

POLITECNICO DI TORINO

Collegio di Ingegneria Chimica e dei Materiali

**Corso di Laurea Magistrale
in Ingegneria Chimica e dei Processi Sostenibili**

Tesi di Laurea Magistrale

**Development of freeze-drying cycles and
evaluation of uncertainty on heat and mass
transfer**



Relatore

prof. Roberto Pisano

Candidato

Estefany Carolina Flores Brun

Ottobre 2017

To my beloved parents and sister....

Introduzione

La liofilizzazione è un processo d'essiccamento molto utilizzato nell'industria farmaceutica. Tale processo ha lo scopo di rimuovere il solvente tramite sublimazione. A differenza di altre tecniche di essiccamento, la liofilizzazione permette di lavorare a basse temperature, rappresentando un importante vantaggio specialmente se il prodotto d'interesse è termolabile, come nel caso delle proteine.

Il processo di liofilizzazione è costituito da tre fasi principali: nella prima fase (congelamento del prodotto), la temperatura del prodotto si abbassa in modo tale da congelarlo. La seconda fase (essiccamento primario) si basa sulla sublimazione sottovuoto del ghiaccio e la terza (essiccamento secondario) consiste nel desorbimento della umidità residua, seguito dalla rottura del vuoto.

Delle tre fasi prima menzionate, l'essiccamento primario rappresenta la fase più lunga e costosa del processo. Di conseguenza l'ottimizzazione di questa fase costituisce uno step importante nello sviluppo del ciclo di liofilizzazione.

Nell'essiccamento primario ci sono due parametri di processo che devono essere ottimizzati: la pressione nella camera del liofilizzatore e la temperatura dei ripiani. Inoltre, durante l'essiccamento primario la temperatura nel fronte di sublimazione non deve superare la temperatura di collasso del prodotto in modo da ottenere un prodotto senza collasso macroscopico nella sua struttura. Quindi, durante l'essiccamento primario da un lato si deve cercare di lavorare in condizioni di essiccamento conservative in modo da ottenere un prodotto senza collassi strutturali macroscopici ma d'altra parte è necessario ridurre i tempi d'essiccamento primario e quindi bisogna lavorare con la più elevata temperatura del ripiano (T_{shelf}) possibile e con una pressione in camera (P_c) che porta alla minimizzazione del tempo di essiccamento. Soltanto un ciclo di liofilizzazione ottimizzato soddisfa entrambe le richieste (domanda di tempo e domanda di qualità del prodotto).

Inoltre, nell'ottimizzazione di un ciclo di liofilizzazione è anche richiesto lo sviluppo di una formulazione farmaceutica che non soltanto assicuri la stabilità dell'API, ma anche una formulazione che abbia adeguate proprietà termiche (i.e. temperatura di collasso sufficientemente alta).

L'uso di un approccio tentativi ed errori per la definizione delle condizioni di processo consuma molto tempo e richiede la conduzione di molte prove sperimentali. Di conseguenza, l'uso di modelli matematici che simulano il fenomeno di sublimazione per definire il design space del processo è un approccio molto usato. L'uso di questi modelli richiede la definizione di una serie di variabili che cambiano con l'avanzare del processo. Per esempio L_{dried} (lo spessore del prodotto secco) aumenta con il tempo e quindi il valore di R_p (resistenza al trasferimento di materia) cambia durante il processo. Questo porta ad avere condizioni ottimali di pressione e temperatura che sono funzioni dal tempo, conseguentemente, l'uso di un modello dinamico rappresenta un vantaggio.

Un modello matematico è una rappresentazione approssimativa della realtà che lavora con vari parametri. Questi parametri hanno una incertezza associata dovuta alla variabilità dei prodotti, disturbi nel sistema e semplificazioni del modello. Pertanto l'inclusione di questa incertezza nel modello è necessaria in modo da sviluppare un ciclo robusto di liofilizzazione che garantisca l'ottenimento di un prodotto con la qualità richiesta.

Obiettivo della tesi

L'obiettivo principale di questo lavoro di Tesi è lo sviluppo di un ciclo di liofilizzazione robusto, partendo dalla selezione ed ottimizzazione di una formulazione farmaceutica, per finire nella definizione delle condizioni ottimali di processo.

Con questo scopo, il lavoro di Tesi è stato diviso in 2 parti.

Nella prima parte si presta speciale attenzione allo sviluppo e ottimizzazione di una formulazione farmaceutica. In questo modo diverse formulazioni sono state caratterizzate termicamente. Lo scopo principale di questa parte del lavoro è capire l'effetto dei diversi componenti in una formulazione sulle caratteristiche termiche (principalmente sulla temperatura di collasso), inoltre si cerca di ottenere una formulazione con una temperatura di collasso più alta possibile.

Una volta selezionata una formulazione e definite le sue caratteristiche termiche, nella seconda parte del lavoro si cerca di ottimizzare la fase di essiccamento, avendo conto della presenza di incertezza sui coefficienti di scambio di materia ed energia. Con questo obiettivo si è usato un modello matematico sviluppato nella Università di Ghent per simulare il fenomeno di sublimazione e costruire un design space dinamico. Questo modello tiene conto dell'incertezza legata ai parametri di entrata e, tramite un'analisi d'incertezza, si è cercato di controllare e stimare quantitativamente il rischio di collasso della struttura del prodotto (i.e the Risk of Failure (RoF)). In questo contesto si è prestato speciale attenzione alla definizione della incertezza legata al coefficiente di trasferimento di massa (R_p) e l'influenza della fase di congelamento su questa incertezza.

Struttura dell'elaborato

Il seguente elaborato è stato suddiviso in quattro capitoli. Il primo capitolo è di tipo introduttivo, nel quale sono presentati i concetti base del processo di liofilizzazione e le fasi coinvolte. Inoltre sono stati spiegati gli aspetti principali nello sviluppo di una formulazione farmaceutica, così come l'importanza dell'adeguata selezione di una formulazione. In tale capitolo c'è anche un riassunto delle varie tecniche sviluppate per l'ottimizzazione delle condizioni operative nell'essiccamento primario. Per ultimo si è introdotta una descrizione dello scopo del lavoro di tesi.

Il secondo capitolo tratta la parte della caratterizzazione termica di diverse formulazioni, sviluppata al Politecnico di Torino. Nello specifico riporta i risultati della caratterizzazione termica di soluzioni di mannitolo e saccarosio in diverse soluzioni tampone così come la valutazione dell'effetto delle concentrazioni dei diversi soluti sulla temperatura di collasso. Come alternativa sono state fatte delle prove con formulazioni contenenti PVP (Polyvinylpyrrolidone) / mannitolo e dextranso / mannitolo.

Il terzo capitolo tratta la parte della ottimizzazione dell'essiccamento primario e definizione delle condizioni operative ottimali. Nello specifico spiega la metodologia usata per la determinazione della incertezza associata alla resistenza al trasferimento di massa partendo dalla determinazione della distribuzione della temperatura di nucleazione. Inoltre si presenta una descrizione del modello matematico usato per definire il design space dinamico e le condizioni ottimali di temperatura dei ripiani e pressione nella camera, così come l'analisi di incertezza fatta nel quale otto parametri sono stati considerati incerti.

Infine, nel quinto capitolo, viene riepilogato il lavoro svolto e si presentano le conclusioni finali.

Scelta della formulazione

Lo sviluppo di formulazioni proteiche è un lavoro impegnativo, non solo per la complessità della produzione e della struttura proteica, ma anche per il loro comportamento labile in determinate condizioni e la loro limitata stabilità chimica e fisica.

Anche se la liofilizzazione offre molti vantaggi, durante questo processo la proteina passa attraverso una serie di perturbazioni che potrebbero portare ad una perdita della sua stabilità e totale o parziale perdita della sua attività biologica.

Pertanto, è molto importante lo sviluppo di una formulazione che minimizzi la perdita della attività proteica durante l'essiccamento e congelamento, e che possa assicurare la stabilità del prodotto durante lo stoccaggio.

Di solito una formulazione contiene eccipienti che stabilizzano la proteina durante il congelamento, questi sono chiamati "crioprotettori", mentre quelli che riducono al minimo la perdita di stabilità proteica durante l'intero processo sono chiamati "lioprotettori". Inoltre, dato l'interesse di ottenere una torta con adeguata qualità e resistenza meccanica, vengono aggiunti "bulking agents". I bulking agents sono di solito eccipienti cristallini mentre quelli che stabilizzano la proteina rimangono in fase amorfa.

È importante tener conto che la progettazione e selezione di una formulazione proteica non è basata solo sulla stabilità dell'API. Anche se è vero che è uno dei parametri più importanti durante il disegno della formulazione è necessario considerare i vincoli fisici sulle condizioni di processo per ottenere una torta adeguata senza collassi macroscopici. In questo scenario, uno dei principali obiettivi nel disegno della formulazione è quello di fornire una formulazione con la temperatura di collasso più elevata possibile, che porta ad una riduzione del tempo di essiccamento primario e che allo stesso tempo assicuri la stabilità proteica.

La temperatura di collasso (T_c) rappresenta la temperatura alla quale si verifica una perdita della struttura della torta, causando effetti negativi sull'umidità residua, eleganza del prodotto, tempo di ricostituzione e stabilità di stoccaggio.

A seconda del tipo e delle quantità di eccipienti presenti nella soluzione, la temperatura di collasso varia. Questa è fortemente influenzata dallo stato fisico dei componenti e quindi dipende non soltanto dalla composizione della formulazione, ma anche dalla storia termica della formulazione.

Si è dunque deciso di studiare l'effetto della concentrazione di diversi componenti e la presenza o assenza di una soluzione buffer sulle proprietà termiche, particolarmente su T_c e T_g' . Con questo obiettivo si sono usate tecniche come: Calorimetria Differenziale a Scansione (DSC) e l'uso di un crio-microscopio (FDM), per determinare T_g' e T_c .

Materiali

Sono state preparate combinazioni di mannitolo (come bulking agent) e saccarosio (come lioprotettori) nelle seguenti soluzioni buffer:

- Buffer fosfato (0.05M, pH 7.3)
- Buffer citrato (0.1 M, pH 7)
- HEPES buffer (0.05M, pH 7.3)

Le seguenti concentrazioni di mannitolo e saccarosio sono state usate:

- 5% mannitolo (w/v)
- 4% mannitolo (w/v) e 1% saccarosio (w/v).
- 3% mannitolo (w/v) e 2% saccarosio (w/v).
- 2% mannitolo (w/v) e 3% saccarosio (w/v).
- 5% saccarosio (w/v).

Inoltre, cercando di ottenere temperature di collasso più alte, combinazioni di PVP/mannitolo e destrano/ mannitolo sono state analizzate, anche variando le concentrazioni di mannitolo tra 5 e 2 % (w/v).

Metodi

DSC analisi:

È stata usata la seguente procedura:

- 1) Raffreddamento da temperatura ambiente a -80°C a $1^{\circ}\text{C}/\text{min}$. Nel caso delle formulazioni con buffer citrato il raffreddamento è stato effettuato a differenti velocità (0,5, 1 e $2^{\circ}\text{C}/\text{min}$)
- 2) Riscaldamento da -80°C a 20°C , con una velocità di riscaldamento di $5^{\circ}\text{C}/\text{min}$.

I termogrammi della fase di riscaldamento sono stati analizzati in modo da evidenziare le diverse trasformazioni durante la fase di riscaldamento e determinare le temperatura di transizione vetrosa delle diverse formulazioni.

FDM:

Il protocollo seguito è il seguente:

- 1) Il primo step consiste nel raffreddare il campione da temperatura ambiente a -60°C a $1^{\circ}\text{C}/\text{min}$.
- 2) Il campione viene mantenuto a questa temperatura per 10 minuti e poi la pressione viene abbassata fino a 10 Pa.
- 3) Il campione viene riscaldato con una velocità di riscaldamento di $1^{\circ}\text{C}/\text{min}$ fino a quando si osserva il collasso della struttura nel fronte di sublimazione.

Durante il processo, fotografie del sistema sono state prese in intervalli di 3 secondi. Le temperature di onset, mid-point e collasso totale (T_{oc} , T_{c-50} e T_{fc}) sono state determinate tramite osservazione del sistema durante il processo.

Risultati

I risultati ottenuti mostrano che man mano la concentrazione di mannitolo aumenta, la temperatura di collasso diminuisce, fino ad arrivare ad una concentrazione di mannitolo maggiore rispetto alla concentrazione di saccarosio, momento nel quale la temperatura di collasso comincia ad aumentare.

L'effetto delle diverse soluzioni di tampone è stato valutato e la temperatura di collasso di formulazioni con due diversi rapporti in peso tra mannitolo e saccarosio (4: 1 e 2: 3; mannitolo al saccarosio) in tre diversi buffer è stata confrontata con la temperatura di collasso delle stesse formulazioni ma in questo caso senza buffer. Nel caso della formulazione con un rapporto in peso 4:1 mannitolo al saccarosio, la temperatura di collasso della formulazione senza buffer era significativamente superiore a quella con buffer. Questo potrebbe essere associato all'effetto inibitorio sulla cristallizzazione del mannitolo causato dalla presenza dei buffer. Per la formulazione con un rapporto di peso 2: 3 mannitolo e saccarosio la temperatura di collasso della formulazione senza buffer non ha mostrato la stessa differenza significativa rispetto al caso della formulazione 4: 1 mannitolo - saccarosio.

Inoltre sono state analizzate combinazioni di PVP/mannitolo e dextran/mannitolo. Le temperature di collasso ottenute con queste formulazioni erano significativamente superiori a quelle ottenute utilizzando combinazioni di mannitolo e saccarosio.

Finalmente la seguente formulazione è stata scelta per continuare con lo sviluppo dei cicli di liofilizzazione nelle seguenti sezioni: 4%(w/v) mannitolo e 1%(w/v) saccarosio in buffer fosfato (0.05M; pH 7.3)

Determinazione delle condizioni di processo in presenza di incertezza sui coefficienti di scambio di materia ed energia.

In questa sezione un modello matematico sviluppato alla Università di Ghent è stato usato per costruire un design space dinamico e definire le variabili di processo adattabili (i.e. T_{shelf} e P_c) in funzione del tempo.

Il modello si basa sui principi basilari di trasporto di materia ed energia e descrive il fenomeno di sublimazione facendo uso di diversi parametri, i cui valori di solito sono approssimazioni dei valori reali. Le predizioni del modello hanno quindi un certo livello d' incertezza associato a quella dei parametri e anche alle assunzioni e semplificazioni intrinseche del modello.

Dunque, al fine di sviluppare un ciclo robusto, è necessario tenere conto di queste incertezze. Nel presente lavoro è stata effettuata un'analisi d'incertezza, in modo tale da controllare e stimare quantitativamente il rischio di collasso della struttura del prodotto (i.e. the Risk of Failure (RoF)). Sono stati considerati incerti otto parametri ed è stato utilizzato un sampling-based approach per fare l'analisi d' incertezza.

Due parametri molto importanti tra quelli considerati incerti sono i coefficienti di trasporto di massa e di energia (R_p e K_v). Siccome in precedenti ricerche non è stata effettuata una valutazione dell'incertezza del R_p , nel presente lavoro è stata posta particolare attenzione alla determinazione quantitativa del livello d'incertezza associato a questo parametro.

La resistenza al trasferimento di massa è legata alla morfologia del prodotto essiccato. In questo scenario la temperatura di nucleazione ha un importante effetto nelle dimensioni dei pori ottenuti nel prodotto. La naturalezza stocastica del fenomeno di nucleazione dà luogo alla variabilità nella morfologia del prodotto in una produzione. Quindi il primo step sviluppato nella definizione dell'incertezza del R_p è l'analisi e la determinazione della distribuzione della temperatura di nucleazione.

Determinazione della temperatura di nucleazione

Siccome il fenomeno di nucleazione è stocastico, la distribuzione della temperatura di nucleazione è stata determinata tramite prove sperimentali. In questo modo è stata misurata la temperatura di nucleazione di un numero statisticamente significativo di campioni (213 campioni).

Sono state usate sei termocoppie, che sono state posizionate in 6 diversi campioni, usati come riferimenti. Dopo, il tempo di nucleazione di ogni campione è stato correlato con una temperatura di nucleazione, facendo uso dei profili di temperatura dei riferimenti.

Con l'obiettivo di valutare l'effetto del protocollo di congelamento nella distribuzione della temperatura di nucleazione e quindi nella variabilità in una produzione, sono stati studiati due protocolli di congelamento: uno con una velocità di raffreddamento di $1\text{ }^\circ\text{C}/\text{min}$ e l'altro con una velocità di raffreddamento uguale a $0.1\text{ }^\circ\text{C}/\text{min}$.

È stato sviluppato un ciclo completo di liofilizzazione per ogni protocollo di congelamento. Al fine di ottenere prodotti finali senza collasso macroscopico, sono state utilizzate condizioni di essiccamento primario molto conservative ($T_{shelf} = -32\text{ }^\circ\text{C}$; $P_c = 10\text{ Pa}$).

Una volta ottenuti i prodotti liofilizzati, sono state sviluppate le seguenti analisi:

- Raman analisi; per valutare il contenuto dei diversi polimorfi dal mannitolo nei campioni. Per l'analisi dei dati è stata usata la tecnica di l'analisi in componenti principali (PCA).
- SEM analisi; per fare una valutazione della morfologia dei campioni.
- Karl fischer analisi; per determinare l'umidità residua dopo l'essiccamento secondario.

Risultati:

Analisi della distribuzione della temperatura di nucleazione

La varianza nella distribuzione della temperatura di nucleazione aumenta con l'uso di una velocità di raffreddamento maggiore. Questo potrebbe essere spiegato tenendo conto del fatto che è più probabile che più campioni nucleano all'interno dello stesso intervallo di temperatura se rimangono in questa condizione per più tempo. Questo risultato è anche coerente con l'analisi

effettuata in termini di differenza tra il tempo di onset e il tempo di offset dell'essiccazione primario (utilizzando le curve del rapporto di pressione pirani/baratron). La differenza tra il punto di onset e il punto di offset è leggermente superiore nel caso del ciclo sviluppato con una velocità di raffreddamento di 1 °C/min rispetto a quello sviluppato con una velocità di raffreddamento di 0.1 °C/min. Questi risultati indicano che una velocità di raffreddamento più elevata porta ad una maggiore variabilità in una produzione.

Raman analisi

Sono state trovate leggere differenze nel contenuto dei poliformi dal mannitolo tra i campioni ottenuti usando diverse velocità di raffreddamento. I campioni ottenuti con una velocità di raffreddamento uguale a 1°C/min contengono più delta mannitolo (e meno beta mannitolo) da quelli ottenuti con una velocità di raffreddamento di 0.1 °C/min.

Inoltre la distribuzione dei polimorfi nel campione è omogenea, tranne vicino al top del campione, dove alfa mannitolo e emi-idrate mannitolo sono presenti.

Umidità residua

Non è stata trovata nessuna correlazione tra la temperatura di nucleazione e l'umidità residua nei campioni. I valori dell'umidità residua (%) sono stati distribuiti in modo casuale per entrambi le velocità di raffreddamento. Ciò potrebbe essere spiegato tenendo conto che l'essiccamento secondario è sufficientemente lungo (15h) da portare ad un'umidità residua bassa nel prodotto.

Morfologia dei prodotti

Una volta definite le distribuzioni delle temperature di nucleazione, sono stati analizzati campioni con diverse temperature di nucleazione tramite l'analisi SEM. I risultati mostrano che le temperature di nucleazioni maggiori sono associate a pori più grandi, mentre i pori più piccoli sono presenti nei campioni che hanno nucleato a minore temperatura.

Il diametro medio di un poro, in tutti casi, è maggiore nel centro del campione. Inoltre, è stata osservata una maggiore variabilità della morfologia all'interno di un campione nel caso dei campioni ottenuti con un velocità di raffreddamento maggiore.

Predizione della morfologia dei prodotti

È stato utilizzato un modello matematico sviluppato al Politecnico di Torino per tradurre ogni temperatura di nucleazione a un'associata morfologia di prodotto.

Il congelamento coinvolge tre eventi principali: sottoraffreddamento, nucleazione e crescita dei cristalli. Durante il sottoraffreddamento, la legge di Fourier è stata usata per descrivere l'evoluzione della temperatura del prodotto. Quando si verifica la nucleazione e la crescita dei cristalli il modello considera l'inclusione di due termini sorgenti all'equazione di bilancio di energia, uno legato alla nucleazione e l'altro alla crescita dei cristalli.

Il dimensionamento del cristallo è stato sviluppato utilizzando un modello empirico che correla il gradiente di temperatura (γ) e la velocità del fronte di congelamento (v) con il diametro dei pori

Una volta verificato l'accordo tra il modello e i risultati sperimentali (immagini al SEM), la popolazione dei campioni di ciascun protocollo di congelamento è stata divisa in 9 classi. Ogni classe è correlata a una temperatura di nucleazione (T_n) e contiene tutti i campioni che nucleano tra $T_n \pm \Delta y$, dove Δy è 1°C nel caso della velocità di raffreddamento più lenta e di $1,5^\circ\text{C}$ quando la velocità di raffreddamento è uguale a $1^\circ\text{C}/\text{min}$.

Per ogni classe, si è fatta la predizione della morfologia del prodotto e il diametro medio di poro è stato determinato in funzione dell'altezza del prodotto. Ogni classe ha una frequenza associata (a causa della frequenza associata a ciascuna temperatura di nucleazione) e quindi può essere determinata una distribuzione di pori (al interno del batch) per ogni altezza del prodotto.

Tutte le simulazioni predicono una maggiore dimensione media dei pori al centro del campione. Questo risultato coincide con i risultati ottenuti con l'analisi SEM.

Determinazione del livello di incertezza del R_p .

Utilizzando le informazioni della distribuzione dei diametro di pori in funzione dell'altezza del prodotto, il valore di R_p e il suo livello di incertezza sono stati calcolati in funzione di L_{dried} (spessore del prodotto secco).

Il valore medio del livello di incertezza ottenuto è di 16% e 12%, rispettivamente per una velocità di raffreddamento uguale a $1^\circ\text{C}/\text{min}$ e $0.1^\circ\text{C}/\text{min}$.

Questo risultato è coerente con le distribuzioni di temperatura di nucleazione dei diversi protocolli di congelamento, in cui una maggiore velocità di raffreddamento porta ad una maggiore variabilità in termini di temperatura di nucleazione e quindi si osserva una maggiore variabilità nei prodotti all'interno di una produzione.

Design Space dinamico dell'essiccamento primario

Il modello matematico che descrive l'essiccamento primario usa un approccio di grid-search e ha conto di due restrizioni nel sistema:

- 1) La temperatura al fronte di sublimazione durante l'essiccamento primario non deve superare il valore della temperatura critica del prodotto (in questo caso definito come $T_{c-50} = -34.8^\circ\text{C}$) in modo da evitare il collasso macroscopico nella struttura del prodotto.
- 2) Il choked flow deve essere evitato, tanto a livello dei flaconi come a livello del liofilizzatore.

Quindi per ogni punto della griglia (i.e. ogni combinazione di T_{shelf} e P_c) e ad ogni intervallo di tempo, è calcolato il valore della temperatura del prodotto, così come il flusso di vapore e l'avanzamento del L_{dried} . In questo modo è costruito un design space dinamico che permette di determinare ad ogni tempo le condizioni di T_{shelf} e P_c che garantiscono il compimento delle due

restrizioni previamente menzionate. Tra questi valori di pressione e temperatura ad ogni tempo è scelta quella combinazione che porta a una massimizzazione del flusso di vapore.

La griglia di pressione e temperatura è limitata. La pressione è limitata tra 10-30 Pa, mentre i limiti della temperatura dei ripiani dipende dalla massima velocità di raffreddamento /riscaldamento raggiungibile con l'apparecchiatura (1°C/min), e quindi è funzione dell'intervallo di tempo.

Analisi d'incertezza

Otto parametri sono stati considerati incerti, e tramite l'uso della tecnica "sobol sampling" è stata definita una matrice d'entrata contenente 1000 campioni. Ogni campione è una combinazione degli otto parametri, e i campioni sono ottenuti come risultato di far variare indipendentemente gli otto parametri tra i suoi limiti massimi e minimi.

Quindi, ad ogni tempo, ed per ogni punto della griglia (combinazione di T_{shelf} e P_c), 1000 simulazioni sono state fatte e quindi sono state ottenute 1000 temperature nel fronte di sublimazione (T_i). Questo porta ad avere una distribuzione di temperature al fronte di sublimazione per ogni combinazione di T_{shelf} e P_c .

Quando il valore di output di T_i è definito come il valore corrispondente al 99% upper percentile, c'è un 1% di probabilità che il vero valore di T_i ottenuto sperimentalmente sia maggiore al T_i determinato dal modello, e quindi si sta lavorando con un valore di rischio di collasso (Risk of Failure) di 1%.

Il rischio di fallimento (Risk of Failure, RoF) è definito come la probabilità che il collasso macroscopico della struttura avvenga su uno o più campioni nel batch.

L'elenco degli otto parametri definiti come incerti è mostrato nella tabella 3.3 (capitolo 3).

È importante menzionare che il livello di incertezza su alcuni parametri è definito come un valore assoluto, mentre che per altri parametri è definito come un'incertezza relativa, espressa in percentuale.

Nel caso del L_{dried} , siccome si tratta di un parametro di input e output, si tiene conto dell'accumulazione dell'errore con l'avanzare del processo, e quindi il valore dell'incertezza di L_{dried} aumenta col tempo.

Nel particolare caso del valore del K_v (coefficiente di scambio di energia), si è fatto la differenziazione tra due gruppi di flaconi:

- I flaconi posizionati al centro
- I flaconi posizionati nei bordi (flaconi con al meno un lato di fronte alla parete o porta del liofilizzatore); questi hanno un valore di K_v significativamente più alto.

E quindi i tre coefficienti del K_v (Eq. 3.9) sono definiti per ogni gruppo.

I coefficienti del K_v appartenenti ai flaconi dei bordi sono stati usati come input dal modello. Questa scelta è stata fatta in quanto questo gruppo di flaconi sono considerati critici rispetto al collasso causato da un maggiore valore di K_v .

Dovuto a questa scelta, il tempo d'essiccamento primario calcolato dal modello è sottovalutato. Quindi una volta che si arriva al punto finale dell'essiccamento primario, le condizioni di pressione e temperatura finali si mantengono per ulteriori ore in modo da assicurare la completa sublimazione del ghiaccio in tutti i campioni.

Il tempo richiesto per finire l'essiccamento primario nei campioni del centro è stato calcolato definendo come input dal modello i valori di P_c e T_{shelf} previamente calcolati e usando i K_v appartenenti ai campioni del centro.

Convalida del modello

Le condizioni ottimali di T_{shelf} e P_c sono state definite per tre RoF (1%, 50%, 99%) al variare del protocollo di congelamento.

Come atteso, le condizioni di essiccamento più conservative sono associate a RoF più bassi.

In seguito, sono state sviluppate delle prove sperimentali per due valori di RoF (1% e 50%) al variare del protocollo di congelamento. Durante l'essiccamento primario la temperatura di tre campioni (uno posizionato al centro e gli altri al bordo) è stata misurata via termocoppie in contatto con il fondo dei flaconi. Finalmente, i campioni ottenuti sono stati analizzati visualmente.

In tutti i casi non si è verificato il collasso macroscopico delle strutture dei campioni. Inoltre la temperatura nel fronte di sublimazione determinata sperimentalmente è maggiore per i campioni nel bordo (rispetto a quella dei campioni posizionati al centro).

Infine, il tempo di essiccamento primario calcolato sperimentalmente (via rapporto di pressioni Pirani/ Baratron) è maggiore rispetto a quello calcolato per il modello tenendo conto dei flaconi del centro.

Per spiegare queste differenze, ulteriori prove devono essere fatte. Inoltre l'analisi delle immagini al SEM dovrebbe essere ripetuta, siccome i risultati associati ad un importante errore (dovuto alla tecnica usata e la percezione del operatore) danno valori di diametro di pori significativamente più grandi a quelli trovati in letteratura

INDEX

Introduction	1
1.1 The importance of Freeze - Drying.....	1
1.2 Basic principles and equipment	2
1.3 Freezing step	5
1.3.1 Physico-chemical processes during freezing phenomena	6
1.3.2 Nucleation temperature and the impact on the final product	8
1.4 Primary Drying	9
1.5 Secondary Drying	10
1.6 Development of a freeze–drying cycle: from formulation to processing conditions.	11
1.6.1 Drug formulation.....	12
1.6.2 Optimization of primary drying	13
1.7 Motivation of the thesis	16
Notation	17
Abbreviations.....	17
References.....	18
Pharmaceutical formulations.....	21
2.1 Using thermal properties to improve a freeze-drying cycle.....	21
2.1.1 Selection of Formulation Composition	24
2.2 Materials and methods	26
2.2.1 Equipment and instrumentation	26
2.2.2 Pharmaceutical formulations.....	29
2.2.3 Thermal characterization.....	30
2.2.4 Freeze-Drying Cycle	32
2.3 Results and discussion	34
2.3.1 Thermal characterization.....	34
2.3.1.1 Formulations Sucrose-Mannitol	34
2.3.1.2 Formulations PVP/Dextran – Mannitol.....	47
2.3.2 Evaluation of cake appearance: cycle performed.....	49
Notation	52

Abbreviations.....	52
References.....	52
Uncertainty analysis.....	55
3.1 Material and methods.....	56
3.1.1 Nucleation temperature distribution.....	56
3.1.2 Characterization tests	59
3.1.3 Experimental determination of the K_v	60
3.1.4 Experimental determination of the R_p	61
3.1.5 Prediction of the product morphology	62
3.1.6 Dynamic Design Space of primary drying.....	63
3.1.6.1 Determination of the optimal process conditions	65
3.1.6.2 Uncertainty analysis	68
3.1.6.3 Determination of the mass transfer resistance.....	70
3.1.6.4 Verification of the Dynamic Design Space	71
3.2 Results.....	72
3.2.1 Nucleation Temperature distribution	72
3.2.2 Impact of freezing conditions and T_n on within-batch and within-vial heterogeneity	79
3.2.3 Experimental determination of the heat transfer coefficient.....	89
3.2.4 Prediction of the product morphology.	89
3.2.5 Determination of the mass transfer resistance.....	92
3.2.6 Dynamic Design space of primary drying for different risk of failure	93
3.2.7 R_p predicted and R_p experimentally determined.....	99
Notation	100
Abbreviations.....	102
References.....	102
Conclusions	105
Acknowledges	109

Chapter 1

Introduction

1.1 The importance of Freeze - Drying

The past decade has seen the rapid increase in the production at large scale of protein, peptides and complex organic molecules for pharmaceutical purpose.

These kinds of substances have a limited long-term stability in aqueous environments and could experiment a variety of chemical reactions as hydrolysis, cross-linking, oxidation, aggregation and disulfide rearrangements (Franks, 1998).

During storage, some of these chemical reactions could affect the product performance, reduce the specific biological activity and even cause problems of safety.

In addition, during the transport of pharmaceutical formulations is important a precise control of the shipping conditions. Usually, this is expensive and difficult to guarantee. During the process, the product could be under different stresses as agitation, high or low temperatures and freezing (Carpenter *et al.*, 1997). Consequently, the development and optimization of processes and techniques aimed to face these problems are a major concern in the pharmaceutical field.

Drying is one of the most challenging and important operations in the industry, this process consists in removing water to slow down adverse chemical reactions, improving the long-term stability and the shipping conditions.

Nowadays, drying technology has evolved and passed from the use of simple solar energy to technologies as tray drying, tunnel drying, spray drying, drum drying, microwaves and others. Among these techniques, the selection of a drying technique should be done depending on the entire manufacturing process, the materials used and the desired final product (Vega-Mercado *et al.*, 2001).

The water in a solution or in a wet solid exerts a characteristic vapor pressure; this vapor pressure depends on the temperature and on the nature of the solid. If this vapor pressure is higher than the water partial pressure of the surrounding environment, the water tends to evaporate or sublimate.

One of the most common basic principles used to drying consists in providing heat to increase the temperature of the product and support the evaporation of the water. There is a wide number of different techniques using this basic principle. Depending on the technique, the heat can be supplied by conduction, convection, radiation or a combination of them. In the case of thermolabile products, a major disadvantage of these techniques is that the

increase in the product temperature could cause adverse reactions, loss of the activity of the API or loss of the product quality (Vega-Mercado *et al.*, 2001)

Therefore, in this complex scenario, freeze-drying appears as one of the most popular methods to dry a product and it is widely used in the pharmaceutical industry (Abdul-Fattah *et al.*, 2007).

1.2 Basic principles and equipment

Lyophilization was introduced in the 1940s for the production of dry plasma and blood products on large scale during the World War II. Later, it was started to be used in food and pharmaceutical companies at large scale (Vega-Mercado *et al.*, 2001).

The process has many advantages compared with traditional drying methods; some of these advantages are (Khairnar *et al.*, 2013; Vega-Mercado *et al.*, 2001):

- The product deterioration due to the oxidation and other chemical reactions is avoided due to the low processing temperature.
- Drying at lower temperatures than room temperature, makes the process appropriate for delicate products, avoiding undesirable changes in the structure, appearance and chemical activity of the product.
- Owing to the highly porous structure, the dried product has a rapid reconstitution time.
- The process fulfills the demands of sterility.
- Good long-term stability because of the removing 95-99% of the water.

Freeze-drying is based on removing water by sublimation from frozen products; this phenomenon involves the phase change from solid to gas without passing through the liquid state. To achieve this objective, it is necessary to develop the drying process using conditions under the equilibrium triple point. Consequently, lyophilization involves two main steps, freezing and drying under vacuum. A typical structure of the process could actually be defined as the development of 3 steps (Rey and May, 2011):

1. Freezing.
2. Primary drying.
3. Secondary drying.

In Figure 1.1, the phase diagram of water is represented. There, it is possible to identify the equilibrium thermodynamic state of the substance in function of the temperature and the pressure values. The different stages during the freeze-drying are represented by the red lines while a common thermal drying technique is represented by the blue line.

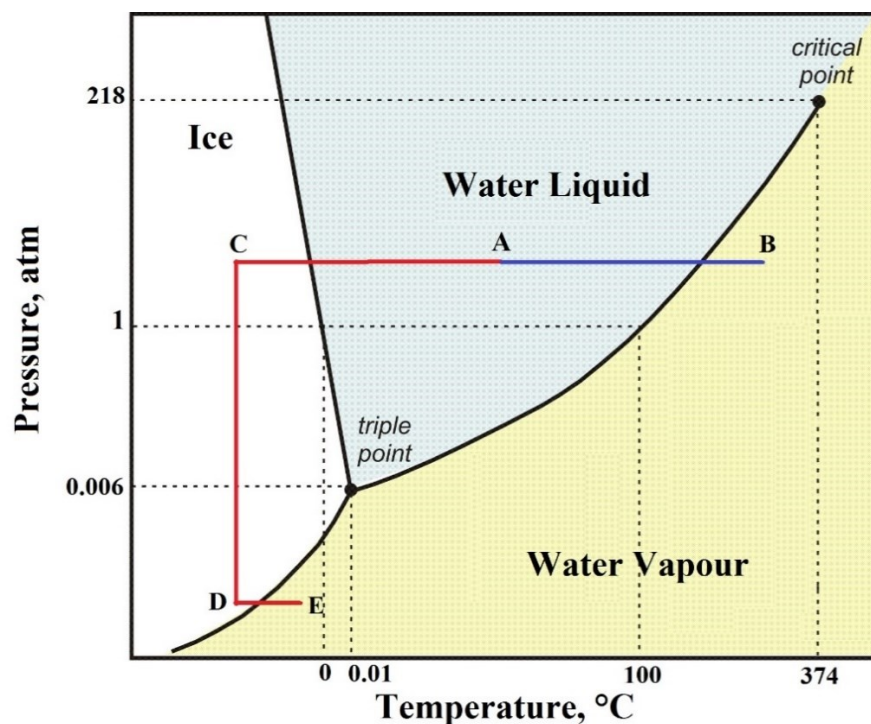


Figure 1.1: Phase diagram of water. The blue line represents a thermal drying technique, the red line represents the different stages during primary drying.

At the beginning of a freeze-drying cycle, the formulation is liquid (point A in Figure 1.1), therefore, the first stage consists in decreasing the temperature to permit the passage of liquid water to ice (point C in Figure 1.1). The next step is primary drying, where sublimation under vacuum occurs.

Primary drying or sublimation starts when chamber pressure decreases (point D) and shelf temperature is high enough to supply the necessary heat in order to promote the sublimation (point E) (Tang and Pikal, 2004).

After primary drying, all the ice has sublimated, but the amorphous product still contains bounded water that needs to be removed; typically, the residual moisture is between 5-20 %, and it depends on the degree of crystalline and amorphous phases on the final product. Therefore, the residual moisture depends on the formulation itself (Tang and Pikal, 2004).

In this scenario, the secondary drying is performed in order to remove the residual moisture; a higher temperature allows the desorption of bounded water. This step has a duration of several hours in order to achieve a residual moisture within the product below 1% (Khairnar *et al.*, 2013; Nireesha *et al.*, 2013).

The shelf temperature and the different physical mechanisms of the steps during the lyophilization are shown in Figure 1.2. Freezing aims to separate water from the drug by its solidification, primary drying removes ice by sublimation and the secondary drying promotes the separation of residual moisture by desorption.

In Figure 1.3 is shown a scheme of a classical freeze dryer in which the main components are (Ratti, 2012):

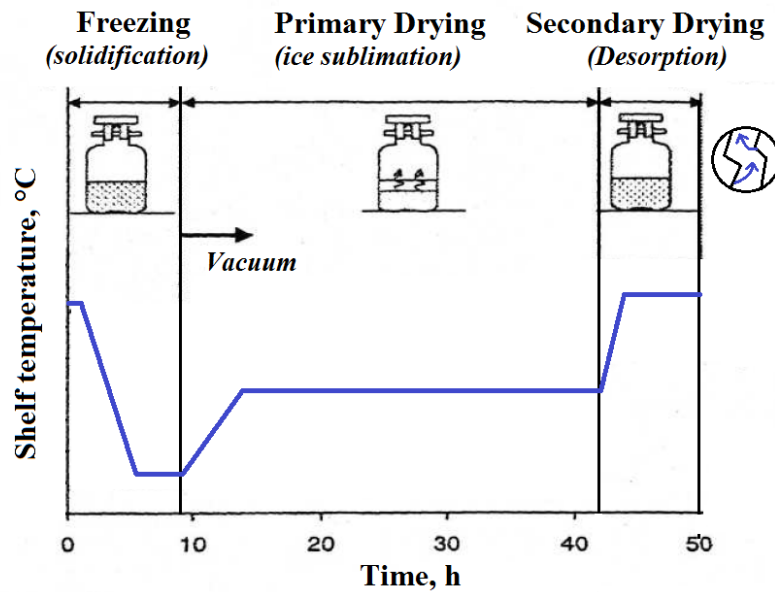


Figure 1.2: Temperature profile during a typical freeze-drying cycle.

- A drying chamber
- A vacuum system; in order to evacuate air from the equipment and work under vacuum during drying. Usually, the vacuum level varies from 4 to 30 Pa.
- A heat transfer system that allows the system to reach low temperatures (-55°C) during freezing while during drying provides the necessary heat.
- A condenser; which temperature allows freezing of the vapor evacuated from the drying chamber.

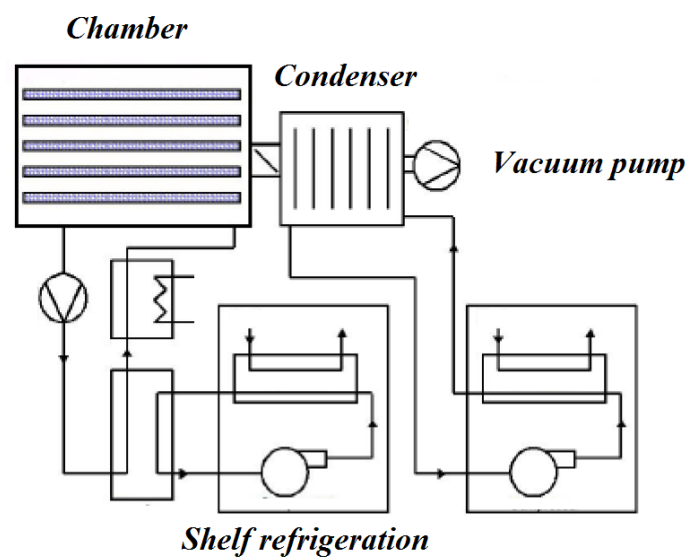


Figure 1.3: Scheme of a classical freeze-dryer (from Pisano (2009), with modifications)

In the typical scheme represented in Figure 1.3, the vials are situated on temperature-controlled shelves contained within the drying chamber. Usually, the shelves are fluid-filled and during the freezing stage, the temperature is controlled using silicon oil as heat transfer fluid. An electrical heater controls the shelf temperature during the drying.

Due to the great amount of vapor generated through primary drying, a water vapor flux is sent to the condenser, which conditions allow to freeze it. The vacuum pump removes only the non-condensable gases from the environment (Ratti, 2012).

1.3 Freezing step

Freezing is one of the most important and complex step during a freeze-drying cycle. It has an impact on quality attributes of the freeze-dried product, such as the stability of the active pharmaceutical ingredient (API) and the physical state and the morphology of the product. This step has also an influence on the process performance and on the development of the next stages.

Shelf-ramped freezing is one of the most common freezing technique used in lyophilization. In this technique, the filled are positioned on the shelves in the freeze-dryer. The shelf temperature is linearly decreased (with a cooling rate from 0.1°C/min to 5 °C/min) until the desired temperature is reached. This final temperature should allow the solidification of the liquid water and must be lower than the eutectic temperature (T_{eu}) (in the case of crystalline solutes) or than glass transition temperature (T_g') (in the case of amorphous materials) (Kasper and Friess, 2011). Depending on the fill depth and the filling volume, the final temperature is held for a determined amount of time in order to allow the complete solidification of water.

This first step constitutes by itself the main dehydration stage during freeze-drying. The solvent water is taken off from the formulation in form of pure ice, generating a biphasic system with the consequence of an important concentration of the solutes; this phenomenon is called “cryoconcentration”(Rey and May, 2011).

In Figure 1.4, the state diagram for a water/solute system is represented. The equilibrium-freezing curve represents how the composition of the concentrate solution changes as the temperature decrease and more water is removed in form of ice. Then, at some point the equilibrium-freezing curve intersects the equilibrium-solubility curve; in these conditions, the concentrated solution is saturated, which means that the solute will crystallize (Kasper and Friess, 2011).The temperature at which the solution is saturated is the eutectic melting temperature (T_{eu}).

Commonly, the solute crystallizes only after a certain degree of supercooling. In the case of some solutes or mixtures of solutes, the crystallization is inhibited. When the temperature is below the glass transition temperature of the maximal freeze-concentrate solution (T_g'), the solutes are transformed into a rigid amorphous solid; this phenomenon is called glassification or vitrification (Liu, 2006). The glass transition temperature of the maximal freeze-concentrate solution is shown in Figure 1.4.

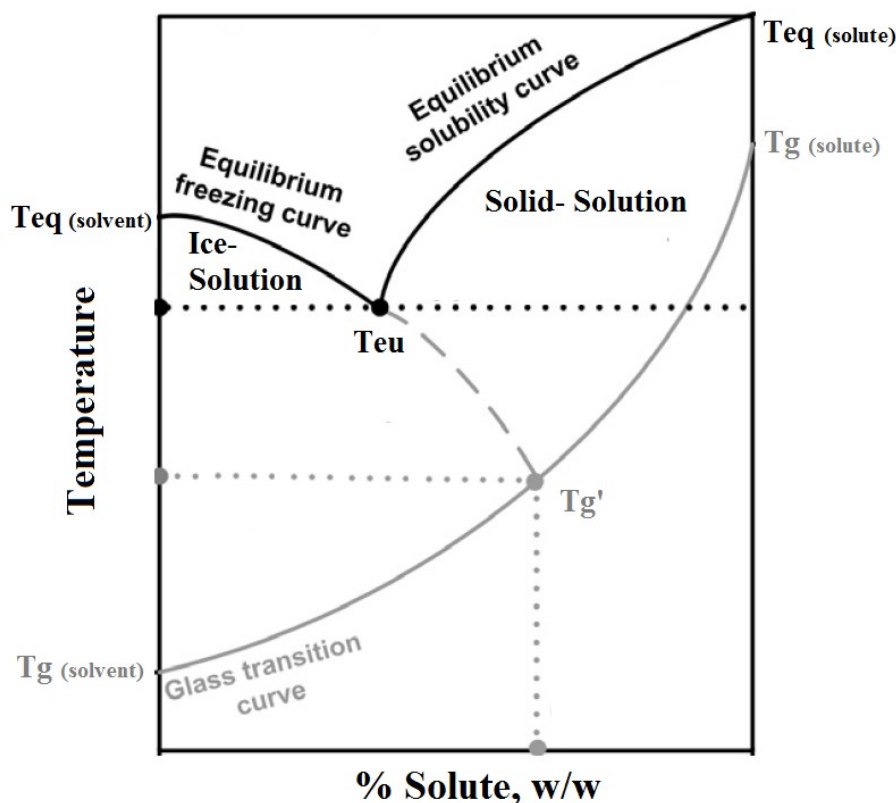


Figure 1.4: State diagram for a water/solute system (From Kasper and Friess, 2011, with modifications).

The product obtained after the freezing step is significantly different in the case of vitrification compared to the case of eutectic crystallization. In the first case, the product consists in ice crystals and on the interstitial region there is a glassy state formed by a solid solution and amorphous water. While in the second case, the structure consists in a mixture of small crystals of ice and solute. Therefore, in the case of amorphous solutes, about 20% of the water remains in the form of associated water with the solid solution after primary drying and the secondary drying is mandatory in order to remove it by a diffusion and desorption process. In crystalline solutes, most of the water can be removed by sublimation of the ice during primary drying (Kasper and Friess, 2011).

1.3.1 Physico-chemical processes during freezing phenomena

The crystallization phenomenon involves two major stages: the nucleation or formation of new crystalline lattice structure (nuclei) from the solution and the crystal growth. The rate of these stages will define the morphology and size of the crystals.

Before the phase change occurs, an energy barrier should be overtaken; the existence of this energy barrier explains the necessity of a degree of supercooling.

The degree of supercooling is defined as the difference between the nucleation temperature and the equilibrium freezing temperature. It constitutes the main driving force for the

formation of stable nucleus and depends on process conditions and product properties (Petzold and Aguilera, 2009; Tang and Pikal, 2004).

The classical theory of nucleation defines the necessary work to create a nucleus as the sum of two terms: a volume term and a surface term.

In terms of reduction of the Gibbs free energy, the volume term represents an exothermal phenomenon (negative term) which supports the nucleation due to the crystalline state constitute a more stable phase in the present conditions. The surface term is positive and it is associated with the creation of a new interface.

In Figure 1.5, the free energy variation in function of the nucleus radius is shown aside to an illustration of the different steps associated.

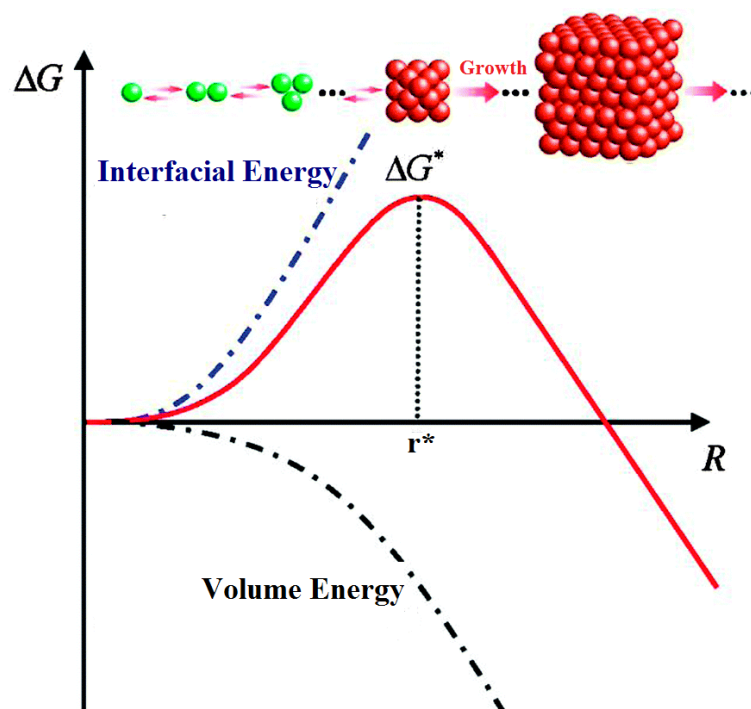


Figure 1.5: Profile of free energy variation in function of the nucleus radius (From Zhang and Liu, 2014, with modifications)

As Figure 1.5 shows, the variation of free energy presents a maximum value at the critical radius r^* ; The ΔG^* represents the energy barrier that should be overcome for the nucleation process (Kiani and Sun, 2011).

Below to the equilibrium freezing temperature, clusters are formed from water molecules. But only when the radius of these clusters is bigger than the critical radius r^* , ice crystallization occurs and the nucleus can continue to the next stage which means the crystal growing.

The typical temperature profile during freezing is represented in Figure 1.6.

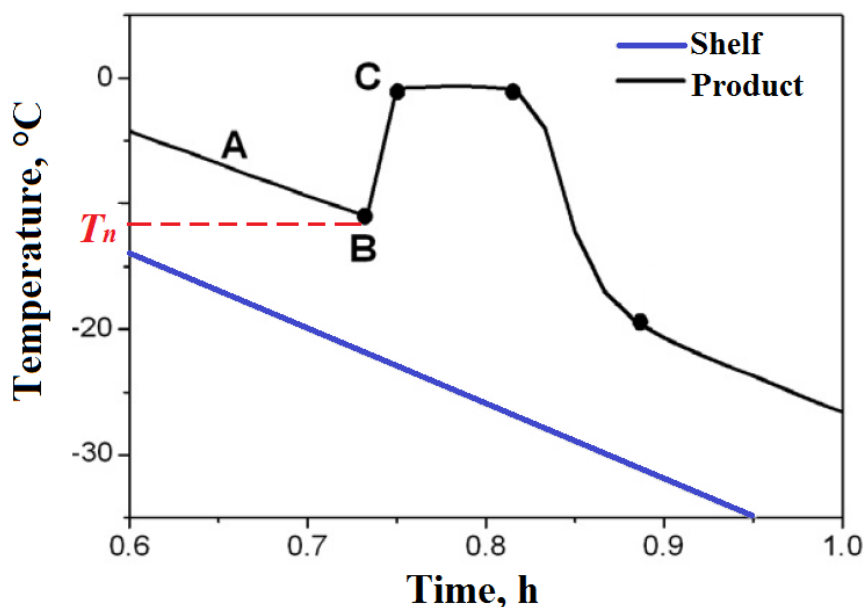


Figure 1.6: Temperature profile of the product and the shelf during the freezing step. Where T_n represents the nucleation temperature (from Kasper and Friess, 2011, with modifications).

Supercooling is represented for the A-B section. On point B, nucleation occurs and the associated temperature is the nucleation temperature (T_n); once the stable nucleus are formed, crystal growth starts and the temperature increases within a short time until a point near to the equilibrium freezing point (point C) (Kasper and Friess, 2011). Then, the temperature remains almost constant and when the solution is completely frozen, the temperature decreases.

In addition, the difference between the homogeneous and heterogeneous nucleation is important. Usually, in the pharmaceutical field, the nucleation is an heterogeneous process and foreign impurities (as large molecules, surface of the containers, impurities) promote the formation of nucleus (Searles *et al.*, 2001).

1.3.2 Nucleation temperature and the impact on the final product

The nucleation temperature is an important parameter of the freezing step because it influences the number and size of the ice crystals and therefore, has an effect on the final product morphology.

Due to the nucleation itself is a stochastic phenomenon, it promotes vial-to-vial heterogeneity in terms of product morphology, which promotes different behaviors during primary and secondary drying (Oddone *et al.*, 2016).

1.4 Primary Drying

Once the freezing step has finished, primary drying starts. The first step is the pressure reduction.

To allow the sublimation, the chamber pressure should be lower than the vapor pressure of ice at the sublimation front which depends on the product temperature. If this requirement is not fulfilled, no mass transfer from the product to the chamber is possible and the sublimation does not occur. Therefore, this gradient of pressure is the driving force for the sublimation during primary drying (Khairnar *et al.*, 2013).

Conventionally, chamber pressure values from 5 to 30 Pa are used (Mortier *et al.*, 2016) and when the sublimation proceeds, water vapor is sent to the condenser.

The sublimation also requires energy; this energy is supplied by increasing the shelf temperature until a certain value.

In Figure 1.7, the phenomena involved during the primary drying are represented schematically. As it is shown, this step includes heat and mass transfer phenomena.

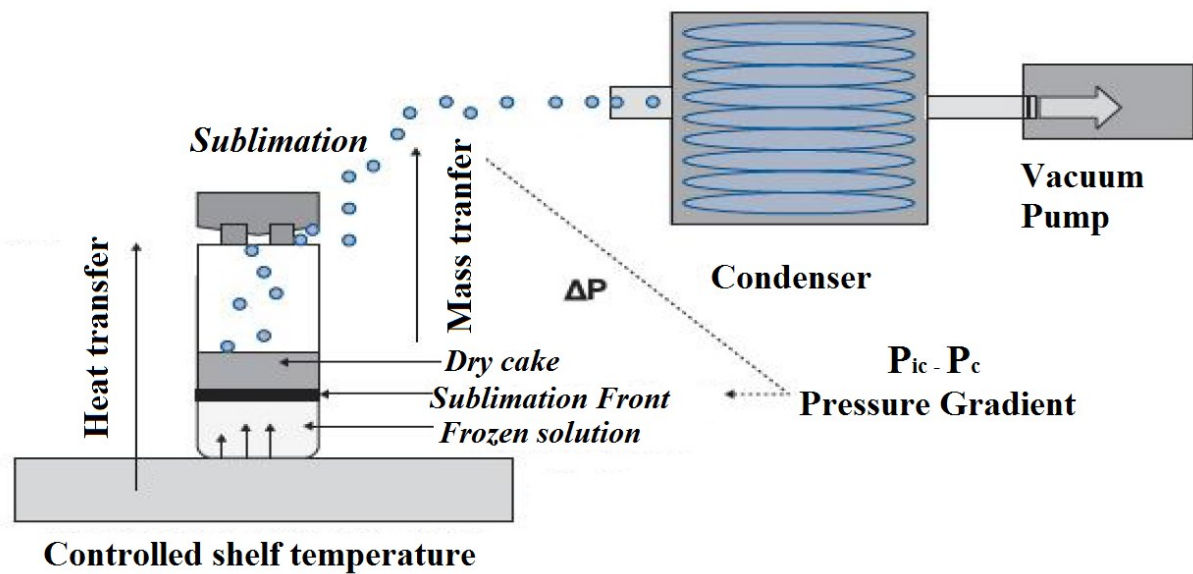


Figure 1.7: Schematic representation of primary drying, showing the mass and heat transfer phenomena (From Khairnar *et al.*, 2013, with modifications).

The heat flux is represented by the Eq. 1.1, where the temperature difference between the shelf and the bottom of the product is the driving force; the heat flux is proportional to this difference, $(T_{shelf} - T_i)$. The coefficient K_v is the overall heat transfer resistance (Fissore *et al.*, 2014).

$$J_q = k_v (T_{shelf} - T_i) \quad (1.1)$$

Eq. 1.2 represents the solvent flux from the sublimation front and it is proportional to $(P_{w,i} - P_{w,c})$.

$$J_w = \frac{1}{R_p} (P_{w,i} - P_{w,c}) \quad (1.2)$$

R_p is the resistance to the vapor flow, $P_{w,i}$ and $P_{w,c}$, are the partial vapor pressure at the sublimation front and at the drying chamber, respectively (Fissore *et al.*, 2014).

From Eq.1.1 and Eq.1.2, is easy to conclude that the chamber pressure and shelf temperature constitute two key process parameters which have an important influence on the primary drying performance. Consequently, it is important to optimize these parameters in order to optimize the freeze-drying cycle.

It is imperative to keep in mind, as previously mentioned, that the drying step is influenced and directly correlated with the previous step (freezing). A number of researchers have reported the influence of the nucleation temperature in primary drying (Searles *et al.*, 2001).

The nucleation temperature has a relevant effect on the crystal morphology and size distribution; this fact affects the mass transfer resistance of the dried cake, which has a direct influence on the sublimation rate (see Eq. 1.2). Therefore, higher nucleation temperatures are associated with large ice crystals; large ice crystals generate bigger pores which offer a lower resistance to vapor flow throughout the sublimation. The opposite occurs in the case of lower nucleation temperatures, which lead to structures with a higher amount of small pores and higher R_p (Geidobler and Winter, 2013).

Another important fact to take into account is the maximum temperature of the sublimation front in the product during primary drying (T_i). If this temperature reaches a higher value than the collapse temperature, the porous structure near to the sublimation front could undergo viscous flow, leading to formation of holes within the cake and collapse structure. The collapse temperature is defined as the temperature where a structure loss within the product will occur. The cake collapse has an impact not only on quality attributes but also affects the residual water content, the reconstitution time and the protein stability (Khairnar *et al.*, 2013).

In the case of crystalline solutes, the collapse temperature (T_c) is associated to the eutectic temperature (T_{eu}). For amorphous phases, the collapse temperature is usually higher than T_g' because the high viscosity near to T_g' prevents the viscous flow (Depaz *et al.*, 2016).

1.5 Secondary Drying

The last stage of lyophilization is secondary drying. After the sublimation of the ice during primary drying, a great amount of bounded water is still within the structure. About 5-20% of residual water could be in the structure and this amount depends on the nature of the

formulation. Therefore, the objective of the secondary drying is removing the bounded water in order to reduce the final moisture of the product (Tang and Pikal, 2004).

The temperature of the process is further increased to promote water desorption. In this stage, it is also possible to observe the loss of cake structure. Therefore, the product temperature should remain below the $T_{g(solute)}$ (the glass transition temperature of the dried product), in order to avoid the viscous flow.

It is also important to use a slow heating rate to go from the T_{shelf} of primary drying to T_{shelf} of secondary drying. As it was showed in Figure 1.4, the glass transition temperature depends on the residual moisture content, and $T_{g(solute)}$ value is higher than T_g' of the maximal freeze-concentrate solution. After primary drying, the residual moisture is still high, which makes necessary not to increase the T_{shelf} too fast (Mortier *et al.*, 2016).

Finally, the time of secondary drying depends on the residual moisture required in the final freeze-dried product.

1.6 Development of a freeze–drying cycle: from formulation to processing conditions

Quality by design (QbD) is an approach widely used in the pharmaceutical field. It is based on the principal idea that “*quality is built into the product*”; in this context, the scope of the pharmaceutical development is the design of a quality product and a manufacturing process suitable and optimized in terms of time and resources.

The ICH guidelines on pharmaceutical development (Q8) outline the steps that pharmaceutical development should include. In Figure 1.8, a scheme of these steps is shown.

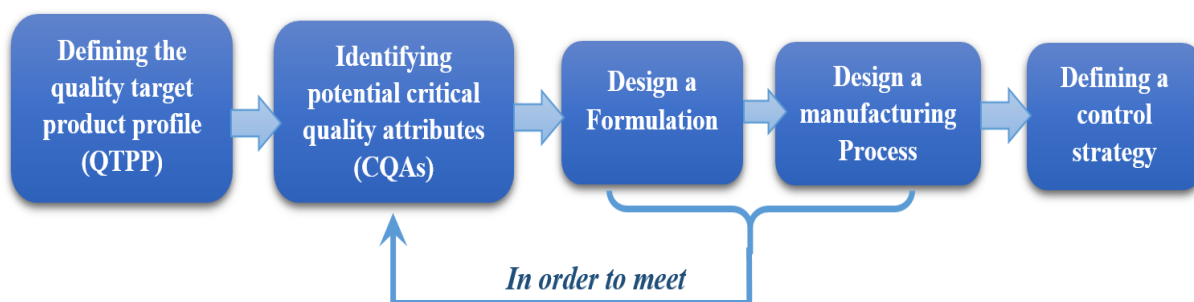


Figure 1.8: Elements that a pharmaceutical development procedure should include.

In the case of a freeze-dried product some of the most important potential critical quality attributes (CQAs) are (Koganti *et al.*, 2011):

- The stability of the API throughout the freeze-drying process.
- The residual moisture of the freeze-dried product should ensure the long term–stability of the product.

- The reconstitution time.
- The freeze-dried cake appearance should fulfil aesthetic requirements.

Once the CQAs are identified, the definition and selection of the type and amount of excipients to obtain a quality drug product is necessary. The concept of QbD is applied to the formulation process and the manufacturing process.

The following sections describe the basic design principles of a stable protein lyophilized formulation and the design of an optimized freeze-drying cycle by using the QbD approach.

Since the drying step is the most time and energy consuming step and also the most expensive, the optimization of this step is fundamental.

1.6.1 Drug formulation

The development of a protein formulation is a challenging work, not only due to the complexity of protein production and structure but also because of their labile behavior under certain conditions and their limited chemical and physical stability (Wang, 1999).

Although, all the advantages that freeze-drying offers, during this process, the protein goes through a number of stresses or perturbations which could lead to a loss of its stability in terms of its primary structure or its native conformation and the complete or partial loss of its biological activity (Bhatnagar *et al.*, 2008)

Therefore, it is quite important the development of a formulation that minimizes the loss of the protein stability during freeze-drying, and could assure the storage stability of the freeze-dried product.

In order to develop a protein formulation, a key step is the definition of specific conditions (e.g. pH and specific stabilizing ligands) and nonspecific stabilizing additives that optimize the protein stability.

There are different mechanisms of destabilization of the protein during the freezing and the drying steps (e.g. the change of phase, the freeze concentration and the pH shift). The excipients that stabilize the protein during the freezing are called “cryoprotectants” and those that minimize protein unfolding throughout both freezing and drying are denoted as “lyoprotectants”(Rey and May, 2011).

One relevant CQA is the cake appearance; in order to obtain an elegant and mechanical strong cake, bulking agents are added. Usually, the bulking agents are crystalline excipients while those that stabilize the protein remain in amorphous phase.

It is important to take into account that the design of a protein formulation is not only based on the stability of the API, even though, it is true that it is one of the most important parameters. During the formulation design is necessary to consider physical constraints on process conditions to obtain an adequate cake with a low residual moisture (Carpenter *et al.*, 1997).

In this scenario, one of the main goals of the formulation design is to supply a formulation with the highest collapse temperature, which is practical and brings as consequence a time reduction in primary drying, within the constraints of assuring the protein stability (Carpenter *et al.*, 1997).

1.6.2 Optimization of primary drying

The primary drying is one of the most expensive and riskiest step during freeze-drying. Usually, the duration of this stage is the largest of the entire cycle, transforming it into a critical time and energy consuming step.

The energy cost breakdown for a freeze-drying process is shown in Figure 1.9. The main energy-consuming operations of the cycle are: freezing, vacuum, condensation and sublimation.

As it is evidenced in Figure 1.9, sublimation and vacuum are the operations that are more expensive. Therefore, in order to reduce the energetic costs of the cycle it is really important the optimization of the primary drying (Ratti, 2001).

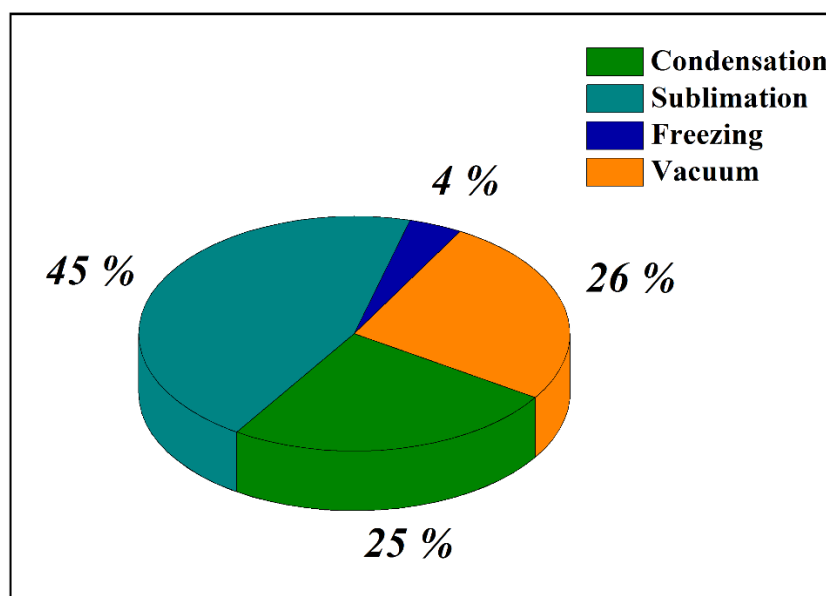


Figure 1.9: Energy cost breakdown for a freeze-drying process (From Ratti, 2001, with modifications)

The process conditions that can be controlled during primary drying are shelf temperature and chamber pressure. These process conditions are considered Critical Process Parameters (CPPs) due to the fact that they affect the CQAs and have a direct influence on the duration of primary drying (Koganti *et al.*, 2011).

In pharmaceutical freeze-drying process, usually the operations constraints are two (Fissore *et al.*, 2011):

- During process, the product temperature should be below the collapse temperature in order to avoid the cake collapse.
- In order to avoid the choking flow within the duct between the condenser and the chamber, the vapor flow must remain under a limit value.

With the purpose to define the two CPPs of the primary drying, T_{shelf} and P_c , in-line and off-line methods can be used (Pisano *et al.*, 2013).

Off-line optimization

The set of operating conditions that allow the preservation of the CQAs defines the design space. Therefore, in this two-dimensional map it is possible to identify all the combinations of T_{shelf} and P_c which lead to obtain the desired level of quality of the product and to satisfy the process constraints.

On Table 1.1, different methods off-line used for the freeze-drying cycle design are compared in terms of technical and general information.

Table 1.1: Technical and general information of different off-line methods currently used for the freeze-drying cycle design (From Pisano, *et al.* 2013, with modifications).

	<i>Trial & error</i>	<i>DS via DOE</i>	<i>Static DS via modelling</i>	<i>Dynamic DS via modelling</i>
Equipment scale wherein the process design is done	Lab	Lab	Lab/industrial	Lab/industrial
Need of cycle scale-up to a manufacturing unit	yes	yes	no	no
Experimental effort & human resources	high	high	low	low
Ease of introducing some margins of safety on processing conditions	no	yes	yes	yes
Accounting for batch unevenness	no	no	yes	yes
Freeze-drying cycle optimization	no	no	no	yes
Availability of comprehensive data for better process understanding	no	yes	yes	yes

The design space can be developed by means of experimental investigation, using a trial and error approach, but this process consumes a lot of time, resources and involves high cost. In this context, mathematical modeling can reduce the number of experiments and the necessary effort. Depending on the mathematical model, we could obtain a static design space or a dynamic design space (Pisano *et al.*, 2013).

Traditionally, a set of process conditions (T_{shelf} and P_c) are maintained constants during primary drying, leading to a static design space that not necessary optimize process conditions during the whole primary drying. Nowadays the use of a dynamic design space is widely used and preferred. Since the L_{dried} (thickness of the dried layer on the product) is constantly changing during primary drying, the R_p is also changing and therefore, the optimum T_{shelf} and P_c change throughout primary drying. With a dynamic simulation we could optimize the cycle and determining the optimum combination of T_{shelf} and P_c that varies with time (Fissore *et al.*, 2011).

It is relevant to take into account the fact that the mathematical model is a representation of the reality, which uses several parameters. These parameters have an uncertainty associated due to the inter-vial variability, process disturbances and simplifications of the model.

As previously mentioned, the freezing has an important impact on the inter-vial variability and due to the stochastic nature of the nucleation temperature a morphology variability is present. This derives into a R_p variability within the batch.

In order to design a robust cycle, it is necessary to include the uncertainty on the mechanistic model; this could be done using different strategies (Pisano *et al.*, 2013):

- A margin of safety on the T_{shelf} and P_c is added.
- Model parameters are overestimated.
- Doing an uncertainty analysis, in order to determinate quantitatively the parameter uncertainty (Mortier *et al.*, 2016; Pisano *et al.*, 2012).

In-line Optimization Methods

In this approach, a predefined cycle recipe is used to carry out the freeze-drying cycle, while a closed loop controller manipulates in-line the process conditions in order to achieve the desired product characteristics.

Figure 1.8 shows that one of the steps in the pharmaceutical development is the definition of a control strategy. An important number of researchers are focused on developing control systems that can evaluate process changes while process conditions are in-line manipulated. In this scenario, in-line optimizations methods can be used to design an optimal cycle and as a part of process control strategy.

There are various techniques developed in this field. These different tools differ principally in the number and type of manipulated process variables and the constraints defined. Furthermore, the type of the information required from the process is another important characteristic because it define the monitoring technique necessary to close the control loop (Pisano *et al.*, 2013).

It is important to note that the in-line optimization method does not always assure that the quality attributes defined on the dried-product will be achieved. In order to obtain a robust cycle, it might be necessary to use a margin of safety. On the other hand, this approach presents the advantage of avoiding the necessity of scaling up the cycle.

1.7 Motivation of the thesis

The aim of this thesis work is the design of a freeze-drying cycle, from the formulation to the definition of the principal process conditions. The work is divided into two different parts, described in chapter 2 and 3, respectively.

The first part involves the selection of a pharmaceutical formulation for a specific protein. Lactate dehydrogenase (LDH) was selected; once the potential formulations are selected, the thermal characterization of these formulations is performed in order to obtain the necessary information to continue with the next step, which is the optimization of the primary drying step.

In the second part, a dynamic design space for the primary drying was calculated using a mechanistic model developed by Mortier *et al.*, (2016). This model accounts for the parameter uncertainty and it was necessary to quantify experimentally the uncertainty of R_p .

With this pursue, a determination of the nucleation temperature distribution was done with the help of a mathematical model for the freezing step developed by Pisano and Capozzi (2017) and the product morphology of lyophilized drugs was estimated; the variability of product structure within a production was determined and the uncertainty of the R_p was quantitatively defined.

In Figure 1.10, the structure of the work is schematized. The first part of the work (chapter 2) was performed at Politecnico di Torino, while the second part was developed at Ghent University.

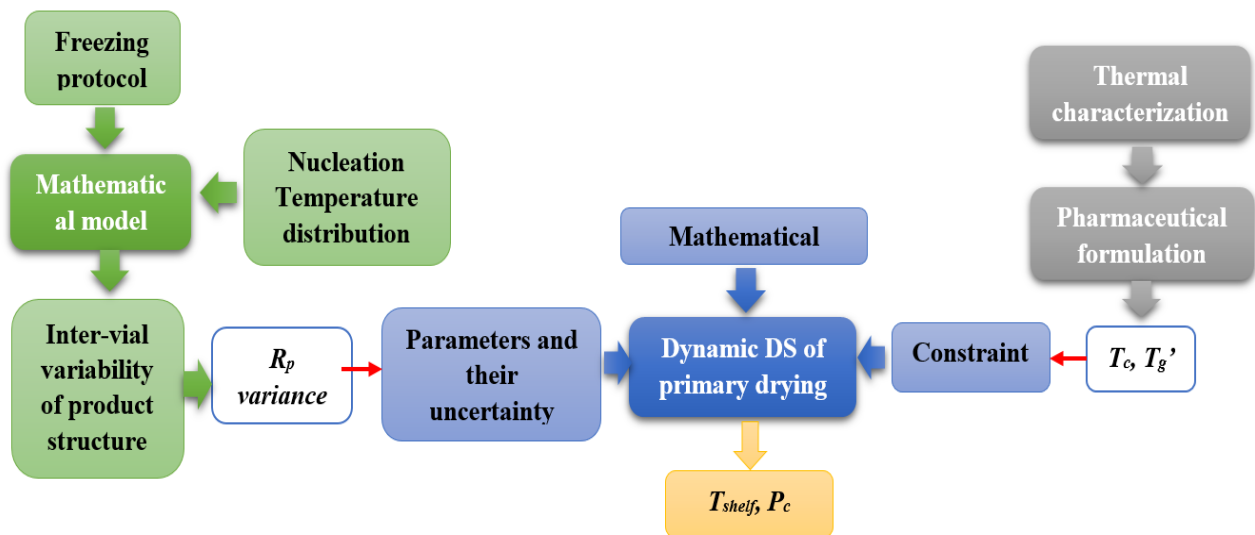


Figure 1.10: Workflow in order to achieve the aim of the project

Notation

J_q	Heat flux, W/m^2
J_w	Solvent flux, $\text{Kg m}^{-2} \text{ s}^{-1}$
K_v	Heat transfer coefficient between, $\text{J m}^{-2}\text{s}^{-1}\text{K}^{-1}$
L_{dried}	Dried layer thickness, m
P_c	Pressure in the drying chamber, Pa
$P_{w,c}$	Partial vapor pressure in the drying chamber, Pa
$P_{w,i}$	Ice vapor pressure at interface temperature, Pa
R	Nucleus radius, m
r^*	Critical radius, m
R_p	Dried product resistance to vapor flow, m s^{-1}
T_c	Collapse Temperature, $^{\circ}\text{C}$
T_{eq}	Equilibrium freezing temperature, $^{\circ}\text{C}$
T_{eu}	Eutectic melting temperature, $^{\circ}\text{C}$
T_g	Glass transition temperature, $^{\circ}\text{C}$
T_g'	Glass transition temperature of the maximal freeze-concentrate state, $^{\circ}\text{C}$
T_i	Product temperature at the sublimation front, $^{\circ}\text{C}$
T_n	Nucleation temperature, $^{\circ}\text{C}$
T_{shelf}	Shelf temperature, $^{\circ}\text{C}$
ΔG	Free energy variation, J
ΔG^*	Critical free energy variation, J

Abbreviations

API	Active Pharmaceutical Ingredient
CPP	Critical Process Parameter
CQA	Critical Quality Attribute
DOE	Design of Experiments

DS	Design Space
QbD	Quality by Design

References

- Abdul-Fattah, A. M., Kalonia, D. S., & Pikal, M. J. (2007). The challenge of drying method selection for protein pharmaceuticals: Product quality implications. *Journal of Pharmaceutical Sciences*, **96**(8), 1855-2177.
- Bhatnagar, B. S., Pikal, M. J., & Bogner, R. H. (2008). Study of the individual contributions of ice formation and freeze-concentration on isothermal stability of lactate dehydrogenase during freezing. *Journal of Pharmaceutical Sciences*, **97**(2), 798–814.
- Carpenter, J. F., Pikal, M. J., Chang, B. S., & Randolph, T. W. (1997). Rational design of lyophilized protein. *Pharmaceutical Research*, **14**(8), 969-975
- Depaz, R. A., Pansare, S., & Patel, S. M. (2016). Freeze-Drying above the glass transition temperature in amorphous protein formulations while maintaining product quality and improving process efficiency. *Journal of Pharmaceutical Sciences*, **105**(1), 40–49.
- Fissore, D., Pisano, R., & Barresi, A. A. (2011). Advanced approach to build the design space for the primary drying of a pharmaceutical freeze-drying process. *Journal of Pharmaceutical Sciences*, **100**(11), 4922–4933.
- Fissore, D., Pisano, R., & Barresi, A. A. (2014). Applying quality-by-design to develop a coffee freeze-drying process. *Journal of Food Engineering*, **123**, 179–187.
- Franks, F. (1998). Freeze-drying of bioproducts: putting principles into practice. *European Journal of Pharmaceutics and Biopharmaceutics*, **45**(3), 221-229.
- Geidobler, R., & Winter, G. (2013). Controlled ice nucleation in the field of freeze-drying: Fundamentals and technology review. *European Journal of Pharmaceutics and Biopharmaceutics*, **85**(2), 214–222.
- Kasper, J. C., & Friess, W. (2011). The freezing step in lyophilization: physico-chemical fundamentals, freezing methods and consequences on process performance and quality attributes of biopharmaceuticals. *European Journal of Pharmaceutics and Biopharmaceutics*, **78**(2), 248-263
- Khairnar, S., Kini, R., Harwalker, M., Slaunkhe, K., & Chaudhari, S. (2013). A Review on freeze drying process and pharmaceuticals. *International Journal of Research in Pharmacy and Science*, **4**(3), 76–94.
- Kiani, H., & Sun, D. W. (2011). Water crystallization and its importance to freezing of foods: A review. *Trends in Food Science and Technology*, **22**(8), 407-426
- Koganti, V. R., Shalaev, E. Y., Berry, M. R., Osterberg, T., Youssef, M., Hiebert, D. N., Kanka F. A., Nolan M., Barrett R., Scalzo G., Fitzpatrick G., Fitzgibbon N., Luthra S., Zhang, L. (2011). Investigation of design space for freeze-drying: use of modeling for primary drying segment of a freeze-drying cycle. *AAPS PharmSciTech*, **12**(3), 854–861.

- Liu, J. (2006). Physical characterization of pharmaceutical formulations in frozen and freeze-dried solid states: techniques and applications in freeze-drying development. *Pharmaceutical Development and Technology*, **11**(1), 3–28.
- Mortier, S. T. F. C., Van Bockstal, P. J., Corver, J., Nopens, I., Gernaey, K. V., & De Beer, T. (2016). Uncertainty analysis as essential step in the establishment of the dynamic Design Space of primary drying during freeze-drying. *European Journal of Pharmaceutics and Biopharmaceutics*, **103**, 71–83.
- Oddone, I., Van Bockstal, P. J., De Beer, T., & Pisano, R. (2016). Impact of vacuum-induced surface freezing on inter- and intra-vial heterogeneity. *European Journal of Pharmaceutics and Biopharmaceutics*, **103**, 167–178.
- Petzold, G., & Aguilera, J. M. (2009). Ice morphology: fundamentals and technological applications in foods. *Food Biophysics*, **4**(4), 378–396.
- Pisano, R. (2009). Monitoring and control of a freeze-drying process of pharmaceutical products in vials. PhD Thesis, Department of Applied Science and Technology, Politecnico di Torino.
- Pisano, R., Fissore, D., & Barresi, A. A. (2013). In-Line and Off-Line Optimization of Freeze-Drying Cycles for Pharmaceutical Products. *Drying Technology*, **31**(8), 905–919.
- Pisano, R., Fissore, D., Barresi, A. A., & Rastelli, M. (2013). Quality by design: scale-up of freeze-drying cycles in pharmaceutical industry. *AAPS PharmSciTech*, **14**(3), 1137–49.
- Pisano, R., Fissore, D., Barresi, A. A., Brayard, P., Chouvinc, P., & Woinet, B. (2013). Quality by design: optimization of a freeze-drying cycle via design space in case of heterogeneous drying behavior and influence of the freezing protocol. *Pharmaceutical Development and Technology*, **18**(1), 280–295.
- Pisano, R., & Capozzi, L. C. (2017). Prediction of product morphology of lyophilized drugs in the case of Vacuum Induced Surface Freezing. *Chemical Engineering Research and Design*, **125**, 119–129.
- Ratti, C. (2001). Hot air and freeze-drying of high-value foods: A review. *Journal of Food Engineering*, **49**(4), 311–319.
- Ratti, C. (2012). Freeze-Drying Process Design. *Handbook of Food Process Design Vol 1*, Chap. 2 , 621–647.
- Rey, L., & May, J. C. (2011). Freeze-drying/ lyophilization of pharmaceutical and biological products, *second Edition, Revised and Expanded*. Drugs and the Pharmaceutical Sciences. Taylor & Francis.
- Searles, J. A., Carpenter, J. F., & Randolph, T. W. (2001). The ice nucleation temperature determines the primary drying rate of lyophilization for samples frozen on a temperature-controlled shelf. *Journal of Pharmaceutical Sciences*, **90**(7), 860–871.
- Tang, X., & Pikal, M. J. (2004). Design of Freeze-Drying Processes for Pharmaceuticals: Practical Advice. *Pharmaceutical Research*, **21**(2), 191–200.
- Vega-Mercado, H., Marcela Góngora-Nieto, M., & Barbosa-Cánovas, G. V. (2001). Advances in dehydration of foods. *Journal of Food Engineering*, **49**(4), 271–289.
- Wang, W. (1999). Instability, stabilization, and formulation of liquid protein

pharmaceuticals. *International Journal of Pharmaceutics*, **185**(2), 129-188.

Zhang, T. H., & Liu, X. Y. (2014). Experimental modelling of single-particle dynamic processes in crystallization by controlled colloidal assembly. *Chemical Society Reviews*, **43**(7), 2324–2347.

Chapter 2

Pharmaceutical formulations

Freeze-drying is commonly used to stabilize biopharmaceutical drugs that are unstable in aqueous environments. However during freeze/drying, proteins experiment several stresses, therefore, an important challenge is to avoid structural and chemicals changes and assure that the protein bioactivity remains (Bhatnagar *et al.*, 2008); the capacity of the protein structure to resist these stresses is related to the formulation.

In this context, the design of a pharmaceutical formulation is required. An adequate selection of the formulation composition is critical in order to develop a robust and short freeze-drying cycle and to assure the protein stability during the process.

The pharmaceutical formulation should fulfil the following demands (Rey and May, 2011):

- The protein unfolding should be inhibited.
- T_g (Glass transition temperature of the dried product) must be higher than the storage temperature.
- Loss of cake structure should be avoided.
- The protein stability must be assured during the storage.

The importance of the thermal properties and the physical state of the excipients on the formulations is analyzed in this chapter. In addition, the effect of the concentration of the different excipients on the formulation is assessed in order to design a formulation that makes possible the development of a short and optimized freeze-drying cycle.

On the first part of this chapter, there is a brief introduction about how the thermal properties are used in order to improve a freeze-drying cycle; the next sections describe the experimental work performed in the Politecnico di Torino.

2.1 Using thermal properties to improve a freeze-drying cycle

Primary drying should be performed with conservative drying conditions in order to keep the product temperature below the critical formulation temperature (i.e. the collapse temperature); on the other hand, it is necessary to develop this step at the maximum possible temperature to reduce the required time for the cycle.

In Figure 2.1, the relation between primary drying and the formulation development is schematized. It is required to fulfil a demand of time and quality in order to optimize the cycle; therefore, a key step in the cycle optimization is the development of a pharmaceutical

formulation with adequate thermal properties (enough high T_c) which assures the protein stability.

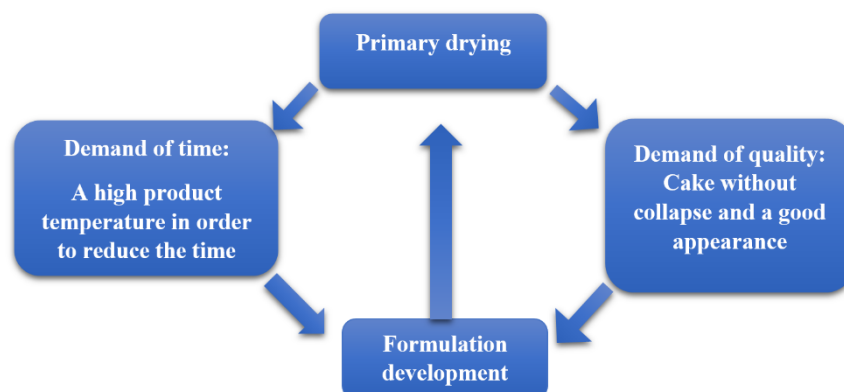


Figure 2.1: Relation between primary drying, formulation development and cycle optimization.

The collapse temperature (T_c) represents the temperature at which there is a loss of the cake structure. Figure 2.2 shows three freeze-dried products with different cake appearances. The freeze-dried product C) represents the product appearance desired at the end of the cycle; In B), it is showed the shrinkage phenomenon that involves a volume contraction with a preservation of the structure; In A) is possible to see a severe loss of the cake structure, big holes and foamy appearance.

The collapse of the cake has a negative impact on (Depaz *et al.*, 2016):

- The residual moisture; an increase of the residual moisture has a negative effect on the API stability.
- The product elegance.
- The storage stability.
- The reconstitution time.

Thermal properties of the formulation such as the eutectic melting temperature (T_{eu}), the crystallization temperature (T_{cr}) or the glass transition temperature of the maximal freeze-concentrate state (T_g') are relevant information in order to determinate the collapse temperature (Rey and May, 2011).

Depending on the type and the amounts of excipients present on the solution, the collapse temperature varies. For amorphous solutes, the T_c is associated with the T_g' ; when the sample has surpassed for some degrees T_g' (but it is still under T_c) the high viscosity of the solution will prevent viscous flow and the collapse. That is the reason why T_c is usually several degrees higher than the T_g' (Kasper and Friess, 2011).

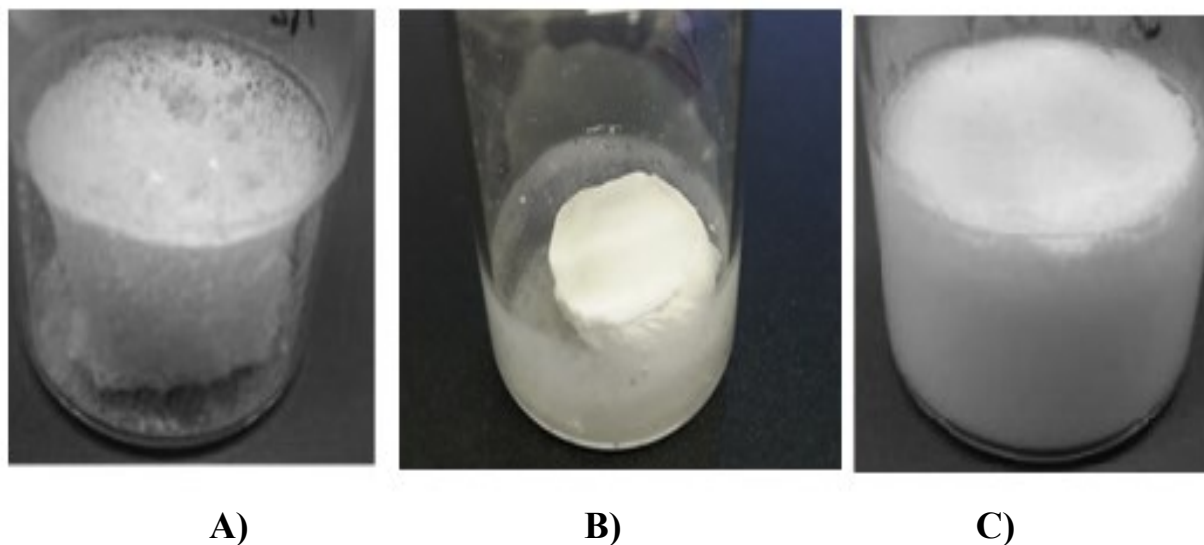


Figure 2.2: Freeze-dried products. A) Severe collapse is present in the freeze-dried product. B) Shrinkage present in the freeze-dried product C) Freeze-dried product with a high-quality cake.

In the case in which amorphous solutes and crystalline bulking agents are mixed, different scenarios can occur depending on the degree of solute crystallization and the different concentrations of the components.

For instance, microscopic collapse could occur in case of complete crystallization of the bulking agent between T_{eu} and T_g' due to the collapse of the amorphous phase; in this case macroscopic collapse will not occur (unless the product temperature is above or near to T_{eu}) because the crystalline phase will provide mechanical support. On the other hand, if the crystallization of the bulking agent is completely inhibited, the collapse temperature is related with the T_g' . While, if there is no complete crystallization, the value of T_c will be between T_g' and T_{eu} (Rey and May, 2011; Tang and Pikal, 2004).

Multiple researchers have informed that the physical state of the excipients has a relevant effect on the thermal properties of the formulation and on the stability of the active pharmaceutical ingredient (API) (Al-Hussein and Gieseler, 2012; Izutsu and Kojima, 2002).

For example, in the case of mannitol, depending on its physical state, it will have a different behavior. This bulking agent can be present in several physical forms, including three different polymorphs forms (α , β and δ). Its amorphous form has a protective and stabilizing effect on proteins during the freeze-drying, due to the hydrogen bonds that it can form with the protein. Therefore, its crystallization has a negative effect in terms of protein stability (Izutsu *et al.*, 1994). On the other hand, the mannitol crystallization gives mechanical support to the cake improving the thermal properties of the formulation and leading to a quality cake.

The physical state of the excipients on the pharmaceutical formulation not only depends on the composition of the formulation but also is a function of process conditions and the thermal history. For instance, the cooling rate in the freezing step can affect the physical state of the excipients, as well as the presence of an annealing stage on the process can modify the final physical state of the solutes.

The concomitant use of tools as Differential Scanning Calorimetry and Freeze-Drying microscope allows the determination of thermal properties as well as they can be used to: predict the physical state of the excipients under certain condition and to understand the effect of the different excipients on the formulation behavior (Rey and May, 2011).

The Differential Scanning Calorimetry is a powerful tool to identify the transformations that could happen in the product during the freeze-drying cycle, but not all the transitions impact in the same way on the structure of the final product, and not all the transitions cause the collapse of the structure (Kasraian *et al.*, 1998). For this reason, nowadays another tool is used to determine the collapse temperature of the product (i.e. the maximum temperature that the product could achieve during primary drying).

The freeze-drying microscopy is a useful technique, which allows the quick determination of the collapse temperature thanks to direct observations of the evolution of the system during the freeze-drying process.

2.1.1 Selection of Formulation Composition

Usually a freeze-dried protein formulation is formed by five principal components (Rey and May, 2011):

- **A stabilizer:** Commonly, amorphous excipients as polysaccharides are used to freeze-dried formulations in order to stabilize the protein against denaturation during the freezing and drying stages. The protein stability depends principally on the interaction by hydrogen bonds of the protein with stabilizers, such as polyol or sugars. Some of the most effective lyoprotectors are non-reducing disaccharides, as sucrose and trehalose (Carpenter *et al.*, 1997).
- **A bulking agent:** In the formulations, usually the API is present in low concentration ($\mu\text{g/ml}$); therefore, a bulking agent is added to increase the dry matter. The bulking agent also provides mechanical support to the cake. In order to obtain an elegant freeze-dried product, crystalline bulking agents as glycine and mannitol are widely used.
- **A nonionic surfactant:** During freezing, the proteins tend to be adsorbed at the ice water-interface, leading to the protein denaturation, therefore, surfactants are added to prevent the surface induced denaturation.
- **A buffer:** The buffer selected should not have an important pH shift during the freezing, some examples that fulfil this condition are: histidine, citrate buffer, and so on (Kasper and Friess, 2011).
- **Specific pH/ligands:** They are added with the aim of increase the thermodynamic stability of the protein.

A key factor in the design of a short and robust cycle is the definition of a formulation composition that fulfils operational constraints; this means a formulation with a high enough T_c and at the same time, a formulation that guarantees the protein stability during freeze-drying and storage.

A small variation in the concentration of one excipient can have an important effect on the thermal properties of the formulation and therefore, the effect of the different excipients in the formulation is an essential knowledge to design the process. In this context, the concentration of excipients that usually have negative effects on the thermal properties can be reduced or directly these excipients can be replaced for others that increase the T_c (Rey and May, 2011).

In the case of mixtures of amorphous components the glass transition temperature of the maximum concentrated phase T_g' is correlated with the T_g' of each component in aqueous solution. Fonseca *et al.* (2001) proposed a linear relationship to predict the T_g' of an amorphous mixture using the T_g' value of each excipient on aqueous solution Eq. (1):

$$T_g' = \frac{\sum_{i=1}^n C_i T_{gi}'}{\sum_{i=1}^n C_i} \quad (2.1)$$

Where T_{gi}' and C_i are the T_g' of the excipient and its solute concentration in aqueous solution, respectively.

The same relation could be done with the T_c of each component instead of the T_g' to determinate approximately the T_c of the mixture (Fonseca *et al.*, 2004). This support the argument about the non-desired effect of the presence of components with low T_g' and low T_c on the formulation.

Therefore, components with high T_g' have a positive effect on the formulation and their use is preferred rather than the use of components with low T_g' . For example, the use of polymers or polysaccharides with a relatively high T_g' , such as Dextran or PVP, improves the thermal properties of the formulation (Rey and May, 2011).

In the case of the presence of crystalline bulking agents, they present a complex physical behavior during the process. Their physical behavior depends on the thermal history of the formulation, the presence and the nature of the co-solutes and the concentration of the bulking agents (Kim *et al.*, 1998).

A number of studies have found that the presence of amorphous species (such as sucrose) could difficult the mannitol crystallization during freeze-drying. In addition, the presence of buffering salts reduces or inhibits mannitol crystallization (Al-Hussein *et al.*, 2012; Cavatur *et al.*, 2002; Izutsu *et al.*, 2007). The cooling rate in the freezing step has also an influence on the final physical state of the mannitol, as well as, the presence of an annealing step that favors the crystallization of mannitol.

The weight fraction of the bulking agent affects the degree of crystallization. Usually, the minimum weight fraction of crystalline solute that allows an extensive crystallization should be determined. Therefore, when a formulation development is performed, a relevant characteristic to evaluate is the degree of crystallization of the solutes.

The aim of this chapter is the development of a formulation using the Quality by design approach. In this context, in order to develop and improve a formulation in terms of its thermal characteristics, the following steps were performed:

- Potential pharmaceutical formulations were chosen in order to stabilize a API (in this case: LDH).

- For the sake of the determination of the collapse temperature and the optimization of primary drying, a thermal characterization of the formulations was done using powerful tools such as DSC and a freeze-drying microscope.
- A freeze-drying cycle was performed in order to assess visually the final freeze-dried product in terms of cake quality.

The success of a formulation design involves two different requirements: to guarantee the stability of the API during the cycle and obtaining a final product with a quality cake (i.e. without macroscopic collapse). In order to fulfil these two requirements, in the present work, different solutions of mannitol (as bulking agent) and sucrose (as lyoprotectant) in phosphate buffer were selected.

Mannitol shows optimal characteristics as bulking agent, it is inert, provide good cake supporting properties and has a high T_{eu} (-1.5°C). Usually, mannitol crystallizes readily, but its tendency to crystallize depends on the formulation composition and process parameters such as the freezing rate. On the other hand, sucrose forms an amorphous phase that stabilizes the protein during the process, interacting with the protein by hydrogen bonds.

An important problem that phosphate buffer presents is the remarkable pH shift that the system experiments during a freeze-drying cycle. In this buffer solution, a selective crystallization of the salts is present, and the basic disodium salt tends to precipitate first because it is less soluble and has a higher eutectic point compared with the monosodium salt. This leads to a pH decrease of 3 pH units or more (Bhatnagar *et al.*, 2007).

Therefore, different buffers are tested as alternatives in order to evaluate their effect on the physical state of the components and on the T_c of the formulation.

Alternatively, formulations with Dextran/mannitol and PVP/mannitol are evaluated, with the attempt of improving the thermal properties.

It is important to underline that one of the principal objectives on this chapter is to understand the effect of different components on the thermal characteristics of the formulation.

2.2 Materials and methods

2.2.1 Equipment and instrumentation

Freeze- Drying Microscopy

As it was previously discussed, the freeze-drying microscopy or cryo microscopy is a powerful tool widely used to acquire the necessary information for formulation development.

This technique has the advantage to operate with similar conditions (in terms of temperature and pressure) than a real freeze-drying cycle. During the analysis, the sample is freeze with a cooling rate (set for the user) and then is dried under vacuum, simulating in this way the first two steps of a freeze-drying cycle.

Different events on the formulation during freezing and drying can be evaluated for direct observation with a microscope through the process, for example, the FDM provide information about (Rey and May, 2011):

- The eutectic melting temperature (T_{eu}) of a formulation.
- The collapse temperature and the presence of micro-collapse in certain cases.
- Information about the formation of a crust or surface skin (in some cases).
- During the process, the nucleation of the sample can also be visualized. (but taking into account the stochastic nature of the nucleation, this value is not representative).

Freeze-drying microscopy is the only technique that allows determining the collapse temperature and crust formation. In the case of the crust formation, the phenomenon depends on the cooling rate and the temperature gradient (therefore, it could be the result of the FDM conditions itself), but it was reported that some formulations show higher tendency to form this surface skin than others (Rey and May, 2011).

During this experimental work, a Lyostat2 freeze-drying microscope was used. The system is composed by:

- A microscope (Olympus, BX51).
- A Freeze-drying stage (FDCS 196, linkam), formed by : a Vacuum pump, Pirani gauge, Liquid nitrogen cooling system, a programmable temperature controller and a digital.
- A FDM software, in this case the Linksys 32 (linkam, UK), that allows the control of the process and the evaluation of the data.

In Figure 2.3, can be seen a picture of the involved equipment in a FDM

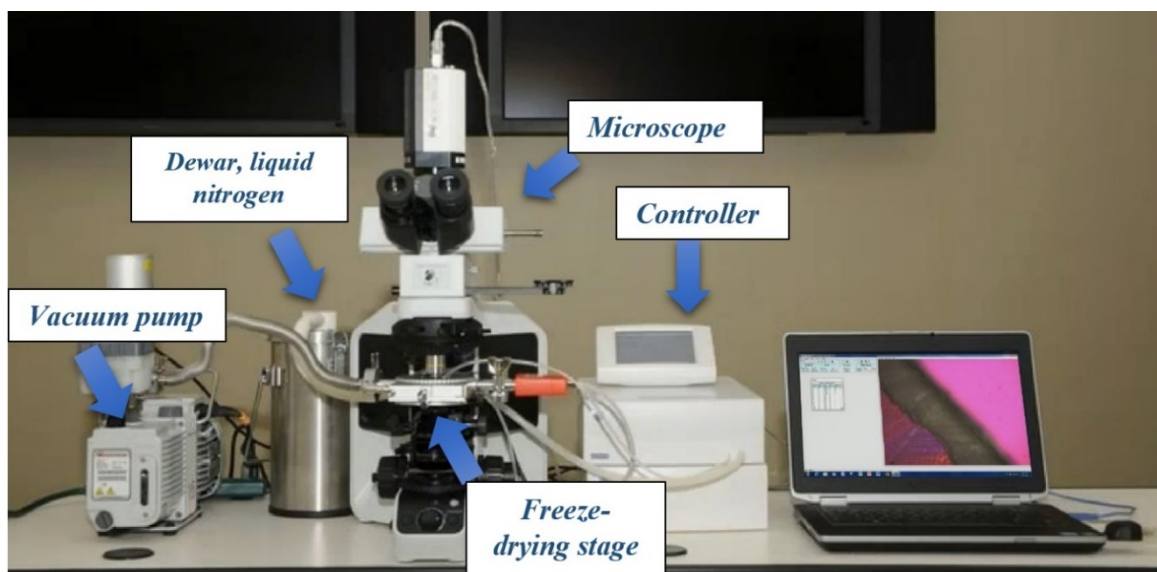


Figure 2.3: Picture of the equipment that involve a FDM. The principal components are shown with the blue arrows.

Differential Scanning Calorimetry (DSC)

The differential scanning calorimetry is one of the most frequently used techniques in thermo analysis, this thermo-analytical tool is used in order to test the behavior of materials and determine the different physical transformations of the sample in function of the temperature.

The technique consists in measuring the difference of heat flow rate between a reference sample and a real sample while both are under temperature-control. When the sample experiments a physical transformation, the necessary heat to keep the sample at the same temperature changes, therefore, the difference in the heat flow rate between the sample and the reference also changes (Höhne *et al.*, 2004).

The DSC is widely used in the pharmaceutical field for the thermal characterization of formulations. Some of the properties obtained are: the glass transition temperature of the maximum freeze-concentrate state (T_g'), the eutectic temperature (T_{eu}), crystallization temperature (T_{cr}), the degree of crystallization and so on. Between those, the T_g' represents one of the critical parameters on a formulation and it is related to the product collapse (Liu, 2006).

On the present work, a DSCQ200 was used to perform the tests.

Confront of the techniques: DSC vs. FDM

In the present study, it is important to underline the fact that the DSC and FDM techniques do not use the same operating conditions. The DSC measurements are performed at atmospheric pressure; therefore, during the process any drying occurs. On the other hand, on the FDM technique, once the freezing of the sample finished, the pressure will drop until a certain set point. There is a precise heat control system to supply the necessary heat for the sublimation. With this dynamic process is possible to determinate the collapse temperature (Meister and Gieseler, 2009).

Summarizing, the DSC is a static method, which allows measuring of physical transformations. However, it is important to consider that not all the transformations lead to a collapse; therefore, the FDM is used to determinate the T_c .

In Table 2.1, there is a resume of the difference between these two techniques. As it is showed the T_g' is not necessarily equal to the T_c and they are different properties.

Table 2.1. Differential scanning calorimetry and freeze-drying microscopy confront.

DSC	FDM
<ul style="list-style-type: none"> • Static phenomenon. The amorphous matrix is in contact with ice. • Simple method. • Measurement of physical transformation. In the present study, a focus on the T_g' is done. 	<ul style="list-style-type: none"> • Dynamic phenomenon; during the process the ice sublimation occurs under vacuum. • Extra costs. • Time and experience. • Measure of the T_c

2.2.2 Pharmaceutical formulations

The API considered in this work is lactate dehydrogenase, an enzyme widely used in the pharmaceutical field.

Combinations of Mannitol (as a bulking agent) and sucrose (as lyoprotectant) were prepared in different buffers solutions, with different weight ratios of mannitol to sucrose to analyze the effect of the excipient's concentration on the physical state of the components and on the formulations thermal characteristics.

Four different buffers were selected. One of the buffer solutions selected was phosphate buffer. It presents a good buffer capacity in the pH range of interest; but as previously mentioned, it has a tendency to produce a remarkable pH shift during the freeze-drying (Al-husseini and Gieseler, 2013). It has been reported that during the lyophilization of LDH in phosphate buffer the pH decreased from 7.5 to 4.5, leading to the denaturation of the protein (Anchordoqui and Carpenter, 1996). Therefore, Citrate/Acid Citric buffer and HEPES (4-(2-hydroxyethyl)-1-piperazineethanesulfonic acid) buffer are also selected as alternatives.

In an attempt to determine the effect that the buffer solution has on the formulation, experimental tests without buffer solutions are also performed.

Table 2.2, shows the detailed compositions of the different sucrose-mannitol formulations used in this study.

Table 2.2: A) Overview of mannitol/sucrose formulations used in different buffer solutions, (neutral pH). B) Different buffers solutions used in the work.

Sample name	Mannitol %(w/v)	Sucrose %(w/v)
5% S	0	5
2:3 %, M:S	2	3
3:2 %, M:S	3	2
4:1 %, M:S	4	1
5 % M	5	0

A)

BUFFER	PH
Phosphate Buffer, 50 mM	7.3
Citrate Buffer, 100 mM	7
HEPES Buffer, 50 mM	7.3

B)

Moreover, formulations with different ratios of mannitol to sucrose were prepared at acid pH (4-5.5) in citrate buffer. Table 2.3, shows the detailed composition of these formulations.

To evaluate the possible use of other excipients that could improve the thermal characteristics of the pharmaceutical formulation, solutions with different ratios of mannitol to PVP (Polyvinylpyrrolidone) and mannitol to dextran are analyzed. The studied samples are listed in Table 2.4.

Table 2.3: Overview of formulation compositions used in Citrate/Citric Acid buffer solution, (acid PH).

Sample name	Mannitol (mg)	Sucrose (mg)	EDTA Na ₂ (0,5 mM)	PH
<i>PL-E1 (M)</i>	500			4.5
<i>PL-E4 (M:S; 3:1)</i>		500		4.5
<i>PL-E3 (M:S, 1:1)</i>	250	250	SI	5.5
<i>PL-E5 (M:S; 1:3)</i>	375	125	SI	5.5
<i>PL-E2 (S)</i>	125	375		4.5

Table 2.4: Overview of the formulation composition with dextran and PVP.

Mannitol % (w/v)	Dextran % (w/v)	Buffer Solution
4	1	<i>Citrate Buffer (0.1 M) / Phosphate Buffer (0.05 M)</i>
2	3	
1	4	
Mannitol % (w/v)	PVP % (w/v)	
2	3	
1	4	

2.2.3 Thermal characterization

Differential scanning calorimetry

The tests were conducted using a DSCQ200. Different formulations were prepared and pipeted in Tzero-pans. To define the amount of sample introduced, the pans were weighted before and after the introduction of the solution.

The samples were cooled from room temperature to -80°C at 1°C/min. After, there were heated to 20 °C at 5°C/min. In the case of the formulations at acid pH, the cooling was performed at different cooling rates (0.5, 1 and 2 °C/min), in order to evaluate the effect of the process conditions on the behavior of the excipients.

Moreover, the pure buffer solutions were also analyzed with the same protocol of the formulations.

Freezing Drying Microscope

In order to determine the collapse temperature, the freeze-drying microscope “BX51” was used.

The system has a high-vacuum cold stage, a software to control the process conditions and to evaluate the data obtained (Linksys 32, Linkam) and a nikon optical microscope.

Approximately, 2 μl of the sample was placed on a glass coverslip, then a Spacer and another glass coverslip were collocated on the sample. The structure of the sample as a thin layer between the two coverslips assure the minimization of the heat input to the sample by convection. About 5 μl of silicon oil were put between the temperature-controlled block (silver block) and the quartz coverslip, in order to get a better thermal contact. The spacer ensures the presence of a constant thickness of the sample layer. In Figure 2.4, there is a schematization of the sample format used.

The cold stage consists in cooling the sample from room temperature to $-60\text{ }^{\circ}\text{C}$ at $1^{\circ}\text{C}/\text{min}$. The sample is held at this temperature for 10 min and then the pressure is dropped until 10 Pa. The sample is heated with a heating rate of $1\text{ }^{\circ}\text{C}/\text{min}$ until the collapse of the structure is observed. During the process, pictures of the system were taken in intervals of 3 seconds and then they were analyzed with the software Linksys 32.

To determine effectively the temperature at which the collapse occurs and to minimize the subjectivity of the user, in the present work we adopted the same criteria described for Meister and Gieseler (2009), so, three levels of structure loss are defined.

Figure 2.5 shows pictures taken on the FDM representing the different levels of structure loss.

The onset of collapse (T_{oc}) is defined as the point where the first structural changes are observed in the dried phase next to the sublimation interphase (e.g. fissures and small holes). When the dried product next to the sublimation front forms a no coherent product layer anymore, the full collapse occurs (T_{fc}) and a severe structural loss, huge holes and fissures characterize it. (Meister and Gieseler ,2009).

On the midpoint collapse T_{c-50} , due to the elevated viscous flow, there are many holes on the dried product but the structure is still looking dense and coherent. In the present work, the T_{c-50} is calculated as the average of the T_{oc} and T_{fc} . This value is important in order to compare the collapse temperature with the T_g' , because usually the T_g' is reported as the midpoint and not as the onset of the glass transition.

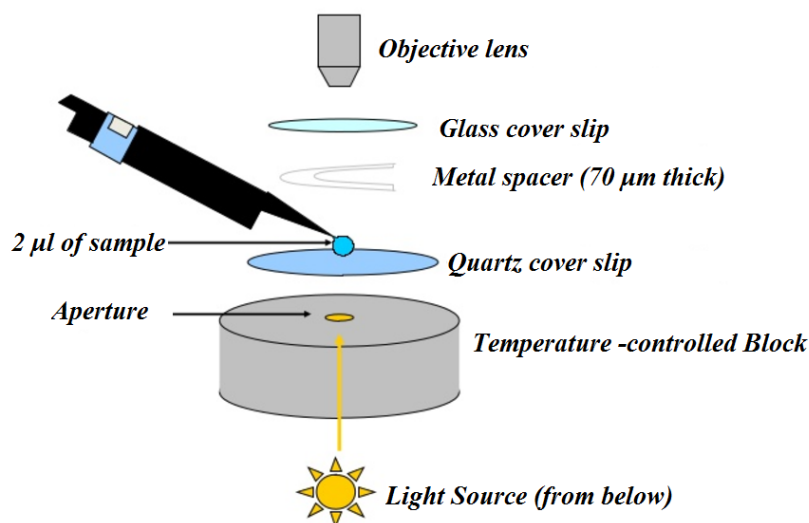


Figure 2.4: Sample format used on a FDM Lyostat2 (Biopharma Technology, Limited, Winchester, U.K, with modifications).

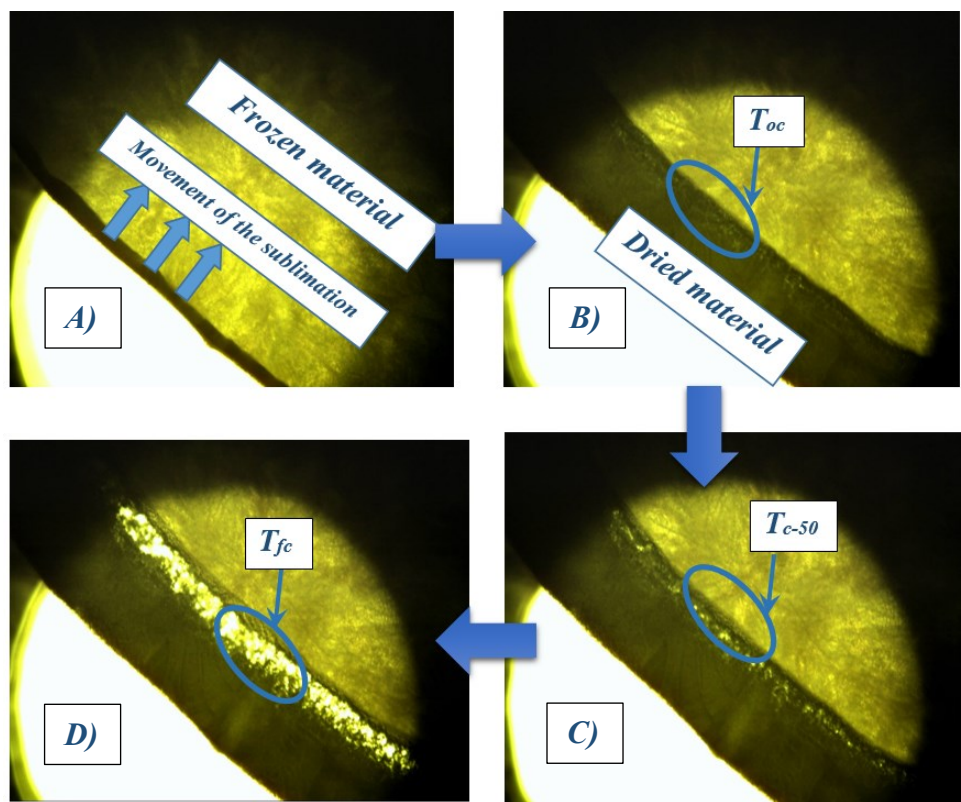


Figure 2.5: Illustration of the criteria chosen to identify the different levels of collapse on the product structure A) Movements of the sublimation front B) Onset Collapse (T_{oc}) C) Midpoint collapse T_{c-50} . D) Full collapse (T_{fc}).

2.2.4 Freeze-Drying Cycle

Freeze-drying experiments were performed using a lyoBeta 25 (Teslar, Terresa, Spain).

Six formulations previously analyzed were selected to develop a freeze-drying cycle. 3 ml of the formulations were pipetted into each vial. The samples were loaded into the chamber at room temperature, with a hexagonal arrange and then cooled to -55°C at $0.5^{\circ}\text{C}/\text{min}$. The primary drying was conducted at -30°C for 60 hours; this temperature was selected considering the collapse temperature of the studied formulations, which were defined by the analysis with the freeze-drying microscope. The secondary drying was performed at 20°C .

As we can note in this cycle, conservative conditions are used to obtain an elegant product and avoid the collapse of the freeze-dried products.

The details of the process conditions are reported in Table 2.5.

Table 2.5: Process conditions during the freeze-drying cycle

Process Conditions				
	T (°C)	Rate (°C/min)	Hold Time (h)	P (Pa)
	20		0.17	
Freezing	-55	-0.55	5	
Primary drying	-30	0.76	60	10
Secondary drying	20	0.09	10	3

In order to study only the effect of the T_{shelf} during the primary drying on the cake structure, it is important to assure that no collapse will occur during the next step of the process. In other words, it is necessary to guarantee that during secondary drying no loss of structure will occur. With this in mind, the following process conditions were defined:

- A slow heating rate to go from the T_{shelf} in primary drying to the T_{shelf} in secondary. As it was mentioned in chapter 1, this is a very important in order to avoid the collapse during this step.
- The duration of the primary drying must be high enough in order to guarantee the complete sublimation of the ice before to pass to secondary drying. Increasing the shelf temperature for secondary drying can cause collapse or eutectic melting if the ice is not completely removed first (Patel *et al.*, 2010).

Moreover, the end of the primary step was monitoring through:

- Comparative pressure measurements: Pirani and Baratron sensors measured the pressure of the system. Baratron sensor measured the absolute pressure inside the chamber and Pirani sensor measured the relative pressure based on the thermal conductivity of the gas.
- The product temperature during the freeze-drying cycle.

The product temperature was measured with four calibrated thermocouples in direct contact with the bottom of the vial. Each thermocouple was introduced in different formulations in a vial positioned on the middle section of the shelf and not on the edge. The vials on the edge of the shelf usually present a higher K_v compared with the vials on the middle; this is due to the radiation contribution coming from the chamber's walls. As consequence, the edge vials present a smaller drying time, which is not representative for the other vials on the batch (Pisano *et al.*, 2012).

The monitoring of the temperature at the base of the product also gives an idea about the temperatures that the product experiment during the process, this information is important during primary drying.

2.3 Results and discussion

2.3.1 Thermal characterization

2.3.1.1 Formulations Sucrose-Mannitol

Formulations with Phosphate Buffer (pH=7.3)

Figure 2.6 shows an example of the appearance of the sublimation front through the process for the sample 3:2 (% w/v) M:S. The pictures were obtained with the FDM at different temperatures.

As the pictures show, the sublimation front starts from the edge of the drop to the center. When the temperature reaches the T_{oc} (-38°C), little holes and a slight change in the dried matrix adjacent to the sublimation interface occurred. At T_{c-50} (-36.7°C) the dried matrix present holes due to the high viscous flow, but the dried matrix is still coherent. When the formulation reaches T_{fc} (-35.5°C), the sublimation front does not form a coherent product layer anymore.

Usually, the DSC thermographs obtained using formulations with crystalline bulking agents, present complex combination of different transformations which depends on the concentration of the different components in the formulation and the process conditions.

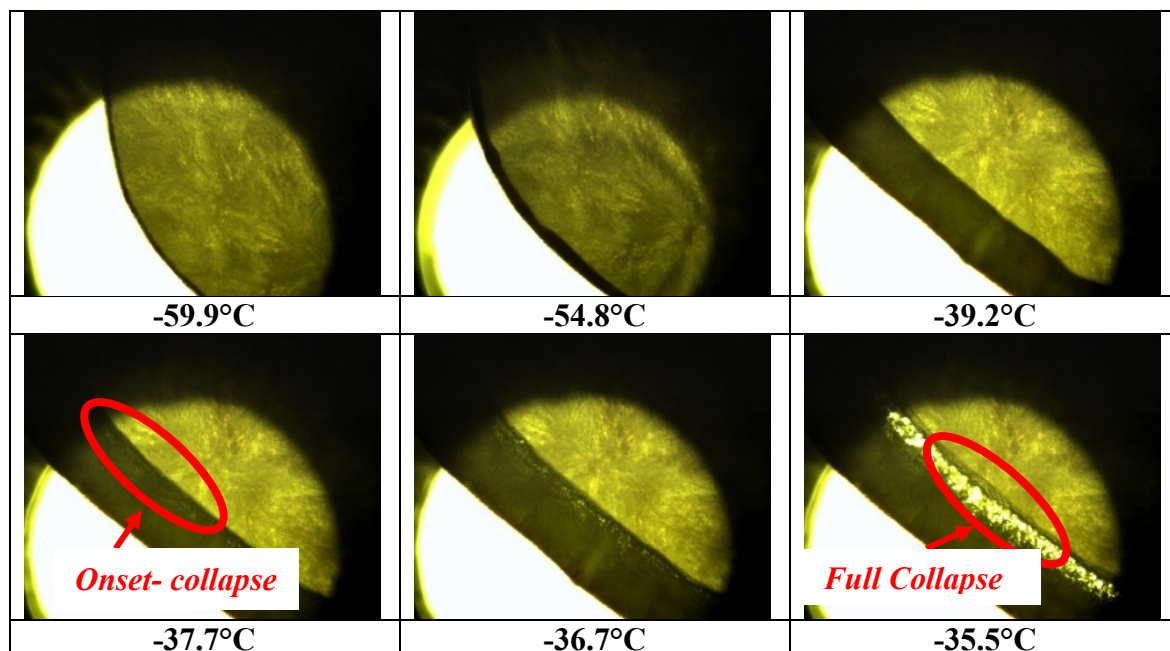


Figure 2.6: Advance of the sublimation front of sample 3:2 (% w/v), MS

In Table 2.6, are reported the results obtained with the DSC and the FDM analysis for different combinations of mannitol and sucrose in phosphate buffer at a pH of 7.3.

In the case of the characteristic glass transition temperatures (T_{g1}' and T_{g2}'), T_{g2}' represents the highest glass transition temperature of the maximal freeze-concentrate state.

Table 2.6: Thermal transitions revealed in the DSC warming thermographs and the collapse temperature determined with the FDM, for combinations of mannitol and sucrose in phosphate buffer at pH of 7.3. ΔT represents the difference between T_{c-50} and T_{g2}'

PHOSPHATE BUFFER (0.05 M)							
Sample	T_{g1}' (°C)	T_{g2}' (°C)	T peak exotherm (°C)	T_{oc} (°C)	T_{c-50} (°C)	T_{fc} (°C)	ΔT (°C)
5% S	-43.06	-33.09	-	-31.8	-31.3	-30.8	1.8
2:3 %, M:S	-47.35	-36.64	-	-37	-36.5	-36	0.1
3:2 %, M:S	-48.98	-38.61	-17.18	-38	-36.8	-35.5	1.9
4:1 %, M:S	-48.95	-39.32	-21.6	-35.2	-34.8	-34.3	4.6
5 % M	-49.49	-40.5	-22.60 ; -9.73	-	-	-	-

The phosphate buffer (alone) shows a flat thermogram in the heating stage.

The DSC warming thermographs with different ratios of mannitol to sucrose in phosphate buffer are represented in Figure 2.7.

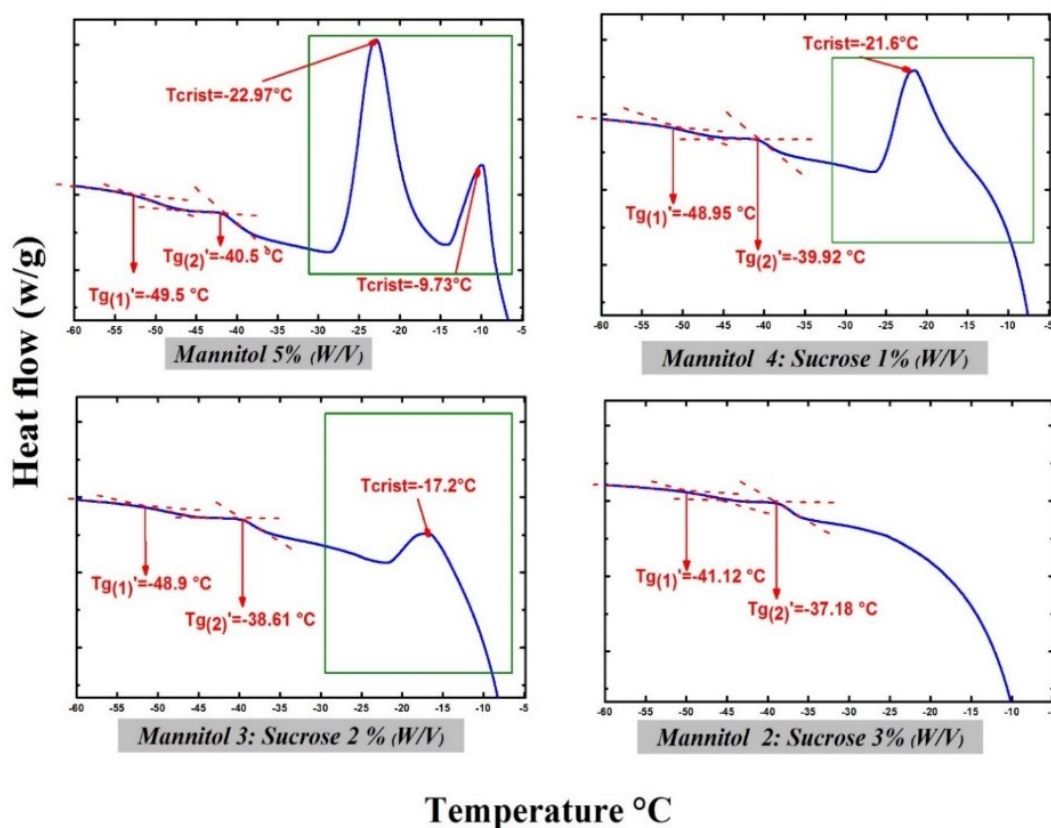


Figure 2.7: DSC warming thermographs of formulations with different ratios of mannitol to sucrose (a zoom of the different thermal transformations)

As it is shown in Table 2.6, all the formulations show two glass transition events and in the case of the formulations with a higher amount of mannitol than sucrose, the glass transition is followed by an exothermal crystallization event. Then an endotherm peak is presented in all the thermograms attributed to the overlapping of eutectic and ice melting phenomena (this event is not shown in Figure 2.7).

The fact that all the thermograms showed a glass-transition temperature T_g' indicates the presence of an amorphous phase.

The T_{g1}' value of the formulations containing both sucrose and mannitol is between the T_{g1}' of the formulations with only the individual components (-43.06 °C, sucrose and -49.49 °C, mannitol). T_{g2}' presents the same behavior.

It is important to note that the glass transition of the mixture of mannitol and sucrose in phosphate buffer is lower than the T_g' of amorphous mannitol (-32°C) or sucrose (-33°C) in aqueous solution. This could be attributed to the presence of buffering salts that usually act as plasticizers giving rise to a shift of the T_g' (Rey and May, 2011).

Moreover, the mixture mannitol-sucrose has also an effect on the T_g' . The T_g' in the case of aqueous solutions of mannitol and sucrose is also lower than the individuals T_g' temperatures of each component in aqueous solution (-32 or -33 C°). Pyne *et al.* (2002) explain this behavior as a consequence of the higher concentration of unfrozen water in the solution of mannitol and sucrose compared with the solutions with only the individual components.

It is also relevant to underline the fact that only the formulations containing a superior concentration of mannitol (than sucrose) exhibit an exothermal peak related with the mannitol crystallization. The formulations that have a higher percent of sucrose than mannitol did not show exothermal peaks, this fact may indicate that mannitol apparently remains in the amorphous phase and the crystallization is inhibited also during the heating.

Several studies reveal that the use of amorphous co-solutes has an inhibitory effect on the mannitol crystallization and this effect increases with the amount of amorphous co-solutes; in this work case, it is referred to the amount of sucrose in the solution (Al-Hussein and Gieseler, 2012; Johnson *et al.*, 2002).

The thermogram of the formulation with only mannitol in phosphate buffer showed a glass transition. Usually, mannitol crystallizes readily, but the presence of the sodium phosphate dibasic and monobasic (phosphate buffer) avoid the complete crystallization of mannitol in frozen solutions (Cavatur *et al.*, 2002; Izutsu *et al.*, 2007).

The degree of mannitol crystallization has an effect on the collapse temperature. Often, the crystallization of the bulking agent provides mechanical support to the cake, increasing the collapse temperature.

In the present case, the collapse temperature decreased with the increasing of mannitol concentration; this happened until the mannitol concentration was at least higher than the sucrose concentration, so, in that moment the mannitol crystallization was not totally inhibited. In addition, we noted that the addition of mannitol to sucrose formulations gave rise to a decreasing in the glass-transition temperature.

The Figure 2.8, shows the effect of the mannitol concentration on the glass transition-temperature and the collapse temperature.

As it was reported in Table 2.6, and it is showed in Figure 2.8, the collapse temperature was 1 to 5 °C higher than the glass transition temperature associated with the collapse.

In the case of the sample of 5 % (w/v) mannitol at $-21.5\text{ }^{\circ}\text{C}$, a change in the sublimation front appeared, this could be associated with a phase change which corresponds with one of the exothermal peaks at $-22.97\text{ }^{\circ}\text{C}$. At first glance, this change was similar to the onset collapse on the structure, but when the temperature increased, the dried layer kept growing forming a homogenous layer without a full collapse.

In Figure 2.9, the evolution of the sublimation front for this specific formulation is showed.

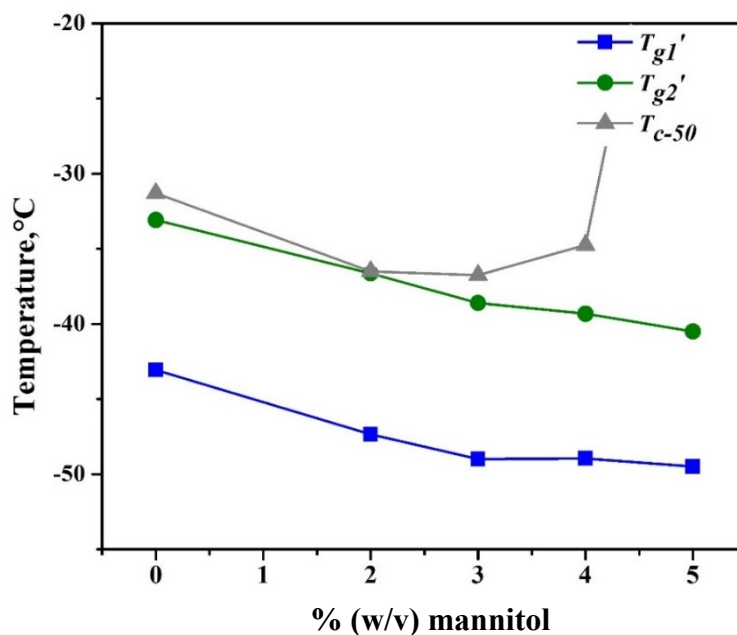


Figure 2.8: Variation of the glass transition temperature and the collapse temperature with the increase of mannitol concentration in formulations with sucrose. The total amount of solid is 5% (w/v)

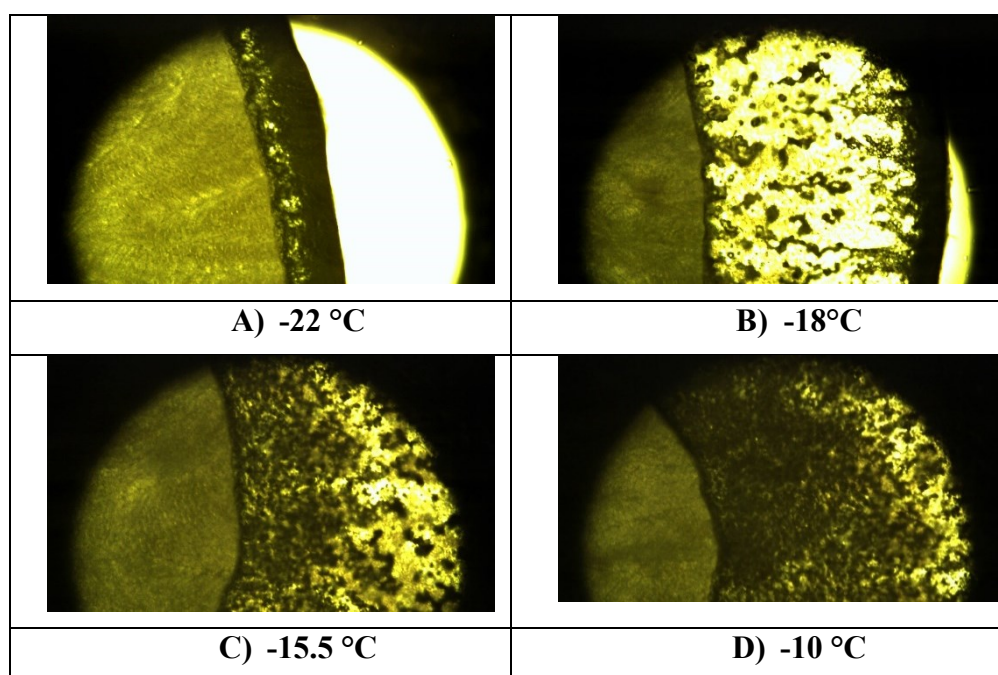


Figure 2.9: Advance of the sublimation front of sample 5 (% w/v), M.

Formulations with Citrate Buffer (pH=7.3)

Figure 2.10, shows warming thermograms of solutions containing different concentrations of sucrose-mannitol in citrate buffer.

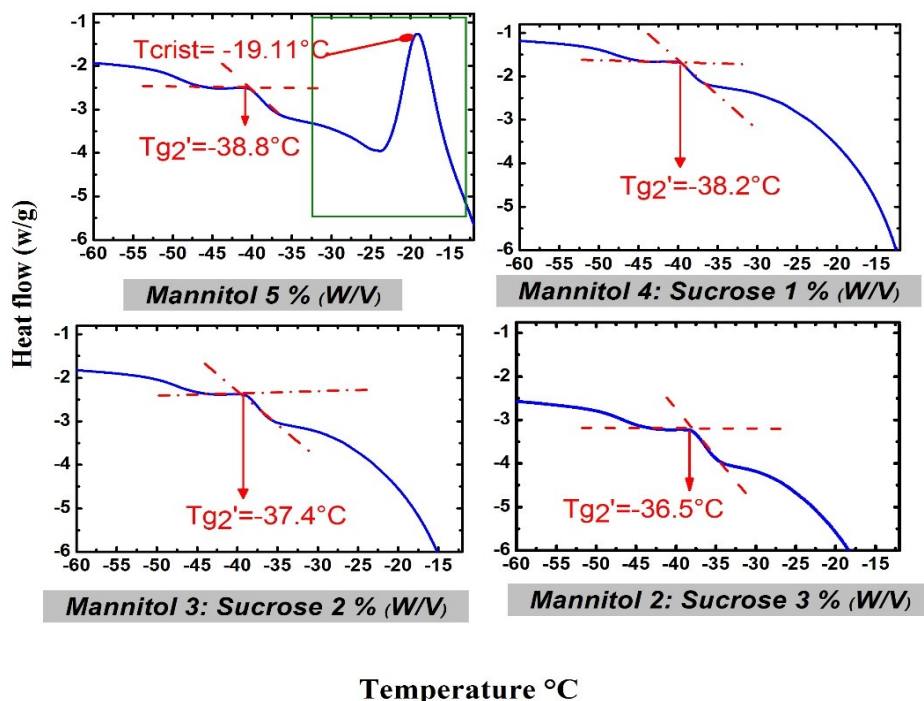


Figure 2.10: DSC warming thermograms of formulations with different ratios of mannitol to sucrose (a zoom of the different thermal transformations)

The thermogram of Citric Acid /Citrate buffer, in contrast to the phosphate buffer, reveals a glass-transition at -42.7°C and -49.5°C (data is not showed), which correspond with the literature (Izutsu *et al.*, 2007).

All the thermograms reveal two glass transition temperatures, T_{g1}' and T_{g2}' , that are lower than the T_g' of amorphous mannitol (-32°C) or sucrose (-33°C) on aqueous solution. As in the case of the formulations with phosphate buffer, this could be explained taking into account the presence of buffering salts and the effect of mixing sucrose with mannitol.

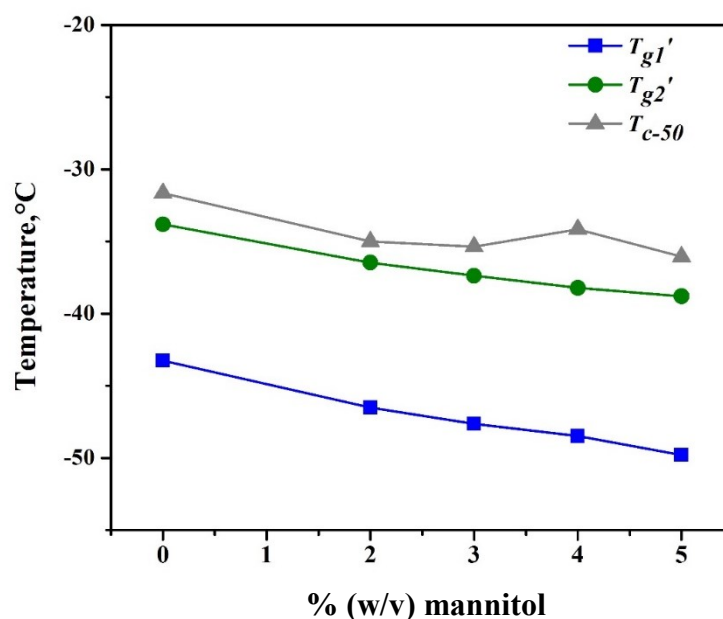
In this case, only the sample of pure mannitol on citrate buffer (without sucrose) presents an exothermal peak, indicating that the effect of citrate buffer and sucrose together probably inhibit completely the mannitol crystallization.

In Table 2.7, are reported all the thermal transitions and the collapse temperature of this group of formulations.

The effect of the mannitol concentration on the glass-transition temperature and the collapse temperature is showed on the Figure 2.11, in all the formulations the total amount of solid in the solution is 5 % w/v.

Table 2.7: Thermal transitions revealed on the DSC warming thermographs and the collapse temperature determined with the freeze-drying microscope.

<i>CITRATE BUFFER (0.1 M)</i>							
Sample	T_{gl}' (°C)	T_{g2}' (°C)	T peak exotherm (°C)	T_{oc} (°C)	T_{c-50} (°C)	T_{fc} (°C)	ΔT (°C)
5% S	-43.26	-33.81	-	-32.4	-31.65	-30.9	2.16
2:3 %, M:S	-46.51	-36.46	-	-36	-35	-34	1.46
3:2 %, M:S	-47.64	-37.37	-	-36.3	-35.35	-34.4	2.02
4:1 %, M:S	-48.47	-38.21	-	-34.5	-34.15	-33.8	4.06
5 % M	-49.8	-38.79	-19.1	-36.7	-36.05	-35.4	2.74

**Figure 2.11:** Variation of the glass transition temperature and the collapse temperature with the increase of mannitol concentration in formulations with sucrose. The total amount of solid is 5% (w/v)

The collapse temperature is between 2 and 4.5 °C higher than the glass transition temperature T_{g2}' .

We noted that the addition of mannitol to sucrose formulations gave rise to a decrease in the glass-transition temperature and collapse temperature. The fact that the collapse temperature did not improve with the addition of mannitol could be related to the inhibition of mannitol crystallization. The introduction of an annealing step could increase the degree of mannitol crystallization and increase the collapse temperature due to the structural support of the crystalline mannitol.

Izutsu *et al.* (2007) have reported that the phosphates and citrates salts prevent the crystallization of mannitol in frozen solutions and freeze-dried solids.

As previously was explained, the thermal history has also an influence on the physical state of the components, in special when crystalline bulking agents are involved.

In order to see the effect of the cooling rate used on the FDM, tests with a slower cooling rate were developed. The sample 4:1 %, M:S and 5 %, M were assessed with two different cooling rates: 1°C/min and 0.5°C/min. The results are not significantly different and no variations on the collapse temperature were found.

On the case of 5% S, a formation of a surface skin was observed during the FDM test.

Formulation with Citrate Buffer (pH=4.5 - 5.5)

The results of the DSC analysis and the collapse temperatures determined with the freeze-drying microscope are reported in Table 2.8.

Table 2.8: Thermal transitions revealed on the DSC warming thermographs and the collapse temperature determined with the freeze-drying microscope.

<i>CITRATE BUFFER (0.1 M) PH= 4.5-5.5</i>								
Sample name	Mannitol (mg)	Sucrose (mg)	T_{g1}' (°C)	T_{g2}' (°C)	T peak exotherm (°C)	T_{oc} (°C)	T_{c-50} (°C)	T_{fc} (°C)
<i>PL-E1 (M)</i>	500	0	-48.93	-40	-16.79	-39.3	-37.2	-35.0
<i>PL-E4 (M:S; 3:1)</i>	375	125	-47.13	-38.9	-	-35.6	-34.8	-33.9
<i>PL-E3 (M:S, 1:1)*</i>	250	250	-46.3	-36.5	-	-34.4	-33.8	-33.2
<i>PL-E5 (M:S; 1:3)*</i>	125	375	-45.53	-36.3	-	-36.1	-35.0	-33.9
<i>PL-E2 (S)</i>	0	500	-41.86	-34	-	-32.0	-31.0	-30.0

*As previously indicated, Samples PL-E3 and PL-E5, have EDTA Na₂ (0.5 mM) and a pH= 5.5 instead of 4,5 like the other samples

As previously specified, in the case of the formulations at acid pH, the cooling stage of the DSC analysis was performed at different cooling rates (0.5, 1 and 2 °C/min), the results of the DSC analysis at different cooling rates did not show significant changes.

The Figure 2.12, illustrates the effect of the mannitol concentration on the glass transition temperature and the collapse temperature.

In the case of the samples PL-E1, PL-E2 and PL-E5 was observed a crust formation.

Through the freezing, a layer of concentrated solute is forced to the edge of the sample, giving rise to this surface skin. The crust difficults the vapor flow and therefore, difficults the drying, leading to a sublimation front that is not parallel with the sample edge.

As previously mentioned, the crust formation depends on the cooling rate and the temperature gradient and in this case could be a result of the FDM conditions, but these formulations exhibited a higher tendency to show this phenomenon.

In Figure 2.13, it is shown a picture of a formulation that has formed this surface skin. The black line in A) at the edge of the drop is the concentrated layer that during drying difficults the vapor flow. When the rupture of the surface skin occurs the sublimation front starts to advance from this point, leading to a not parallel sublimation interface.

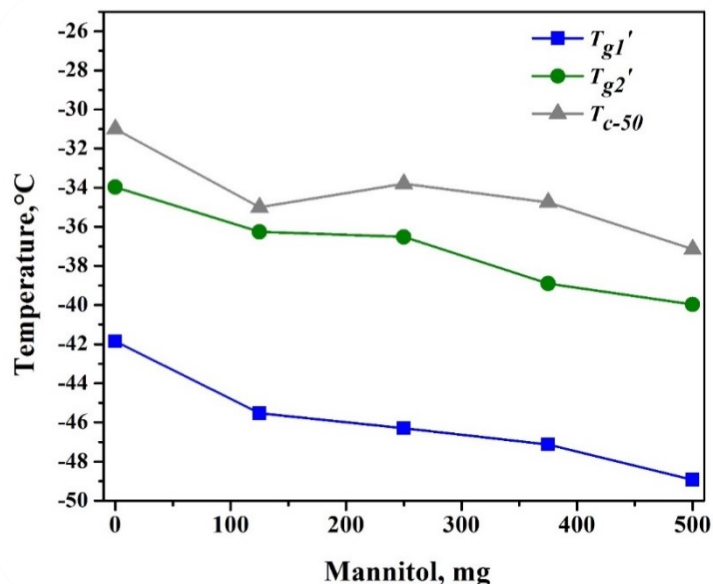


Figure 2.12: Variation of the glass transition temperature and the collapse temperature with the increasing of mannitol concentration in formulations with sucrose. The total amount of solid is 500 mg/ml.

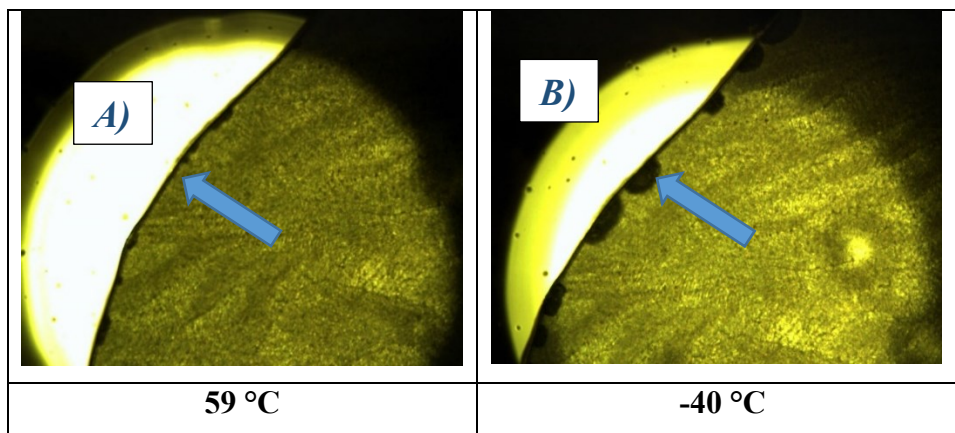


Figure 2.13: Formulation showing crust formation (PL-E1). A) The black line on the surface is the concentrate band that inhibit the drying sample immediately after the drying has started. B) In the sections in which the crust breaks the sublimation interface advance.

Formulations with HEPES Buffer (pH=7.3)

In Table 2.9, are informed all the transitions revealed in the DSC warming thermogram and the collapse temperature for different formulations.

Figure 2.14, shows the warming thermograms of solutions containing different concentrations of sucrose-mannitol on HEPES Buffer.

All the solutions presented glass transition temperatures and only the formulations that had a higher mannitol concentration than sucrose showed exothermal peaks related with the mannitol crystallization. Moreover, as the amount of sucrose increased, the exothermal event was shifted to a higher temperature and the peak was less pronounced. This fact shows the effect of sucrose concentration on mannitol crystallization; as higher the amount of sucrose is, the mannitol crystallization is more difficult.

Figure 2.15, shows the relationship between the mannitol concentration, the glass-transition temperature and the collapse temperature.

It was observed that higher concentrations of mannitol were correlated with lower glass-transition temperatures; this fact happened only with the solutions that contained also sucrose as a co-solute and the solution with only mannitol presented the highest glass-transition temperature of this group of formulations. The collapse temperature showed the same tendency of T_g ; it decreased with the increasing of mannitol concentration, but the formulation of mannitol without sucrose showed the highest temperature. In the case of the sample of 5 % (w/v) mannitol, the sublimation front showed micro-collapses from a low temperature (-37°C). But the advance of the sublimation front continues without total collapse until -14.4°C .

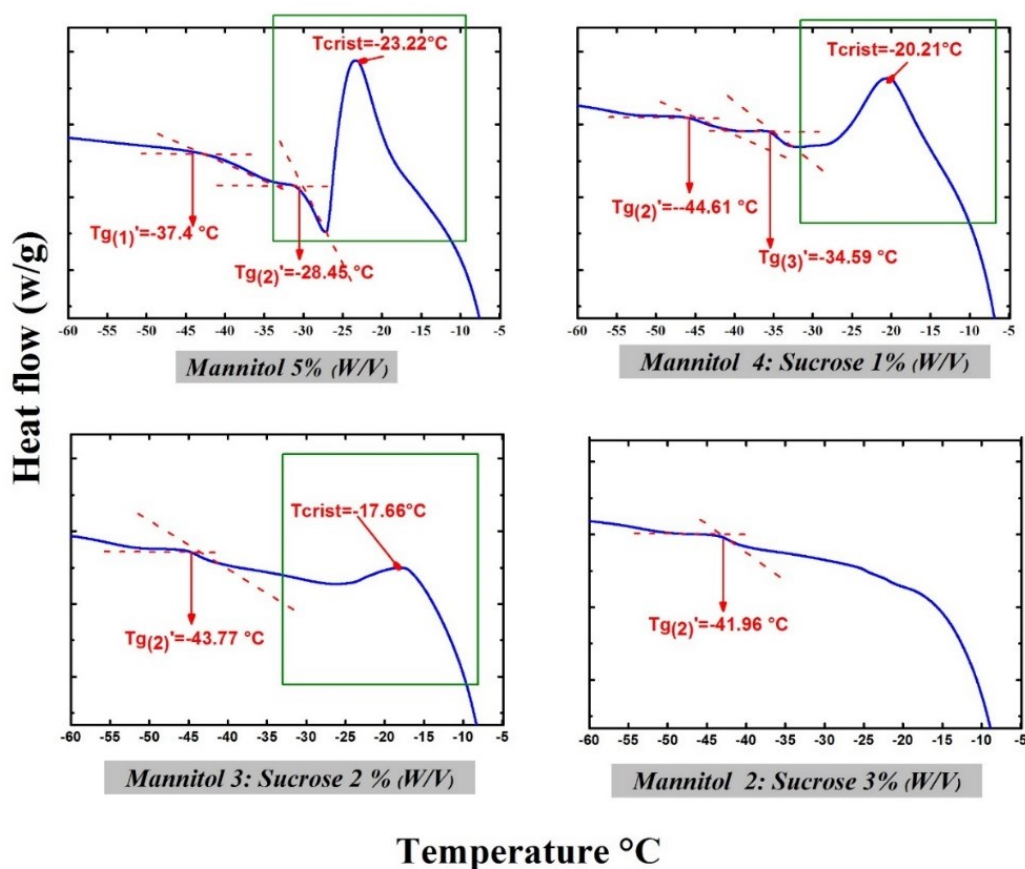
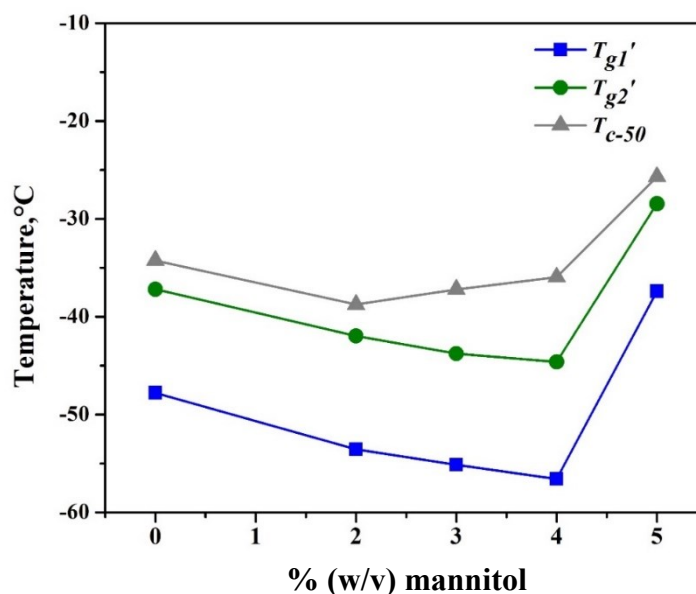


Figure 2.14: DSC warming thermograms of formulations with different ratios of mannitol to sucrose on HEPES buffer (a zoom of the different thermal transformations).

Table 2.9: Thermal transitions revealed on the DSC warming thermographs and the collapse temperature determined with the freeze-drying microscope.

HEPES BUFFER (0.05 M)								
Sample	T _{g1'} (°C)	T _{g2'} (°C)	T _{g3'} (°C)	T peak exotherm (°C)	T _{oc} (°C)	T _{c-50} (°C)	T _{fc} (°C)	ΔT (°C)
5% S	-47.77	-37.19		-	-35	-34.25	-33.5	2.94
2:3 %, M:S	-53.54	-41.96		-	-39.5	-38.75	-38	3.21
3:2 %, M:S	-55.14	-43.77		-17.66	-37.6	-37.2	-36.8	6.57
4:1 %, M:S	-56.57	-44.61	-34.59	-20.21	-37	-35.95	-34.9	-
5 % M	-37.4	-28.45		-23.22	-37	-25.7	-14.4	2.75

**Figure 2.15:** Variation of the glass transition temperature and the collapse temperature with the increase of mannitol concentration in formulations with sucrose. The total amount of solid is 5% (w/v)

Formulations without Buffer

In order to determine the effect of the buffer solution on the formulations, two different aqueous solutions of sucrose-mannitol were tested. The results are shown in the Table 2.10.

Table 2.10: Thermal transformations revealed on the DSC warming thermographs and the collapse temperature determined with the freeze-drying microscope.

WITHOUT BUFFER				
Sample	T _{g1'} (°C)	T _{g2'} (°C)	T peak exotherm (°C)	T _{oc} (°C)
2:3 %, M:S	-54.5	-39.46	-18.79	-36.7
4:1 %, M:S		-32.6	-27.96; -23.17	-10.0

The T_g' in the case of sample 2:3% M:S was lower than the T_g' of amorphous mannitol (-32°C) or sucrose (-33°C) in aqueous solution.

It is relevant to note that the onset of collapse has an important increasing (from -37 to -10 °C) when the mannitol concentration became higher than the amount of sucrose. In fact, it has been reported that in order to obtain a degree of mannitol crystallization, its concentration should be higher or at least equal than sucrose concentration otherwise, the mannitol will not crystallize (Johnson *et al.*, 2002).

Confront

The collapse temperature of sample 4:1 %, M:S and 2:3% ,M:S in different buffer solutions is represented in the Figure 2.16.

In the case of sample 4:1%,M:S, the collapse temperature had an important decrease when there is no buffer in the formulation. This fact confirms the inhibitory effect of buffering salts on the mannitol crystallization.

The presence of an amount of mannitol in crystalline form gives mechanical support to the cake while the amorphous phase stabilizes the protein. However, as was explained previously, it is necessary a minimum mannitol concentration in order to allow its crystallization.

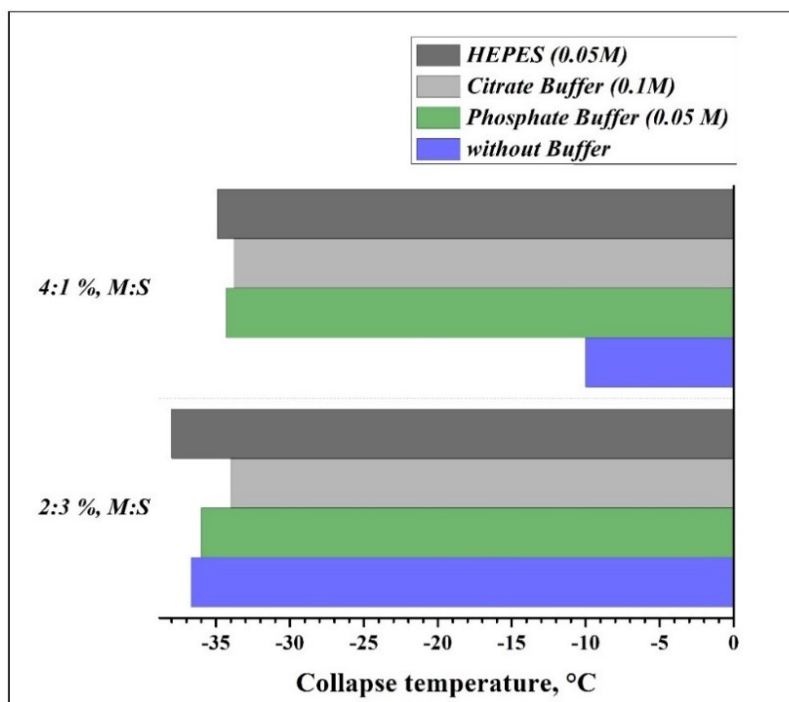


Figure 2.16: Collapse temperature of sample 4:1 %, M:S and 2:3 % M:S, in different buffer solutions.

In the case of the formulation of 2:3 %, M:S, the amount of mannitol was not high enough and the sucrose inhibited its crystallization, leading to a low collapse temperature even in the aqueous solution.

Figure 2.17 illustrates the effect of mannitol concentration on the collapse temperature for formulations in different buffer solutions. The solution in citrate buffer presented the higher collapse temperature in the range of 0 to 4 % (w/v) of mannitol concentration.

On all the cases, the collapse temperature decreased with the amount of mannitol, until the mannitol concentration was higher than the sucrose concentration, in this case, the T_c increased with the amount of mannitol. Therefore, a key parameter to determine on the formulation development is the concentration of the different components.

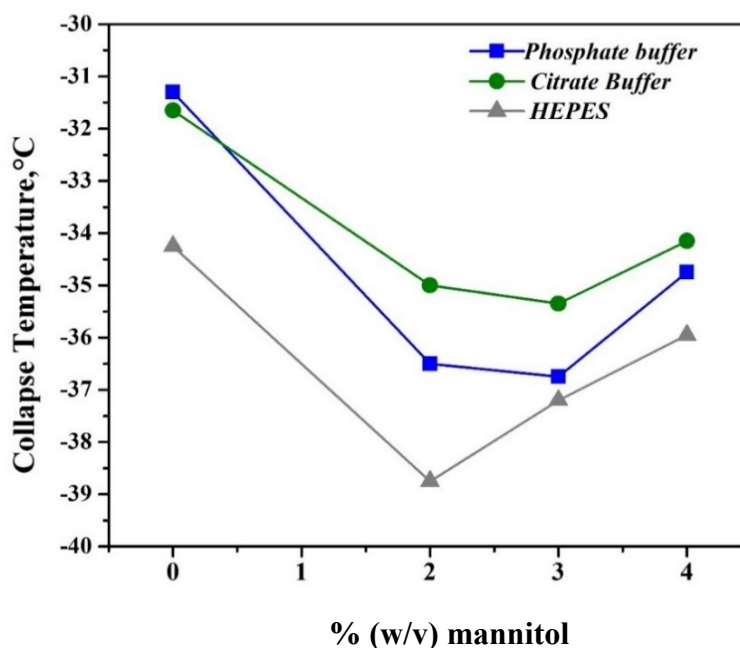


Figure 2.17: Variation of the collapse temperature with the increase of mannitol concentration in formulations with sucrose on different buffer solutions. The total amount of solid is 5% (w/v).

In the Figure 2.18, are shown the warming thermograms of the sample containing 4 % (w/v) mannitol and 1 % (w/v) sucrose in different buffer solutions.

As we can note the sample 4:1 % M:S on aqueous solution showed two exothermal peaks; the sample on phosphate buffer and HEPES showed one exothermal peak and the sample on citrate buffer did not show any exothermal transformation. Moreover, the exothermal event was shifted to a higher temperature when phosphate buffer and HEPES were present.

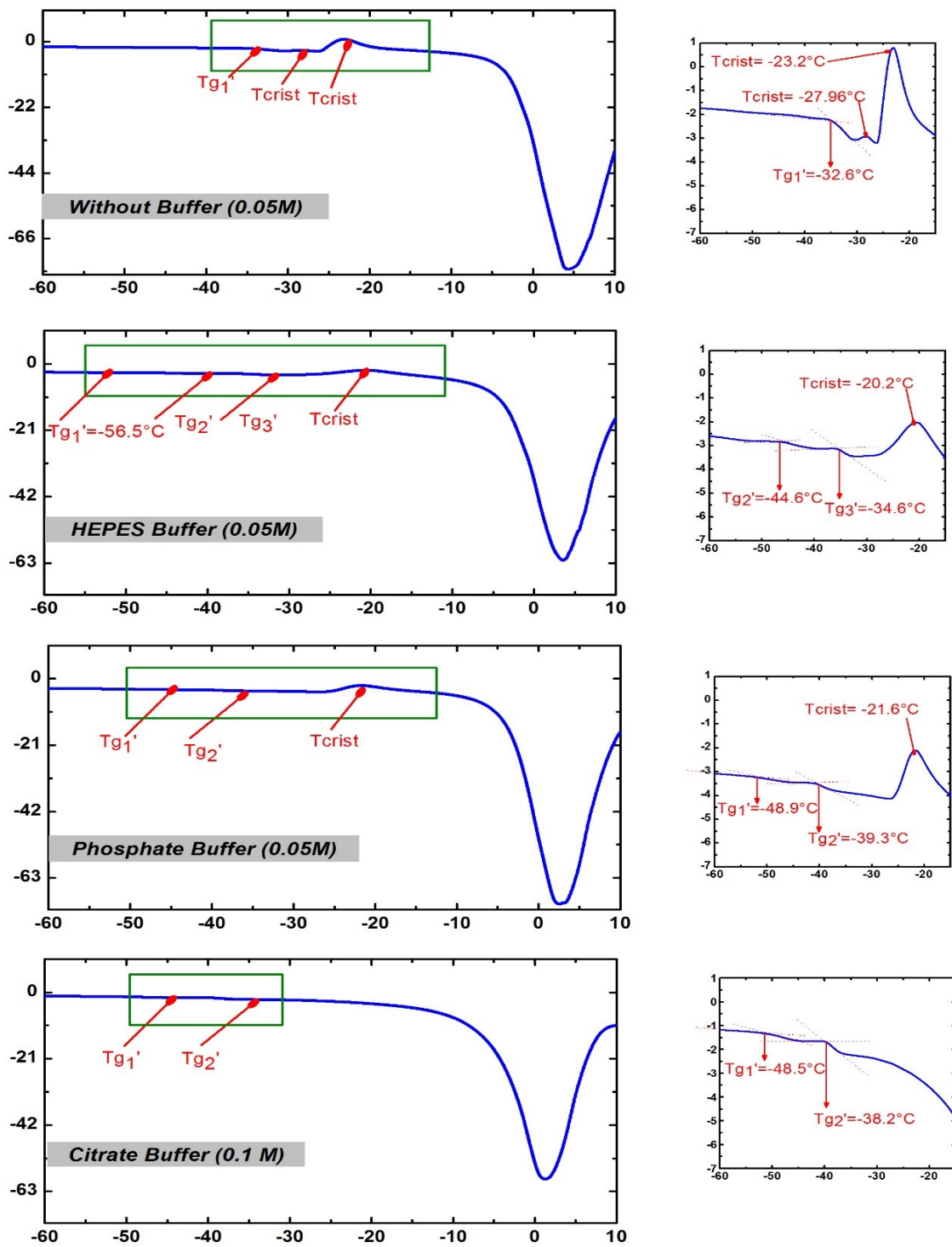


Figure 2.18: DSC warming thermograms of sample 4:1 % (w/w), M:S in different buffer solutions.

2.3.1.2 Formulations PVP/Dextran – Mannitol

Dextran-Mannitol

Formulation dextran-mannitol were assessed in order to evaluate the effect of the excipients on the thermal properties.

The results of the DSC analysis and the collapse temperatures determined with the freeze-drying microscope for formulations dextran-mannitol in different buffers solutions are reported in the Table 2.11.

As the table shows, there is an improvement on the collapse temperature with the use of dextran and compared with the formulation of mannitol-sucrose the T_{c-50} is higher.

The use of polysaccharides as dextran ($T_g'=10$), made possible increasing the maximum temperature value during primary drying. This represents an important advantage in terms of primary drying time. On the other hand, it has been reported that dextran could fail to protect proteins because it forms a separate phase from the protein during the lyophilization (Rey and May, 2011). Sometimes the polymers are too bulky to form hydrogen bonds with the protein, but use them with another stabilizer could be a useful combination in terms of thermal properties and protein stability (Carpenter *et al.*, 1997).

Only on the case of 4% mannitol and 1% dextran in phosphate buffer, there was an exotherm peak attributed to the crystallization of mannitol. The inhibition of mannitol crystallization and presence of its amorphous form could improve the protein stability.

Table 2.11: Thermal transformations revealed in the DSC warming thermographs and the collapse temperature determined with the freeze-drying microscope for formulations with mannitol–dextran.

Mannitol (% v/w)	Dextran (% v/w)	T_{g1}' (°C)	T_{g2}' (°C)	T peak exotherm (°C)	T_{oc} (°C)	T_{c-50} (°C)	T_{fc} (°C)	Buffer solution
4	1	-47.8	-36.88	-	-32.4	-31.7	-30.9	Citrate Buffer (0.1 M)
2	3	-44.9	-31.52	-	-25.7	-25.0	-24.3	
1	4		-27.89	-	-23.0	-22.5	-22	
4	1	-50.8	-36.58	-19.81	-34.7	-33.4	-32.1	Phosphate Buffer (0.05 M)
2	3	-16	-29.77	-	-23.5	-22.3	-21	
1	4		-23.44	-	-15.3	-14.8	-14.2	

The Figure 2.19, shows the effect of the mannitol concentration in the collapse temperature and in the glass transition temperature associated with the two different groups of formulations (one in phosphate buffer and the other in the citric buffer). The collapse temperature and the T_g' increase with the increase of dextran concentration. All the formulations showed has a 5% w/v of solid.

The collapse temperature is between 5 and 10 °C higher than the glass transition temperature associated with the collapse.

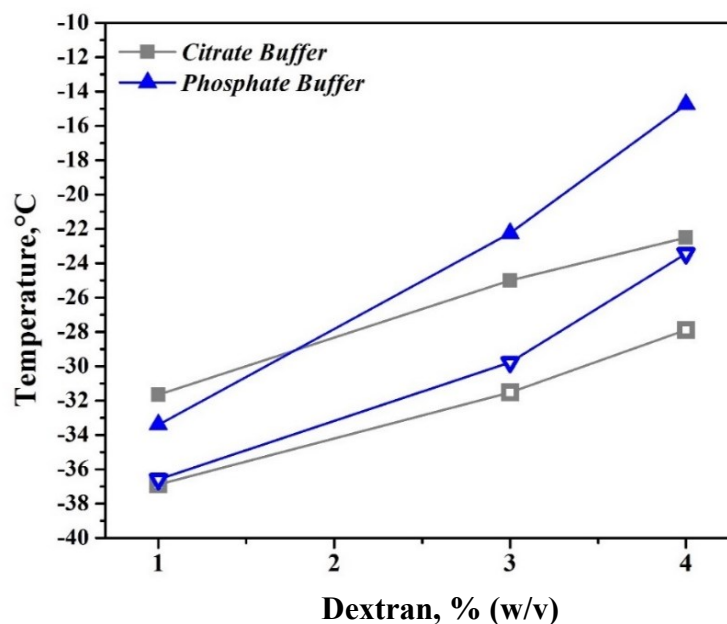


Figure 2.19: Variation of the glass transition temperature and the collapse temperature with the increase of dextran concentration in formulations with mannitol. All the formulations showed a 5% w/v of solid. The empty triangles and squares represent the T_{g2}' of the formulations in phosphate and citrate buffer, respectively.

PVP- Mannitol

In the Table 2.12, are reported all the thermal events revealed in the DSC warming thermogram and the collapse temperature for the formulations with mannitol and PVP.

Table 2.12: Thermal transformations revealed in the DSC warming thermographs and the collapse temperature determined with the freeze-drying microscope.

Mannitol (% v/w)	PVP (% v/w)	T_{g1}' (°C)	T_{g2}' (°C)	T_{g3}' (°C)	T_{g4}' (°C)	T_{oc} (°C)	T_{c-50} (°C)	T_{fc} (°C)	Buffer solution
2	3	-50.58	-37.96	-27.2	-23.01	-23.9	-22.6	-21.3	<i>Citrate Buffer</i>
1	4	-49.39	-39.33	-24.7	-21.07	-22.8	-22.2	-21.6	
2	3		-27.7	-23.44		-22.5	-21.15	-19.8	<i>Phosphate buffer</i>
1	4	-50.04	-31.03	-25.85		-22.2	-21.1	-20	

As it is shown on the Table 2.12, the addition of PVP to the formulation increased the collapse temperature improving the thermal characteristics of the formulation. PVP is also well-known as a macromolecular inhibitor of mannitol crystallization; in this case, the

amorphous mannitol could be used as lyoprotectant. The PVP could present phase-separate from the protein during the lyophilization (Cavatur *et al.*, 2002).

2.3.2 Evaluation of cake appearance: cycle performed

A freeze-drying cycle was performed in order to assess visually the final freeze-dried product in terms of cake quality. Six formulations were selected from the formulations previously characterized. The information of the formulation compositions, the maximum product temperature reached and the presence or absence of shrinkage is reported in the Table 2.13

Table 2.13: Formulation compositions, maximum temperature reached for the product and cake appearance

Sample	Buffer *	Mannitol (% v/w)	Sucrose (% v/w)	Shrinkage	TC	T_c (°C)	T_{max} (°C)
1	<i>Phosphate Buffer</i>	5	-	No	4	-	-29.7
2	<i>Citrate Buffer</i>	5	-	Si**	2	-36	-37.3
3	<i>Citrate Buffer</i>	4	1	Si	3	-34	-36.4
4	<i>Phosphate Buffer</i>	4	1	Si	1	-34.8	-36.14
5	<i>Citrate Buffer</i>	2	3	Si	-	-35	-
6	<i>Phosphate Buffer</i>	2	3	Si*	-	-37	-

*In this case, phosphate buffer (0.05 M) and citrate buffer (0.1 M) are used

Conservative conditions were selected in order to avoid the collapse and to maintain the product temperature below the T_c previously evaluated, therefore, the primary drying was performed at -30 °C for 60 hours. The time of the primary drying was high enough to guarantee the complete ice sublimation.

The temperature profile of the product temperature and the T_{shelf} during the drying is shown in the Figure 2.20. The product temperature was measured at the bottom because that is the warmest part of the ice structure during the sublimation and it is also the last point to dry; therefore, with the product temperature profile it is possible to assess the maximum product temperature reached during the sublimation and to determine approximately the duration of primary drying (Rey and May, 2011).

The maximum temperature reached for the product is determined for the temperature in which appears an important change of the tendency in the temperature profile. For example, as we can see in Figure 2.20, in the case of sample 2, the maximum product temperature was -37.3 °C. In this point, the sublimation front passes through the thermocouple.

For all the formulations, the maximum product temperature reached was below to the collapse temperature by at least one degree.

The product temperature profile in Figure 2.20, could be also used to determinate the end of primary drying. But it is important to take into account that the obtained time for primary drying is only an approximation. The vials with the thermocouples are not considered as representatives (Patel *et al.*, 2010).

The vials with the thermocouples usually nucleate first than the others (higher nucleation temperature) which has an effect on the product morphology and on the R_p ; consequently, these vials dry faster than the entire production.

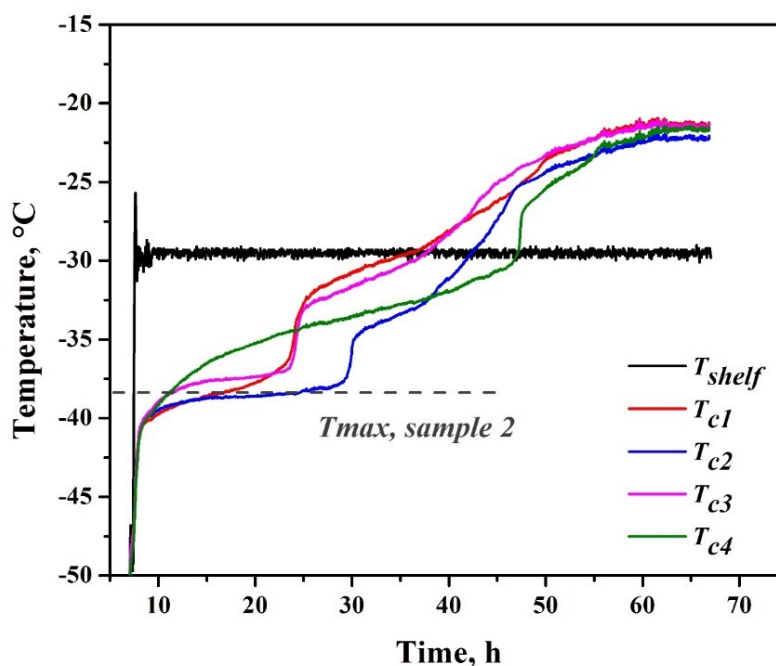


Figure 2.20 Product temperature profile during primary drying

Another technique used to determine the end of the ice sublimation is doing a comparative measurement, Baratron vs Pirani.

The values of Pirani and Baratron pressure allow getting a better approximation of primary drying time.

As it was said previously, Pirani is a manometer that measures the relative pressure based on the thermal conductivity of the gas, so, the pressure value measured depends on the nature of the gas inside the chamber.

Through primary drying, inside the chamber most of the gas is vapor water (gas with higher thermal conductivity than nitrogen, approximately 1.6 times higher), consequently, the measured pressure value is higher than the real chamber pressure (Patel *et al.*, 2010).

Then, when the sublimation is completed in an important number of vials, the amount of vapor water inside the chamber starts to decrease (onset time) until the Baratron and Pirani manometers measure the same value of pressure. At this point, there is only nitrogen inside the chamber and all the vials are dried (offset time) and the primary drying ends.

In the Figure 2.21, we can see this phenomenon and determining the onset time (40 h relative to the start of the cycle) and the offset time (60 h relative to the start of the cycle). Hence, the primary drying ended after 52 hours the step starts.

Once the freeze-dried product was obtained, the quality of the cake structure was determined visually. Pictures of the final dried product are shown in Figure 2.22.

The samples with citrate buffer showed a higher level of shrinkage. In special, the sample mannitol 5% (w/v) in citrate buffer showed an important level of shrinkage. The sample 1 (mannitol 5%, phosphate buffer) showed a cake quality without shrinkage. The samples 4, 5 and 6 also showed a cake quality with a lower degree of shrinkage.

From these formulations, sample 4 (4% (w/v) mannitol and 1% (w/v) in phosphate buffer) was selected to continue with the next steps on this project (chapter 3).

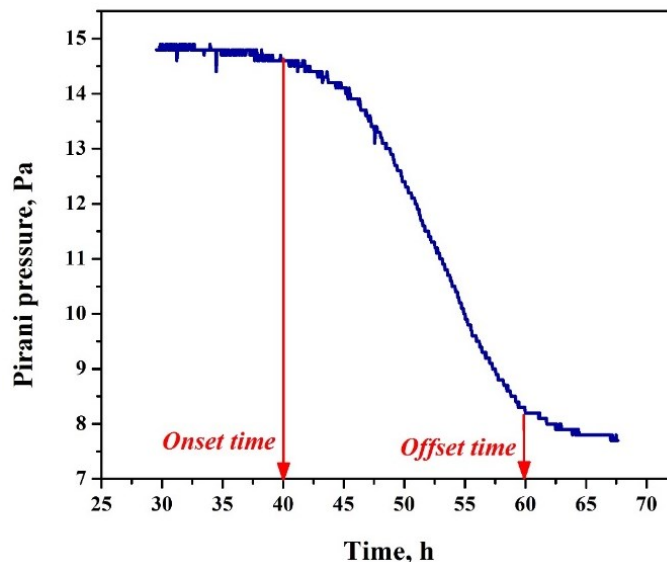


Figure 2.21: Pirani pressure again primary drying time.

<p>Mannitol 5%(w/v), phosphate buffer</p>	<p>Mannitol 5%(w/v), citrate buffer</p>	<p>Mannitol 4 %: Sucrose 1% (w/v), citrate buffer</p>
<p>Mannitol 4 %: Sucrose 1% (w/v), phosphate buffer</p>	<p>Mannitol 2 %: Sucrose 3% (w/v), citrate buffer</p>	<p>Mannitol 2 %: Sucrose 3% (w/v), phosphate buffer</p>

Figure 2.22: Freeze-dried products obtained.

Notation

C_i	Concentration of the component “i” in aqueous solution
T_c	Collapse temperature, °C
T_{c-50}	Midpoint collapse temperature, °C
T_{cr}	Crystallization temperature, °C
T_{eu}	Eutectic melting temperature, °C
T_{fc}	Full collapse temperature, °C
T_g	Glass transition temperature of the dried product
T_g'	Glass transition temperature of the maximal freeze-concentrate state, °C
T_{gi}'	Glass transition temperature of the maximal freeze-concentrate state of the component “i” in aqueous solution, °C
T_{oc}	Onset collapse temperature, °C
T_{shelf}	Shelf temperature, °C

Abbreviations

API	Active pharmaceutical ingredient
LDH	Lactate dehydrogenase
PVP	Polyvinylpyrrolidone

References

- Al-hussein, A., & Gieseler, H. (2013). Investigation of histidine stabilizing effects on LDH during freeze-drying. *Journal of Pharmaceutical Sciences*, **102**(3), 813–826.
- Al-Hussein, A., & Gieseler, H. (2012). The effect of mannitol crystallization in mannitol-sucrose systems on LDH stability during freeze-drying. *Journal of Pharmaceutical Sciences*, **101**(7), 2534–2544.
- Anchordoquy, T. J., & Carpenter, J. F. (1996). Polymers protect lactate dehydrogenase during freeze-drying by inhibiting dissociation in the frozen state. *Archives of Biochemistry and Biophysics*, **332**(2), 231–238.
- Bhatnagar, B. S., Bogner, R. H., & Pikal, M. J. (2007). Protein stability during freezing: separation of stresses and mechanisms of protein stabilization. *Pharmaceutical Development and Technology*, **12**(5), 505–523.

- Bhatnagar, B. S., Pikal, M. J., & Bogner, R. H. (2008). Study of the individual contributions of ice formation and freeze-concentration on isothermal stability of lactate dehydrogenase during freezing. *Journal of Pharmaceutical Sciences*, **97**(2), 798–814.
- Carpenter, J. F., Pikal, M. J., Chang, B. S., & Randolph, T. W. (1997). Rational design of lyophilized protein. *Pharmaceutical Research*, **14**(8), 969-975
- Cavatur, R. K., Vemuri, N. M., Pyne, A., Chrzan, Z., Toledo-Velasquez, D., & Suryanarayanan, R. (2002). Crystallization behavior of mannitol in frozen aqueous solutions. *Pharmaceutical Research*, **19**(6), 894–900.
- Depaz, R. A., Pansare, S., & Patel, S. M. (2016). Freeze-Drying above the glass transition temperature in amorphous protein formulations while maintaining product quality and improving process efficiency. *Journal of Pharmaceutical Sciences*, **105**(1), 40–49.
- Fonseca, F., Obert, J. P., Béal, C., & Marin, M. (2001). State diagrams and sorption isotherms of bacterial suspensions and fermented medium. *Thermochimica Acta*, **366**(2), 167–182.
- Fonseca, F., Passot, S., Cunin, O., & Marin, M. (2004). Collapse temperature of freeze-dried lactobacillus bulgaricus suspensions and protective media. *Biotechnology Progress*, **20**(1), 229–238.
- Höhne, W. H. G., Hemminger, W. H., & Flammersheim, H. J. (2004). differential scanning calorimetry, *second edition*.
- Izutsu, K., & Kojima, S. (2002). Excipient crystallinity and its protein-structure-stabilizing effect during freeze-drying. *The Journal of Pharmacy and Pharmacology*, **54**(8), 1033–1039.
- Izutsu, K., Yomota, C., & Aoyagi, N. (2007). Inhibition of mannitol crystallization in frozen solutions by sodium phosphates and citrates. *Chemical & Pharmaceutical Bulletin*, **55**(4), 565–570.
- Izutsu, K., Yoshioka, S., & Terao, T. (1994). Effect of mannitol crystallinity in the stabilization of enzymes during freeze-drying. *Chem. Oharm. Bull*, **42**(1), 5–8.
- Johnson, R. E., Kirchhoff, C. F., & Gaud, H. T. (2002). Mannitol-sucrose mixtures--versatile formulations for protein lyophilization. *Journal of Pharmaceutical Sciences*, **91**(4), 914–922.
- Kasper, J. C., & Friess, W. (2011). The freezing step in lyophilization: physico-chemical fundamentals, freezing methods and consequences on process performance and quality attributes of biopharmaceuticals. *European Journal of Pharmaceutics and Biopharmaceutics*, **78**(2), 248-263
- Kasraian, K., Spitznagel, T. M., Juneau, J. A., & Yim, K. (1998). Characterization of the sucrose/glycine/water system by differential scanning calorimetry and freeze-drying microscopy. *Pharmaceutical Development and Technology*, **3**(2), 233–9.
- Kim, A. I., Akers, M. J., & Nail, S. L. (1998). The physical state of mannitol after freeze-drying: Effects of mannitol concentration, freezing rate, and a noncrystallizing cosolute. *Journal of Pharmaceutical Sciences*, **87**(8), 931–935.
- Liu, J. (2006). Physical characterization of pharmaceutical formulations in frozen and freeze-dried solid states: techniques and applications in freeze-drying development. *Pharmaceutical Development and Technology*, **11**(1), 3–28.

- Meister, E., & Gieseler, H. (2009). Freeze-dry microscopy of protein/sugar mixtures: drying behavior, interpretation of collapse temperatures and a comparison to corresponding glass transition data. *Journal of Pharmaceutical Sciences*, **98**(9), 3072–3087.
- Patel, S. M., Doen, T., & Pikal, M. J. (2010). Determination of end point of primary drying in freeze-drying process control. *AAPS PharmSciTech*, **11**(1), 73–84.
- Pisano, R., Fissore, D., Barresi, A. A., Brayard, P., Chouvenc, P., & Woinet, B. (2013). Quality by design: optimization of a freeze-drying cycle via design space in case of heterogeneous drying behavior and influence of the freezing protocol. *Pharmaceutical Development and Technology*, **18**(1), 280–295.
- Pyne, A., Surana, R., & Suryanarayanan, R. (2002). Crystallization of mannitol below Tg' during freeze-drying in binary and ternary aqueous systems. *Pharmaceutical Research*, **19**(6), 901–908.
- Rey, L., & May, J. C. (2011). Freeze-drying/ lyophilization of pharmaceutical and biological products, *Second Edition, Revised and Expanded. Drugs and the pharmaceutical sciences*. Taylor & Francis.

Chapter 3

Uncertainty analysis

As it was explained in chapter 1, during primary drying, there are two adaptable process conditions that should be defined (T_{shelf} and P_c) to reduce the primary drying time and to obtain an adequate freeze-dried product. In this context, an approach widely used is the development of a mechanistic model to simulate the sublimation process during primary drying and to construct a design space.

Each combination of T_{shelf} and P_c leads to a value of T_i that depends on the process parameters. Since the process parameters change during primary drying, the optimal combination of T_{shelf} and P_c also changes, and the use of a dynamic design space represents an advantage. For example, with the evolution of primary drying the thickness of the L_{dried} changes, leading to an increase in the mass transfer resistance and consequently an increase of T_i (Fissore *et al.*, 2011)

A mechanistic model gives an approximate representation of the reality and therefore, contain a degree of uncertainty related to the assumptions and simplifications of the model and the uncertainty of the parameters. In this scenario, two critical parameters, defined as input variables, are the heat and mass transfer coefficients, i.e., K_v and R_p . These two parameters are defined for the entire batch, while in reality they vary from vial to vial. Consequently, one of the main concerns in process development and the use of mechanistic models is the inter-vial heterogeneity that leads to uncertainty on the results (Mortier *et al.*, 2016).

In this chapter, a mechanistic model developed by Van Bockstal *et al.* (2017) was used for the determination of a dynamic design space of primary drying. This mechanistic model takes into account the uncertainty of some parameters, and therefore an uncertainty analysis was performed. In this way, the risk of cake collapse (RoF) was estimated and controlled. The Risk of Failure was defined as the chance that one or more samples collapse during primary drying.

Particular attention has been paid in determining the uncertainty of the mass transfer coefficient. Nucleation temperature and cooling rate have a strong influence on the final product morphology, and the stochastic nature of the nucleation phenomenon is usually responsible for product heterogeneity in the batch, and consequently for the vial-to-vial variability of R_p .

With the scope of defining an uncertainty level of the R_p value, the nucleation temperature distribution was determined and then each nucleation temperature was related to a product

morphology using a mathematical model developed by Pisano and Capozzi (2017), the model simulates the freezing step. Then, a mechanistic model was used to construct a dynamic design space and to define the optimal process condition during primary drying.

Figure 3.1 shows a scheme that represents the logic steps performed in this chapter to define the optimal process conditions during primary drying.

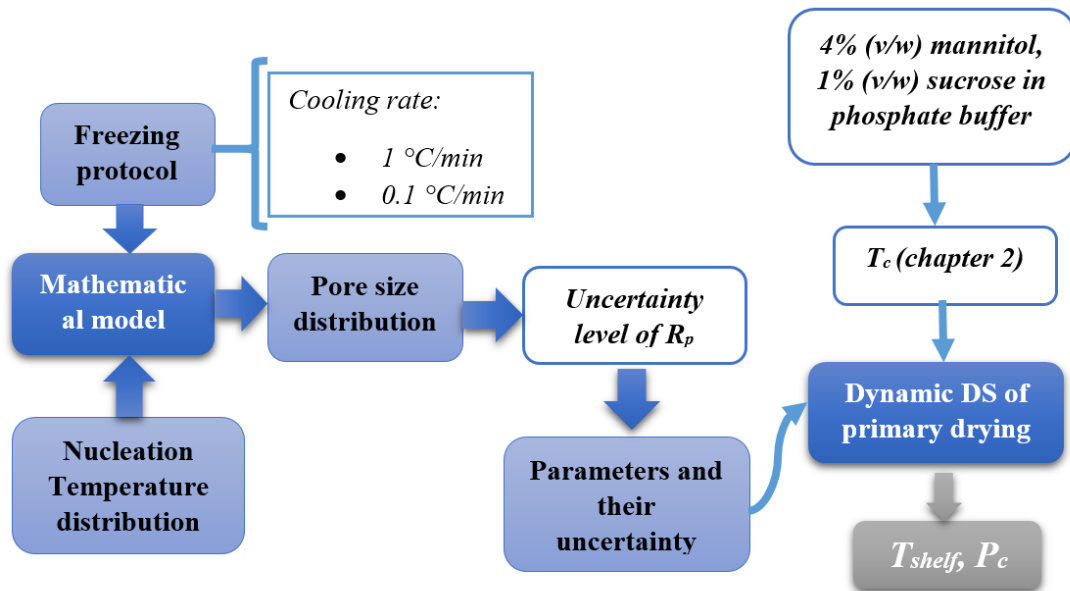


Figure 3.1: Workflow of the work developed in the second part of the thesis work.

Two different freezing protocols were used: one with a cooling rate of 1°C/min and the other with a cooling rate equal to 0.1°C/min. The formulation used in this work was a mixture of 4% (w/v) mannitol and 1% (w/v) sucrose in phosphate buffer. This formulation was previously analyzed in chapter 2 to obtain its thermal characteristics.

3.1 Material and methods

3.1.1 Nucleation temperature distribution

As previously mentioned, the nucleation temperature is a stochastic phenomenon, and its distribution should be experimentally determined.

An experimental campaign was carried out, and the nucleation temperature of a statistically significant number of samples was measured. Two different freezing protocols (cooling rates: 1°C/min and 0.1°C/min) were used to evaluate the effect of the freezing protocol on the nucleation phenomenon and how the cooling rate affects the nucleation temperature distribution.

The nucleation phenomenon is promoted by the presence of foreign impurities; because of this, it is important to work with controlled conditions. Therefore, a solution of 4% (w/v) mannitol and 1% (w/v) sucrose in phosphate buffer, pH 7.4 (0.05M) was prepared using water for injection. The solution was filtered through a 0.2 μm pore size filter and was prepared under laminar flow cabinet.

A total of 48 glass vials (10R type, Schott, Müllheim, Germany) were filled with 3 ml of solution and placed on four shelves in the drying chamber with a linear arrange in order to allow the complete visualization of all the vials during the freezing. Then, the shelf temperature was linearly decreased from room temperature to -55°C with a cooling rate of $1^{\circ}\text{C}/\text{min}$ or $0.1^{\circ}\text{C}/\text{min}$ (depending on the freezing protocol). The product temperature was monitored via 6 thermocouples placed in direct contact with the bottom of different vials. Due to the presence of the thermocouple, these vials usually nucleate at higher temperature than those without thermocouple, therefore, they were used only as reference and its nucleation temperature was not included in the final nucleation temperature distribution. Two webcams were used to record the freezing process and to determine the time when nucleation occurs.

Figure 3.2 shows a picture of the freeze-dryer and the webcams used. Two thermocouples were placed on the first shelf and other two on the fourth shelf (one in the vial near to the wall and the other thermocouple on a center vial). In the second and third shelf, only one thermocouple for each shelf was used.

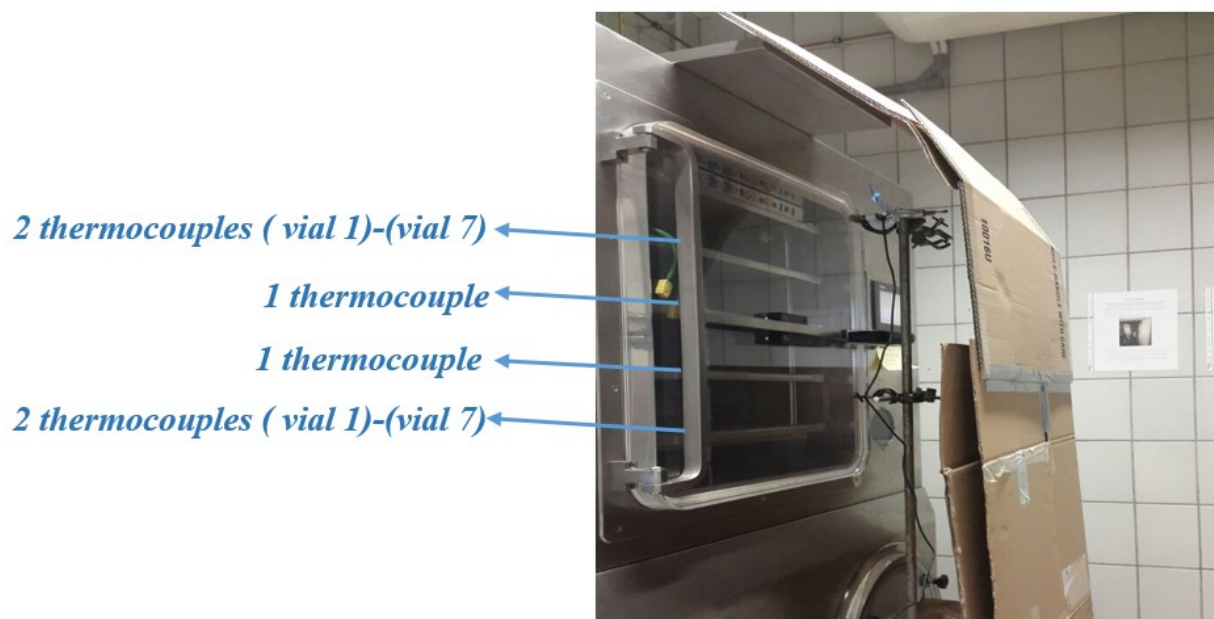


Figure 3.2: Picture of the freeze-dryer used to perform the cycles. The distribution of the thermocouples inside the drying chamber is specified.

The nucleation time of 42 samples was determined and was related to a nucleation temperature using the product temperature profile of the references. Figure 3.3 shows a typical temperature profile during freezing aside to an illustration of the nucleation phenomenon in a vial.

In order to have a direct correlation between the nucleation time and the nucleation temperature for each sample, it is necessary to obtain a reference temperature profile without the typical temperature increase observed when the nucleation occurs. As Figure 3.3 shows, a linear regression was done to have a representative product temperature profile of the whole production (when the product temperature increase).

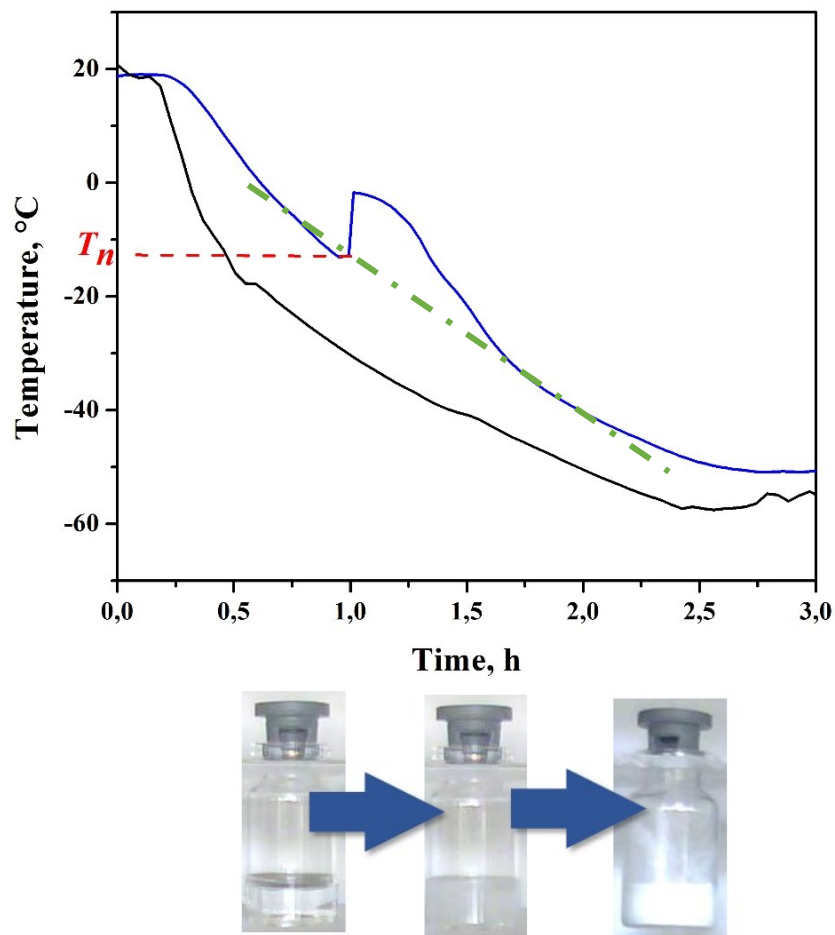


Figure 3.3: Product temperature profile and a schematization of the nucleation phenomenon in a vial.

In total 5 cycles (4 with only a freezing step) were performed following the methodology previously described and 213 nucleation temperatures were obtained. This procedure was developed for each freezing protocol.

One of the five cycles performed includes a primary and secondary drying step. The process conditions of this cycle are summarized in Table 3.1. As we can note, conservative conditions are used in this cycle to avoid the collapse or shrinkage of products after freeze-drying.

The freeze-dried products obtained were analyzed by SEM, Karl Fischer, and Raman analysis.

Table 3.1: Process conditions during the freeze-drying cycle.

<i>Process Conditions</i>				
	T °C	Rate (°C/min)	Hold Time (h)	P (Pa)
	20		0.17	
<i>Freezing</i>	-55	1 /0.1	5	
<i>Primary drying</i>	-32	0.76	46	10
<i>Secondary drying</i>	20	0.09	15	3

3.1.2 Characterization tests

Residual moisture content

The Karl Fisher analysis was used to determine the residual moisture contained in the samples at the end of the secondary drying. Six samples with different nucleation temperatures (from each freezing protocol) were selected.

Polymorphs state of mannitol-based formulations

A Raman Rxn1 spectrometer (Kaiser Optical Systems Ann Arbor, MI, USA) equipped with a laser, 785nm Invictus NIR diode was used to collect the spectra. A laser power of 400 mW was used to record the spectra with a resolution of 4 cm⁻¹. For each spectrum, an exposure time of 10 s and 3 accumulations were used. HoloGRAMS™ data collection software (Kaiser Optical Systems Ann Arbor, MI, USA) was used for the collection and data transfer.

Raman spectra were recorded at three different positions: at the top, center and the bottom of the sample. For each position 6 Raman spectra were obtained. This analysis was performed for five different samples (related to five different nucleation temperature). The procedure described below was performed for each freezing protocol.

The Raman spectra collected was analyzed using Principal Component Analysis (PCA), this powerful technique was selected due to a large amount of spectra collected. In this case, SIMCA software (version 13.0.3, Unimetric, Umea, Sweden) was used to perform the principal component analysis.

Principal analysis component (PCA)–Process analysis

PCA is a multivariate spectral analysis technique, widely used for the analysis of Raman spectra. The technique allows the analysis of multiple variable data set, and the main idea consists of reducing the dimensionality of the data, defining a new set of variables (the principal components, from now on PC in the manuscript) while the variability is retained

as much as possible and the principal components are ordered. In this way, most of the variation shall be kept in the first principal component (Jolliffe, 2002).

The Raman spectra collected were inserted into the data matrix (D). Then an orthogonal bilinear decomposition was done, and the principal components were obtained on a sequentially way (De Beer *et al.*, 2007):

$$D = TP^T \cdot E = t_1p_1' + t_2p_2' + \dots + t_Qp_Q' + E \quad (3.1)$$

Where T is the score matrix ($M \times Q$), P is the loading matrix ($M \times N$), and E is the residual matrix that explains the residual variation of the data set not correlated with a chemical contribution. N is the number of collected spectra at M wavelength. Q is the number of principal components (PCs). Each PC is formed by the score vector t and the loading vector p . There is a score value for each spectrum that provides information about how the spectrum is related to other spectra in the component studied. On the other hand, the loading spectra present the spectral attributes (in the original spectra) captured by the principal component.

The main and most powerful characteristic of PCA is the capacity to transform correlated information from a large number of spectra channels into a small number of orthogonal PCs. In this way, the PCA analysis provides a way visualizing clearly complex data (Zhang *et al.*, 2005). Nevertheless, the PCs do not necessarily represent the real underlying factor that causes the data variation, but they are an orthogonal linear combination of them, and each PC is obtained by maximizing the variance that it can explain (De Beer *et al.*, 2007).

The spectral region of interest ¹ for identify the polymorph of mannitol in the product was 850-1200 cm^{-1} . Before starting with the process described below, the raw data was pre-processed by Standard Normal Variate (SNV) and centered. The preprocessing of the data is necessary to facilitate the obtaining of information in the subsequent data analysis procedure. In this way, unwanted signals and noise in the signals (due to the particle size effect, surface roughness and so on) are attenuated. In the case of SNV, each spectrum is transformed to a spectrum with unit standard deviation and a mean intensity of zero (Zhang *et al.*, 2005).

SEM-Analysis

A Scanning Electron Microscope (SEM, FEI type, Quanta Inspect 200, Eindhoven, the Netherlands) was used to assess the internal structure of five freeze-dried products for each cooling rate, and each samples had a different T_n , spread into the nucleation temperature distribution. SEM images were taken near to the top, center, and bottom of the sample in order to obtain an estimation of the intra-vial heterogeneity. A quantitative analysis was done in terms of pore size distribution.

3.1.3 Experimental determination of the K_v

The heat transfer coefficient (used in section 3.1.5) associated with the linear vial arrangement was determined using a gravimetric method (Pisano *et al.*, 2013).

A total of 48 glass vials, each filled with 3 ml of deionized water, were placed on four shelves in the drying chamber (12 vials per shelf, using a linear arrangement). The shelf temperature was linearly decreased from room temperature to $-45\text{ }^{\circ}\text{C}$ at a rate of $1^{\circ}\text{C}/\text{min}$. This temperature was kept for 1 hour. Then, the shelf temperature was increased until $-20\text{ }^{\circ}\text{C}$ and the pressure was reduced to 10 Pa. Each vial was weighed before it was loaded and after 5 hours of sublimation, allowing the determination of the mass of sublimated ice (Δm) that gives an estimation of the sublimation rate.

The product temperature (T_i) was monitored during drying using K-type thermocouples (WIKA Instruments, Klingenberg, Germany) placed at the bottom of 3 vials randomly spread on the shelves. The K_v was calculated by (Fissore *et al.*, 2011):

$$K_v = \frac{\Delta m \Delta H_{sub}}{\Delta t (T_{shelf} - T_i) A_v M} \quad (3.2)$$

Where Δm is the mass of sublimated ice, Δt is the sublimation time (5h), A_v is the bottom area of the vial and M is the molecular weight of water.

Then, a nonlinear regression was used to fit equation 3.9 to the data previously obtained, and the K_v coefficients (α , β , γ) were determined.

The T_i and T_{shelf} profiles used in this section correspond to the data obtained from the cycles performed in section 3.1.1.

3.1.4 Experimental determination of the R_p

The R_p was determined experimentally to confront the experimental value with those obtained in section 3.1.6.3 (using the model of the freezing step).

The product resistance to vapor flow (R_p) is related to the vapor flow by:

$$R_p = \frac{p_i - P_{w,c}}{J_w} \quad (3.3)$$

Where p_i is the vapor pressure at the sublimation front and $P_{w,c}$ is the water vapor partial pressure in the drying chamber, and since during the primary drying the gaseous phase in the drying chamber is constituted principally by vapor water, $P_{w,c}$ is assumed to be equal to the chamber pressure (P_c) (Fissore *et al.*, 2011); J_w is the sublimation flux.

In order to determine the R_p , two variables were monitored during primary drying: the temperature at the sublimation front (T_i) and the T_{shelf} . Then the sublimation flux was calculated using the equation 3.2 and the K_v value previously determined.

P_i was calculated using the following equation (Murphy and Koop, 2005):

$$P_i = e^{9.55 - 5720/T_i + 3.53 \ln(T_i) - 0.00728 T_i} \quad (3.4)$$

The L_{dried} associated with each R_p was calculated using the equations 3.11 and 3.12. Then, a nonlinear regression was used to fit equation 3.9 and determine the R_p coefficients (R_{po} , A_{Rp} and B_{Rp}).

3.1.5 Prediction of the product morphology

Once the nucleation temperature distribution was defined (for each freezing protocol), a dynamic model developed by Pisano and Capozzi (2017) was used to obtain an estimation of the pore size and its distribution within the product. Moreover, since a profile of pore size in function of the product thickness was calculated for different nucleation temperatures; each nucleation temperature was correlated with a mean pore size, and therefore, the inter-vial variability within a production was predicted.

The mechanistic model consists of three steps (Pisano and Capozzi, 2017):

- 1) Define the values of the input parameters.
- 2) The model predicts the products dynamic during freezing.
- 3) Ice crystal sizing; which involves the prediction of a pore size distribution and a mean pore diameter.

The input parameters can be divided into three groups:

- Manufacturing conditions; such as T_{shelf} during the process, freezing protocol, filling volume.
- Geometrical characteristics of the system; vial geometry (10R vials)
- Experimentally determined parameters; such as the nucleation temperature and the heat transfer coefficient. The procedures followed to determine the K_v and nucleation temperature distribution were described in section 3.1.3 and 3.1.1, respectively.

Once the input parameters were set, the product dynamics were predicted, i.e., the temperature profile and the rate of the freezing front. Freezing involves three main events: supercooling, nucleation and crystal growth. During the supercooling, Fourier's law was used to describe the evolution of the product temperature, due to no phase change occurs. Then when the nucleation and crystal growth occurs, the present mathematical model uses the nucleation-growth method and two source terms were included in the heat balance (Pisano and Capozzi, 2017):

$$\rho c_p^* \frac{\partial T}{\partial t} = \nabla \cdot \kappa \nabla T + Q_c + Q_n \quad (3.5)$$

Where Q_c is the source term related to the growth of ice crystals and Q_n represents the nucleation contribution.

The crystal sizing was developed using an empirical model that correlates the temperature gradient (γ) and the freezing front rate (v) with the pore diameter (Bomben and King, 1982):

$$D_p = \alpha v^{\lambda_1} \gamma^{\lambda_2} \quad (3.6)$$

Where α is product characteristic, and it is calculated by fit the equation 3.6 to experimental data acquired by SEM analysis (section 3.1.2), λ_1 and λ_2 are model parameters.

3.1.6 Dynamic Design Space of primary drying

As previously mentioned, a mechanistic model developed by Van Bockstal *et al.* (2017) was used to determine the optimum value of the two adaptable process variables during the primary drying (T_{shelf} and P_c). In this section, the basic principles of the model are described.

The mechanistic model describes the ice sublimation phenomenon using equations based on principles of energy and mass transfer. As it is common in the model development, two simplifications were done:

- A planar sublimation front was assumed.
- It was assumed that the transferred energy was consumed only for the sublimation of the ice (i.e. steady-state system was assumed).

During the primary drying, the model calculates the evolution of the L_{dried} thickness as a function of the time for a set of input parameters. The following series of equations were used to calculate the temperature at the sublimation front T_i (K) and the difference of temperature through the ice layer ΔT (K) (Mortier *et al.*, 2016):

$$e^{9.550426-5723.265/T_i+3.53068\ln(T_i)-0.00728332T_i} = - \frac{(-A_p \Delta H_{sub} P_c - A_v K_v R_p M T_i + A_v K_v R_p M \Delta T)}{A_p \Delta H_{sub}} \quad (3.7)$$

$$\Delta T = \frac{889200 \frac{(L_{Total} - L_{dried})(P_i - P_c)}{R_p} - 0.0102(L_{Total} - L_{dried})(T_{shelf} - T_i)}{1 - 0.0102(L_{Total} - L_{dried})} \quad (3.8)$$

Where P_c is the chamber pressure, A_p and A_v are the inner and outer area of the vial, respectively; The inner area also corresponds to the product area. L_{total} is the thickness of the product which depends on the filling volume and the geometric characteristics of the vial. L_{dried} is the thickness of the dried product and ΔH_{sub} is the latent sublimation heat that is a function of T_i . K_v and R_p are the vial heat transfer coefficient and the mass transfer resistance respectively.

The heat transfer coefficient depends on the equipment and the type of vial, because the vial contact area could change for different vial models. In addition, the position of the vial in the chamber affects the K_v , in fact, several studies have reported that the vials near to the edge present a higher value of K_v than those in the center of the shelf (Pisano *et al.*, 2013). This fact is explained taking into account the higher contribution of the radiation from the chamber walls in the case of vials place in the edge of the shelf.

In the present work, K_v was described in function of the chamber pressure (P_c) by the following equation (Giordano *et al.*, 2011):

$$K_v = \alpha + \frac{\beta P_c}{1 + \gamma P_c} \quad (3.9)$$

The constants α , β and γ used in the present work, were experimentally determined by Van Bockstal *et al.* (2017) through the same methodology described in section 3.1.3. In this context, two different groups of vials were defined: the edge-vials (vials with at least one side toward the wall or the door of the chamber) and center vials (vials surrounding by other vials). Consequently, a set of parameters for each group of vials were defined.

Figure 3.4 provides information on the heat transfer coefficient as a function of the chamber pressure. An increase of the gas molecule density between the shelf and the bottom of the vial leads to a rise of the K_v value, therefore, the K_v presents an upward trend as the chamber pressure increases (Pisano *et al.*, 2012). Moreover, this figure shows the difference between the K_v of the edge vials and the K_v of the center vials.

The K_v of the vials situated on the edge of the shelf is significantly higher than the K_v of the center vials. As the total energy transferred to the edge vials is higher, this group of vials is considered the limiting factor and they have a higher risk of collapse during the primary drying (Van Bockstal *et al.*, 2017). Consequently, the factors α , β and γ of the edge vials are used as input variables in the mechanistic model.

The R_p can be expressed in function of L_{dried} by the following empirical equation:

$$R_p = R_{p,0} + \frac{A_{Rp} L_{dried}}{1 + B_{Rp} L_{dried}} \quad (3.10)$$

In theory, $R_{p,0}$ is the mass transfer resistance of the product when the primary drying starts. A_{Rp} and B_{Rp} are two constants that describe how the R_p vary with the evolution of L_{dried} and therefore with the evolution of time.

The sublimation rate is calculated by:

$$\dot{m}_{Sub} = A_p \frac{(P_i - P_c)}{R_p} \quad (3.11)$$

Where P_i is the vapor pressure at the sublimation front and it can be calculated once T_i is determined. The mass of ice removed at the time $t+1$ is equal to:

$$m_{sub,t+1} = m_{sub,t} + \dot{m}_{Sub} \Delta t \quad (3.12)$$

The L_{dried} evolution can be obtained taking into account the mass of ice removed, the density of ice, ρ_I and the volume fraction of ice:

$$L_{dried} = \frac{m_{sub}}{\rho_l \xi A_p} \quad (3.13)$$

The L_{dried} is calculated for each time step, and it is both an output value and an input value (for the next time step).

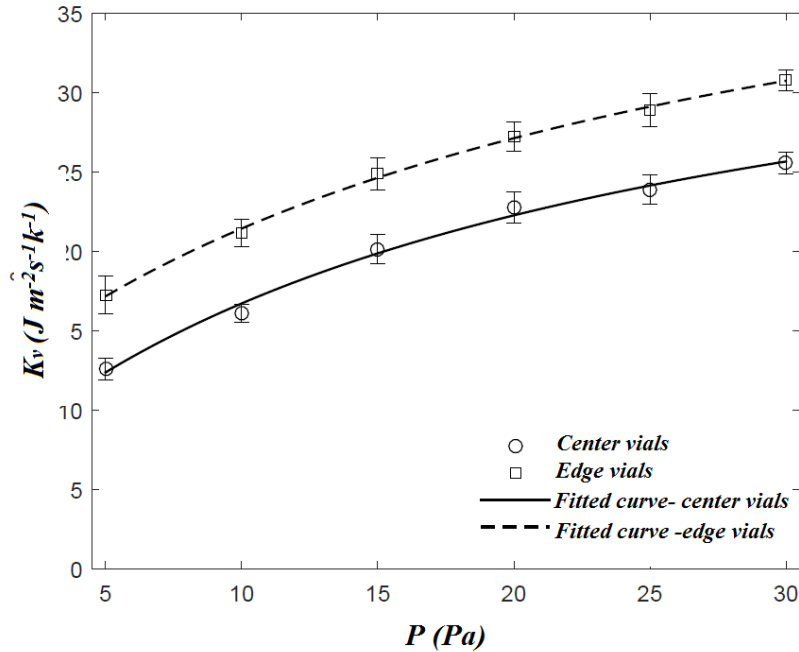


Figure 3.4: Heat transfer coefficient (K_v) in function of the pressure in the drying chamber (P_c) (from Van Bockstal *et al.*, 2017, with modifications)

3.1.6.1 Determination of the optimal process conditions

A grid-search approach is used in order to determine the optimal process conditions at each time step. Therefore, the simulation of the sublimation phenomenon was done for different combinations of P_c and T_{shelf} .

For each grid-point (each combination of P_c and T_{shelf}) two main operation constraints were taken into account:

- The temperature at the ice interface, i.e., the sublimation front, should remain below a critical temperature $T_{i,crit}$ to avoid collapse.
- The choked flow should be avoided.

In the present work, the critical product temperature $T_{i,crit}$ was set at the mid-point collapse temperature (T_{c-50}) of the studied formulation that is -34.8 °C. The collapse temperature was determined via direct observation of the process using a freeze-drying microscope; the procedure used to determine this temperature was described in chapter 2.

The choked flow limitation at both vial and dryer level was taken into account. In the case of vial-level, the choked flow was considered at the vial neck (the narrowest point, related to a local pressure rise) and it is given by (Van Bockstal *et al.*, 2017):

$$\dot{m}_{sub,chock,vial} = \frac{0.3r_{v,n}^2\pi\sqrt{\frac{\kappa T_r R}{M}}M}{RT_r} P_c \quad (3.14)$$

where the maximum sublimation rate in order to avoid choked flow (at vial level) is $\dot{m}_{sub,chock,vial}$ and $r_{v,n}$ is the radius of vial neck, the ratio of the specific heat of water is represented by κ , T_r is the temperature of the water vapor, R the gas constant and M the molecular weight of water.

The maximum sublimation rate allowed to avoid choked flow at dryer level is (Van Bockstal *et al.*, 2017):

$$\dot{m}_{sub,chock,dryer} = \frac{0.3r_d^2\pi\sqrt{\frac{\kappa T_r R}{M}}M}{RT_r} \frac{P_c}{n_{vials}} \quad (3.15)$$

Where r_d depends on the freeze-dryer, and it can be defined as the radius of the dryer duct (duct connecting the chamber and the condenser). In the studied case, since the duct is equipped with a butterfly valve, r_d is defined as the narrowest lumen at the valve connecting the condenser and the chamber; n_{vials} represents the maximum number of vials that fit on the drying chamber.

The procedure used to determine the optimal values of T_{shelf} and P_c is shown in Figure 3.5 A. For each grid-point, at each time step, a simulation was done in order to calculate the associated \dot{m}_{sub} and T_i . Then, the fulfillment of the two constraints was verified. The optimum combination of T_{shelf} and P_c is that which assures the fulfillment of the two constraints and provides the highest sublimation rate.

The grid for T_{shelf} and P_c was limited in order to reduce the computational load. P_c was limited between 10 Pa-30 Pa; 10 Pa represents the lower pressure that can be reached by the freeze-dryer. In the case of T_{shelf} , the upper and lower limits are defined taking into account the maximum temperature ramp that the equipment can provide (1°C/min), therefore, the grid boundaries for T_{shelf} are constantly changing during the simulation and due to the time step increases during the process, the width range of T_{shelf} is constantly changing.

Figure 3.5 B shows an example of how T_{shelf} and P_c are determined at a certain time. The value of the sublimation rate (\dot{m}_{sub}) as well as the temperature at the sublimation front (T_i) are plotted for each grid point. The black line on the center of the Figure (Figure 3.5 B) indicates the value of T_i and thus, the values below the line are lower than the critical temperature (T_{c-50}). The Figure on the right shows whether the constraints related to avoiding the choked flow is fulfilled or no (the value is 0 when the limit value of \dot{m}_{sub} is not exceeded and the value is 1 in the other case).

In Table 3.2 is showed a resume of the values of the model parameters used in the present work.

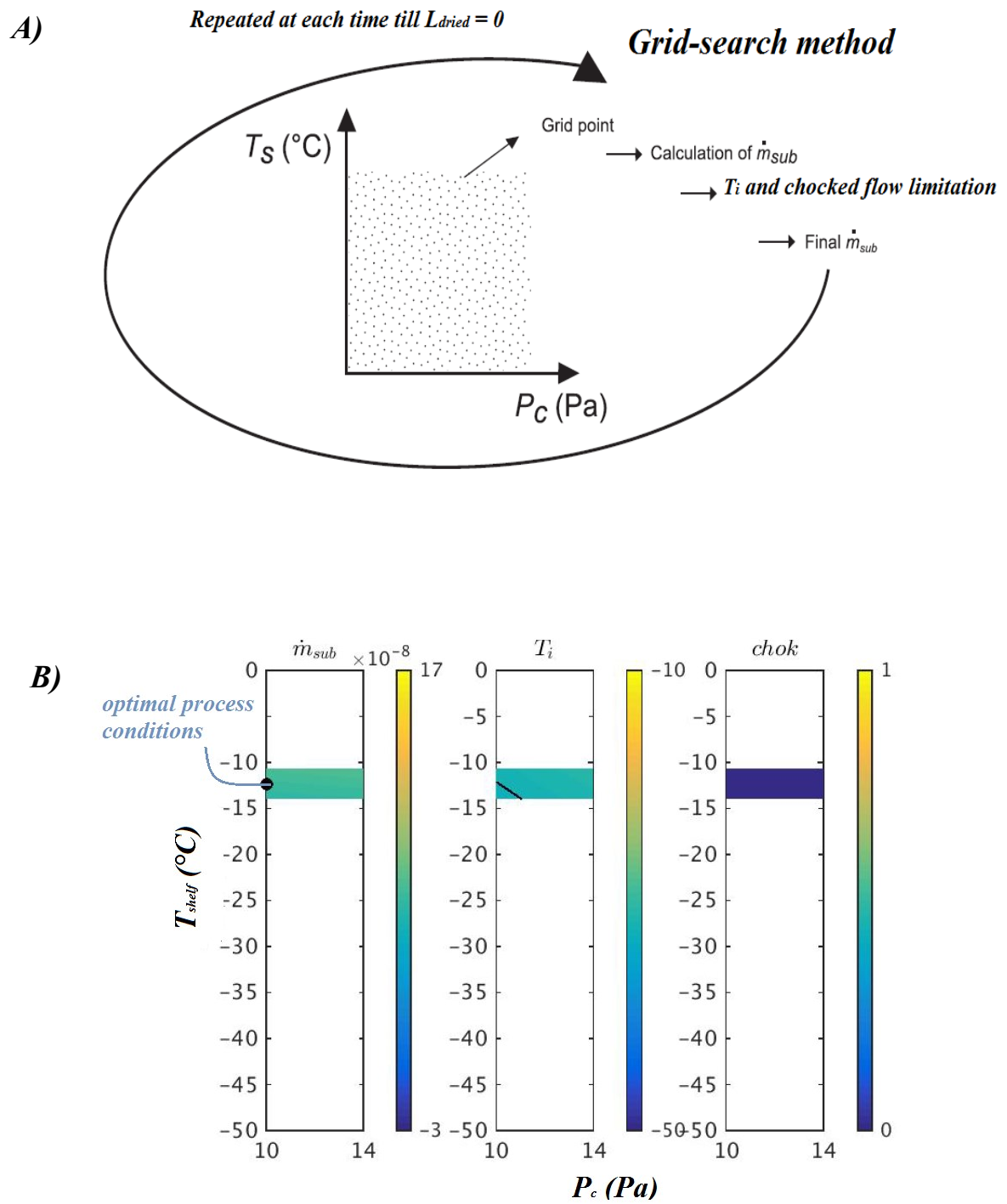


Figure 3.5: Procedure to determine the optimal values of T_{shelf} and P_c . A) Grid search- method. B) Determination of the optimal value of P_c and T_{shelf} for a specific primary drying time (from Mortier et al., 2016 and Van Bockstal *et al.*, 2017, with modifications)

Table 3.2: Values of the model parameters used in the simulations.

Parameter		Cooling rate 1°C/min	Cooling rate 0.1°C/min	
Inner radius of vial	$r_{v,i}$	0.011	0.011	m
Outer radius of vial	$r_{v,o}$	0.012	0.012	m
Radius of vial neck	$r_{v,n}$	0.063	0.063	m
Radius of the duct of the dryer	r_d	0.08	0.08	m
coefficient- R_p	R_{po}	51051.27	55705.63	($m\ s^{-1}$)
coefficient- R_p	A_{Rp}	22817.21	26239.42	(s^{-1})
coefficient- R_p	B_{Rp}	0.00	0.04	(m^{-1})
coefficient- K_v	α	11.18	11.18	($J\ m^{-2}\ s^{-1}\ k^{-1}$)
coefficient- K_v	β	1.435	1.435	($J\ m^{-2}\ s^{-1}\ k^{-1}\ Pa^{-1}$)
coefficient- K_v	γ	0.04008	0.04008	(Pa^{-1})
Filling volume	V	3	3	(mL)
Critical product temperature	$T_{i,crit}$	-34.8	-34.8	°C
Density of ice	ρ_I	914.4	914.4	($Kg\ m^{-3}$)
Volume fraction of ice	ξ	0.97	0.97	
Ratio of the specific heat for water	k	1.33	1.33	
Water molecular weight	M	0.018	0.018	($Kg\ mol^{-1}$)

3.1.6.2 Uncertainty analysis

The uncertainty analysis was performed with the same procedure proposed by Van Bockstal *et al.* (2017). A sampling-based approach was used to perform the uncertainty analysis. In this assessment, 8 factors were considered to be uncertain and an input matrix was created using the Sobol technique. The input matrix is formed by 1,000 samples. In other words, 1,000-factor combinations were obtained as a result of varying 8 factors between their lower and upper limit. Then, 1,000 simulations were run for each grid point (combination of P_c and T_{shelf}) at each primary drying time, leading to an important computational effort.

In Figure 3.6, the procedure previously described is shown. The value of T_i is determined for each simulation, leading to a 1,000 T_i values related to one grid point. For instance, if the output of T_i is fixed at the value corresponding to the 99% upper percentile (of the distribution of the 1,000 T_i values), there is only 1% of probability that the true temperature at the sublimation front is higher than the T_i calculated by the model and the risk of failure (e.i. the risk of cake collapse) is 1%.

Repeated at each time till $L_{dried}=0$

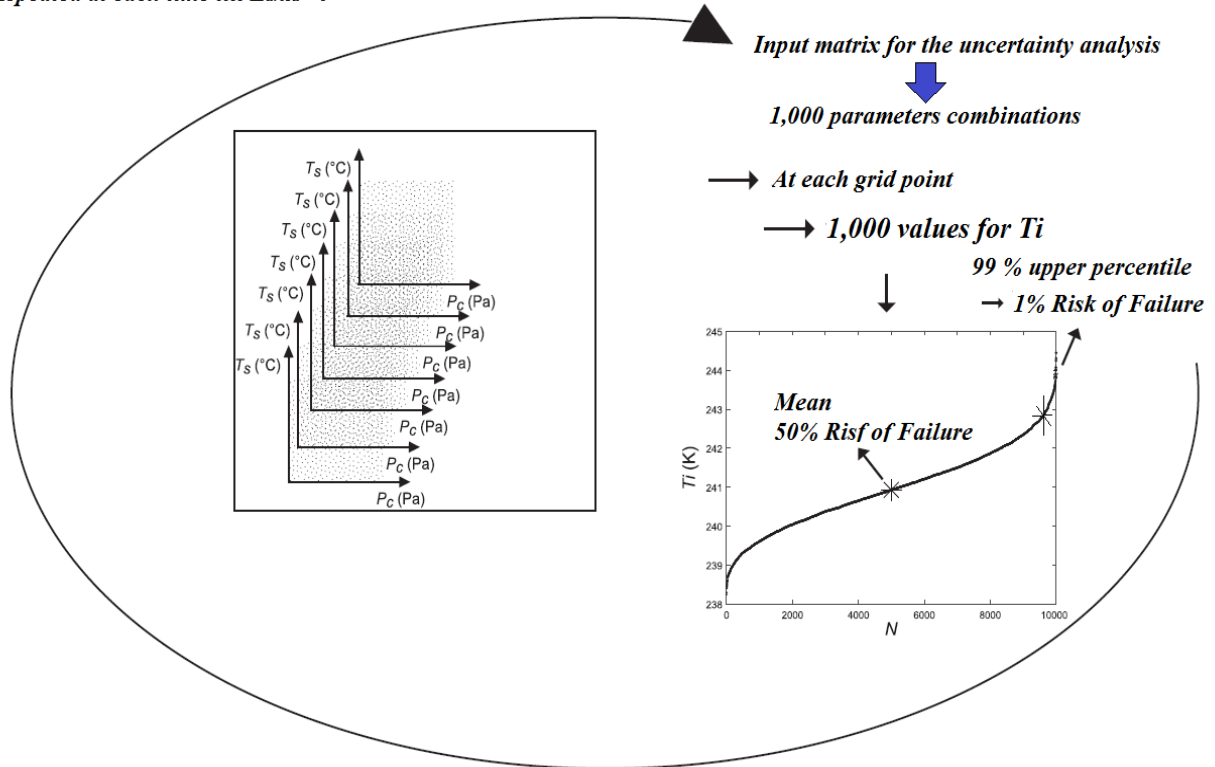


Figure 3.6: A Schematic explanation of the uncertainty analysis. For each sample (i.e. each parameter combination of the input matrix T_i was calculated. The figure shows the mean T_i and the 99% upper percentile T_i corresponding to a RoF of 50% and 1%, respectively (from Mortier *et al.*, 2016, with modifications).

Table 3.3 shows the uncertainty of each factor considered uncertain. In the case of some factors (T_{shelf} , P_c , $r_{v,i}$, $r_{v,o}$) the uncertainty is defined as an absolute value, while in the case R_p , K_v , and V a relative uncertainty is defined.

The supplier of 10R vials (Schott, Müllheim, Germany) provided the uncertainty on the inner ($r_{v,i}$) and the outer ratio ($r_{v,o}$). On the other hand, the uncertainty on P_c , T_{shelf} and K_v have been taken from previous experimental work developed by Van Bockstal *et al.* (2017). In the case of T_{shelf} , two different cases are considered. First, when T_{shelf} remains constant, the uncertainty level is 2.5°C; while in the case of a shelf ramp temperature the uncertainty changes from 2.5 to maximum 10 °C, due to the thermal inertia of the shelves. The uncertainty of R_p was determined based on experimental work and with the help of a mathematical model developed by Pisano and Capozzi, (2017), more details of the procedure are presented in section 3.1.6.3.

It is important to remark that since L_{dried} is an output and input variable, the model developed by Van Bockstal *et al.* (2017) takes into account the accumulation of error on this value, and therefore the uncertainty of L_{dried} increases during the simulation.

Table 3.3: Uncertainty level of the uncertain input parameters.

Factor	Uncertainty level	Reason of inclusion in uncertainty analysis
$r_{v,i}$	0.0001 m	Inherent error
$r_{v,o}$	0.0001 m	Inherent error
R_p	12 % - 16 %	Based in experimental data
P_c	1 Pa	Inherent error
T_{shelf}	2.5 - 10 °C	Based in experimental data (Van Bockstal <i>et al.</i> , 2017)
V	1%	Inherent error
L_{dried}	-	Error propagation considered
K_v	5%	Based in experimental data (Van Bockstal <i>et al.</i> , 2017)

3.1.6.3 Determination of the mass transfer resistance

The value R_p depends on the formulation compositions and the concentration of the excipients (Kuu *et al.*, 2006). Moreover, this parameter is linked to a high inter-vial variability due to the stochastic nature of the nucleation phenomenon that leads to porous diameter heterogeneity (Kasper and Friess, 2011). Therefore, a quantitative assessment of the R_p uncertainty is required.

In previous works, the R_p value and its uncertainty were taken from literature and those were not calculated for the specific system. In the present research, a quantitative analysis of the R_p uncertainty was included.

Once the nucleation temperature distribution has been defined (section 3.1.1), a mathematical model developed by Pisano and Capozzi, (2017) was used to correlate each nucleation temperature to a pore size diameter that changes as a function of the product thickness. Then, for each product thickness, the nucleation temperature distribution is associated with a pore diameter distribution, and consequently, the variability of the product structure within a batch can be predicted. A R_p distribution (for each value of L_{dried}) was calculated using the pore diameter distribution (associated with a product thickness) Therefore, for each L_{dried} a R_p distribution was obtained using the following equation (Geidobler and Winter, 2013):

$$R_p = \frac{3}{2} \frac{\tau^2}{\xi} \frac{1}{D_p} \sqrt{\frac{\pi RT}{2M_w}} \quad (3.16)$$

Where R is the gas constant, τ the tortuosity, D_p the pore diameter (Giordano *et al.*, 2011).

The R_p is a function of the pore size and the pore size changes with the product thickness. Therefore, the value of R_p will be affected for the intra-vial heterogeneity. In the calculation of R_p , this change of pore size as the L_{dried} increases was taken into account.

A nonlinear regression was used to fit Eq. 3.10 to the mean R_p value in function of L_{dried} and the constants R_{p0} , A_{Rp} , and B_{Rp} were obtained. The uncertainty of these coefficients is grouped into the uncertainty of the global R_p value.

The procedure described below was performed for both freezing protocols (cooling rate of 1°C/min and 0.1 °C/min).

3.1.6.4 Verification of the Dynamic Design Space

The process variables T_{shelf} and P_c were defined for three different RoF (1%, 50%, and 99%). Then, two experimental runs were performed in order to validate the dynamic design space (related with a RoF of 1% and 50%) for the studied formulation

The experimental verification of the dynamic design space were performed in a laboratory scale freeze-dryer Lyobeta 25 (Telstar, Terrassa, Spain). The vacuum-tight chamber (0.2 m³ volume) contains 4 shelves, each shelf with a heatable area of 0.16 m². The system is equipped with a condenser (35 kg of ice capacity) and a vacuum pump to evacuate the drying chamber. A capacitance manometer, Baratron Type 626 A (MKS Instruments, Andover; MA, USA) was used to control the pressure. While comparative measurements were performed using a thermal conductivity gauges (Pirani Type PSG-502-S, Inficon, Bad Ragaz, Switzerland) to determinate the primary drying end point.

The validation tests have been carried out using the same formulation studied on the determination of the nucleation temperature, that is a solution of 4% (w/v) mannitol and 1% (w/v) sucrose in phosphate buffer, pH 7.4 (0.05M) was prepared using water for injection. The solution was filtered with a 0.2 µm pore size filter and was prepared under laminar flow cabinet. A total of 100 glass vials were filled with 3 ml of the studied formulation and placed directly on one shelf using a square arrangement. The shelf temperature was linearly decreased (with a cooling rate of 1°C/min or 0.1 °C/min, respectively) until a temperature of -55°C is reached. Then, this temperature was kept constant for 5 hours. The process variables were defined for each verification run, depending on the cooling rate used in the freezing step, and the corresponding RoF. Once the primary drying offset point was determined the secondary drying was performed at 20 °C and 3 Pa, the shelf temperature ramp during the transition from primary drying to secondary drying was 0.1 °C/min in order to avoid the collapse. At the end of each cycle the chamber was vented with dry nitrogen and the vials were stoppered.

As previously mentioned, due to the edge vials were considered the limiting factor, the coefficients α , β and γ (K_v - coefficients) of the edge vials are used as input variables in the mechanistic model. This fact leads to an underestimation of the drying time, related with the slower sublimation rate of the center vials. Therefore, the primary drying stage of each run was extended. The final optimal combination of P_c and T_{shelf} predicted by the model was maintained for additional hours in order to assure the complete ice sublimation on the center vials.

The endpoint of primary drying for the whole production was computed using the K_v - coefficients (α , β , and γ) of the center vials. In this case, P_c and T_{shelf} are input variables and the output variable is the primary drying endpoint (for the center vials). The calculation is based on the complete sublimation of the ice mass and the accumulation of the L_{dried} error was not taken into account (Van Bockstal *et al.*, 2017).

Experimentally, the end point of the primary drying of each cycle was determined using comparative pressure measurements, i.e., ratio of Pirani thermal conductivity gauge and Baratron capacitance manometer, as explained in chapter 2.

The product temperature was measured via thermocouples on direct contact with the bottom of the vials, in order to evaluate whether the temperature at the sublimation front remains below the critical product temperature or not. One thermocouple was positioned on an edge-vial, while the other two were positioned in a center-vial and in a vial on the second line of the arrangement, in order to evaluate the differences between the vial positions. Once the freeze-drying cycle ended, the products were visually evaluated, to see if the cake presents signs of macroscopic collapse. The shrinkage of the cake is not considered collapse and it is attributed to the sucrose and amorphous mannitol.

3.2 Results

3.2.1 Nucleation Temperature distribution

Figure 3.7 shows how the vials were positioned on the shelves and how the nucleation time was determined for different samples; Figure 3.8 shows the product temperature profiles recorded with 6 thermocouples for the two freezing protocols.

Once the nucleation time of the vial selected with the red square was determined, this time was directly correlated with a nucleation temperature. In this particular case, due to the temperature of the vial with the thermocouple 1 and 2 were different, a linear regression was done to determine the temperature of the vial selected with the red square. The same procedure was followed in all of the vials. In the case of the slower cooling rate (0.1 °C/min), the procedure previously described was not necessary, due to the almost inexistent temperature gradient and therefore, the temperature is almost the same in all of the vials.

Figure 3.9 shows histograms of five sampling distributions (5 cycles) intended to estimate the nucleation temperature in the case of the slower cooling rate (0.1 °C/min). While Figure 3.10 shows the histograms related to a cooling rate of 1°C/min.

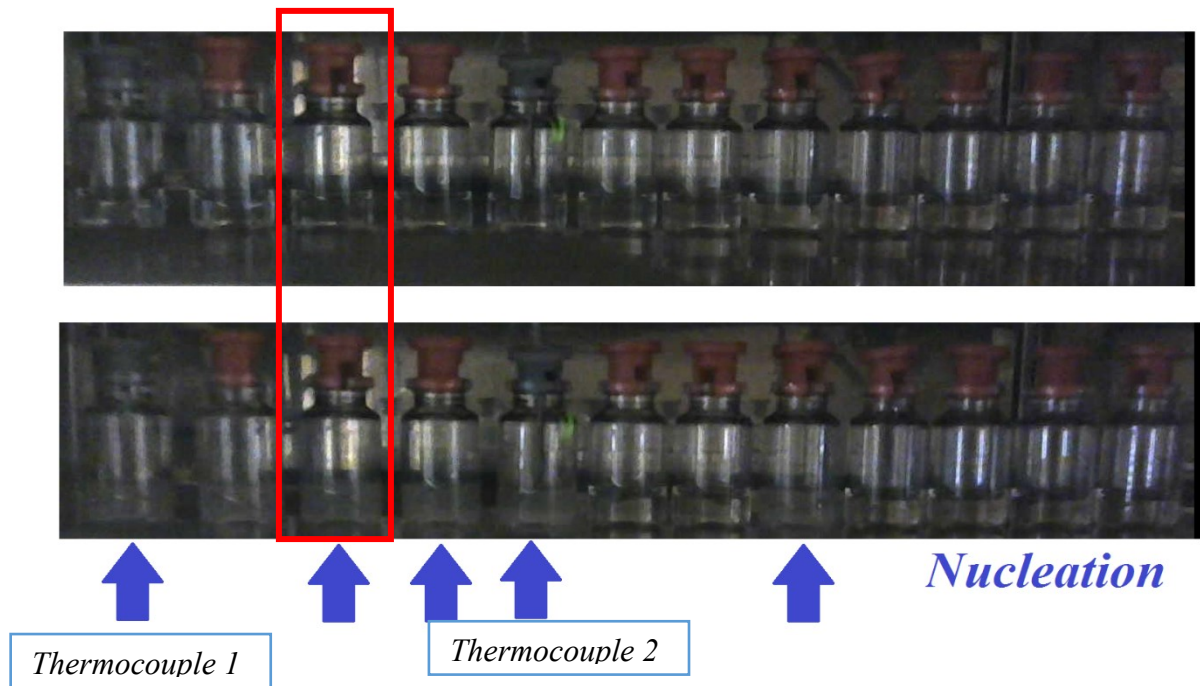


Figure 3.7: Vials positioned in the shelf at two different times (linear arrangement). The blue arrows indicate the vials where the nucleation occurred.

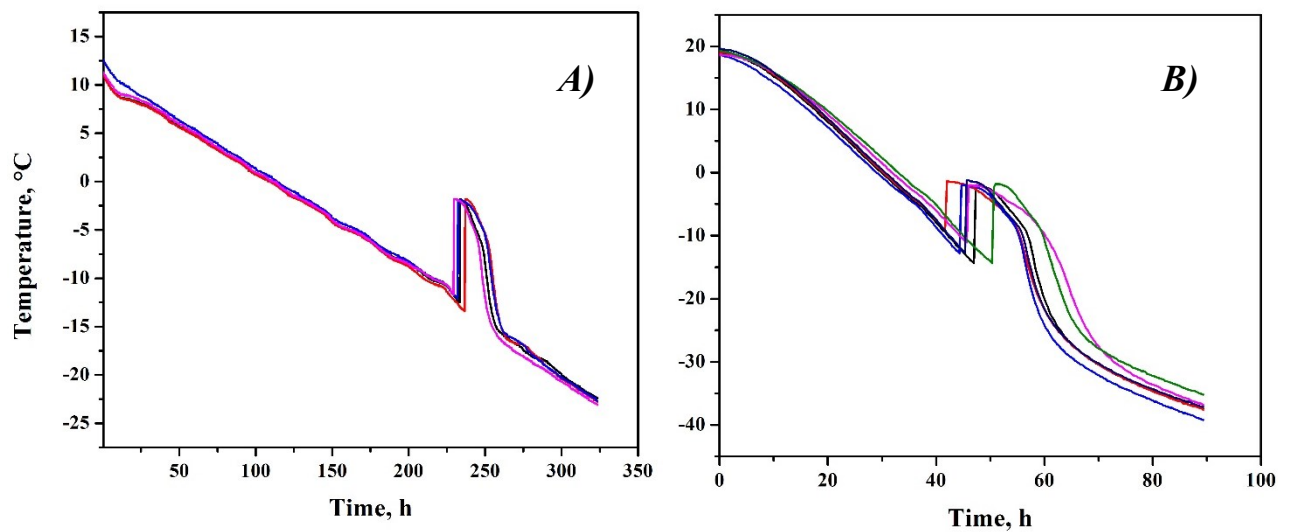


Figure 3.8: Product temperature profiles recorded with 6 thermocouples for two different freezing protocols A) Cooling rate: 0.1°C/min. B) Cooling rate: 1°C/min

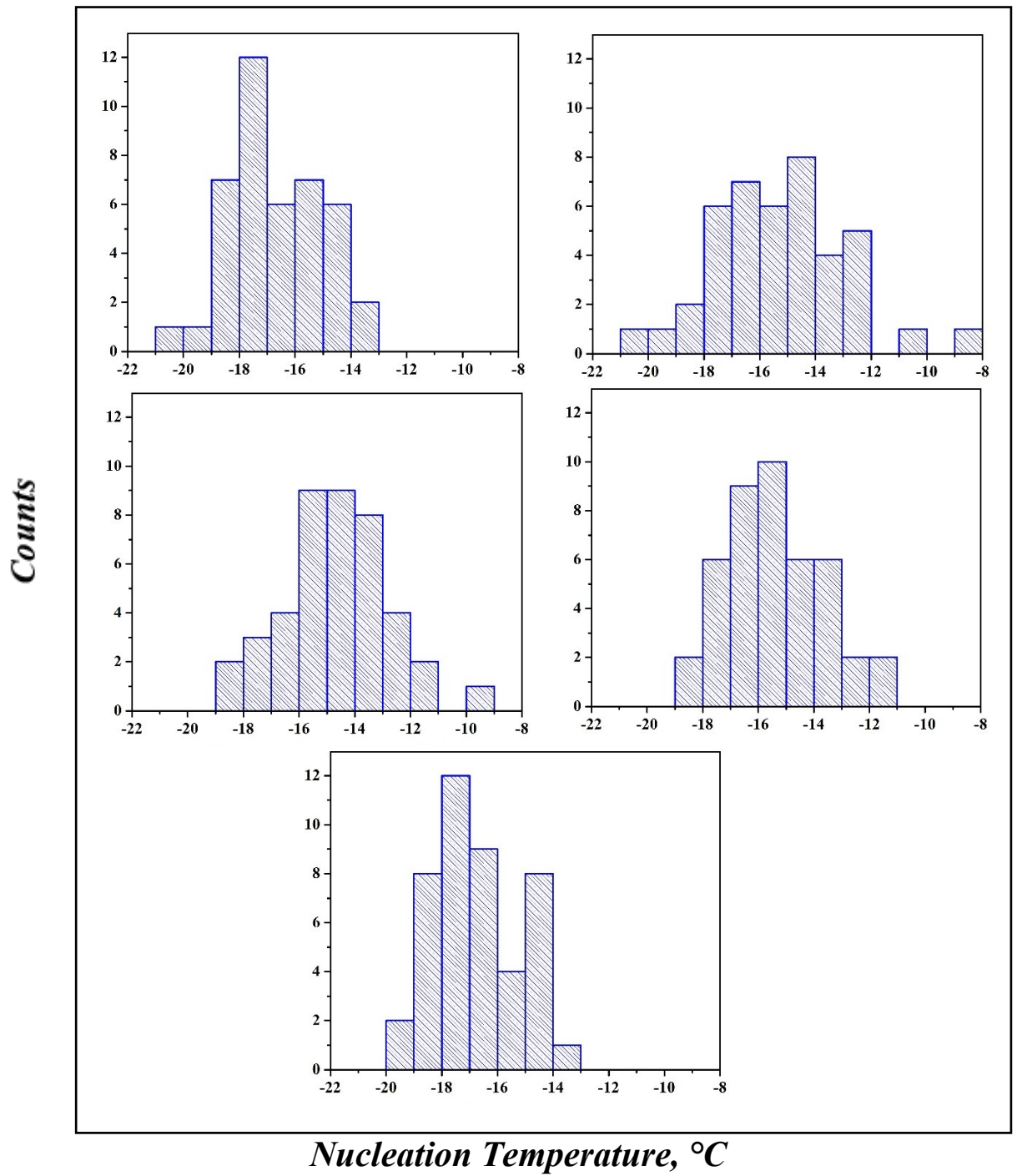


Figure 3.9: Frequency histograms of the nucleation temperature for 5 different cycles in the case of a cooling rate equal to 0.1°C/min.

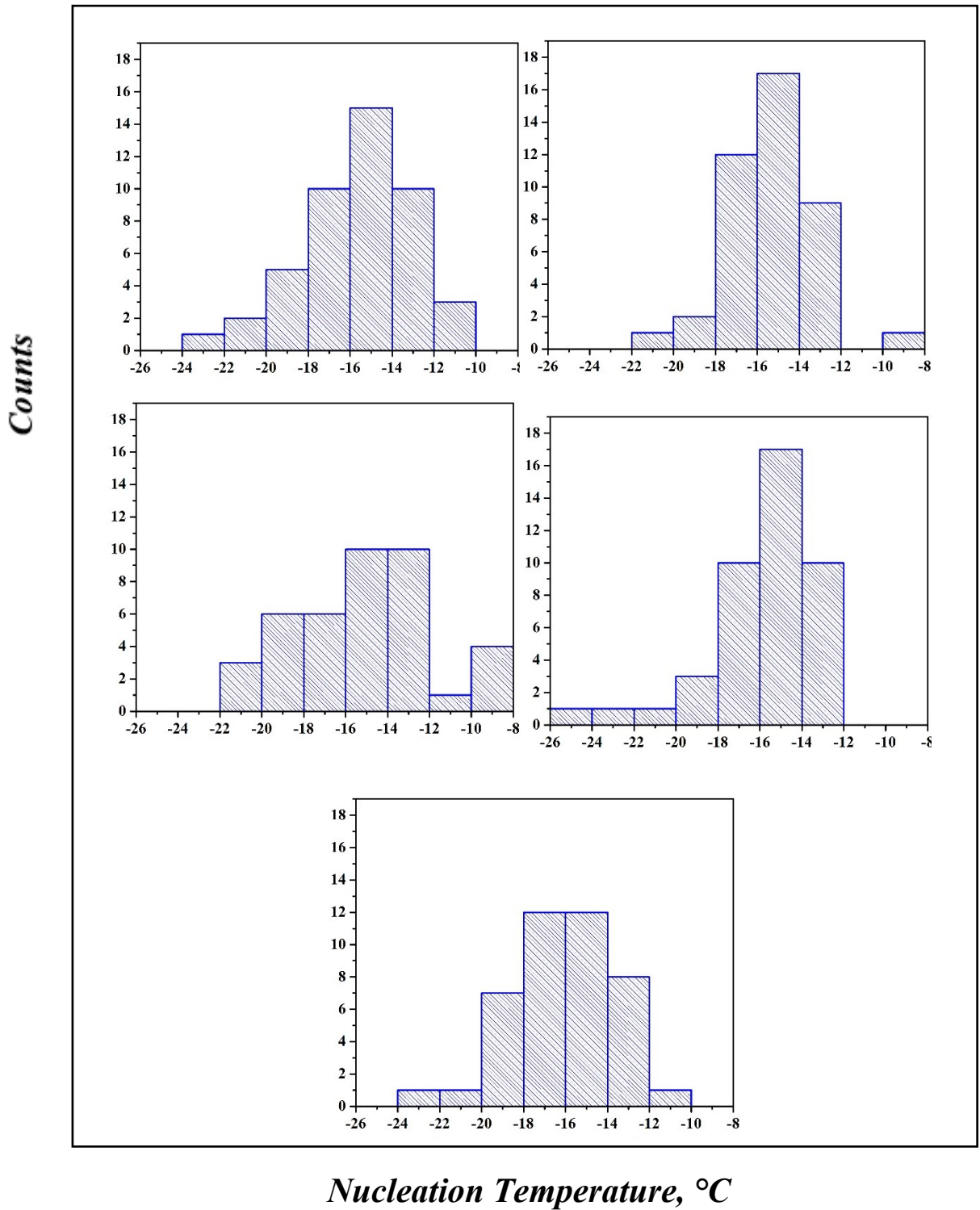


Figure 3.10: Frequency histograms of the nucleation temperature for 5 different cycles in the case of a cooling rate equal to 1°C/min.

Figure 3.11 A shows the box plots of the nucleation temperature distribution for each cycle in the case of the slower cooling rate and B in the case of the higher cooling rate. In the box plots, the top bar is the maximum observation; the bottom bar is the minimum observation. The top and bottom of the box are the third and first quartiles, respectively and the middle bar is the median value. As it is shown in all of the cases, the mean was similar for all of the cycles that belong to the same freezing protocol.

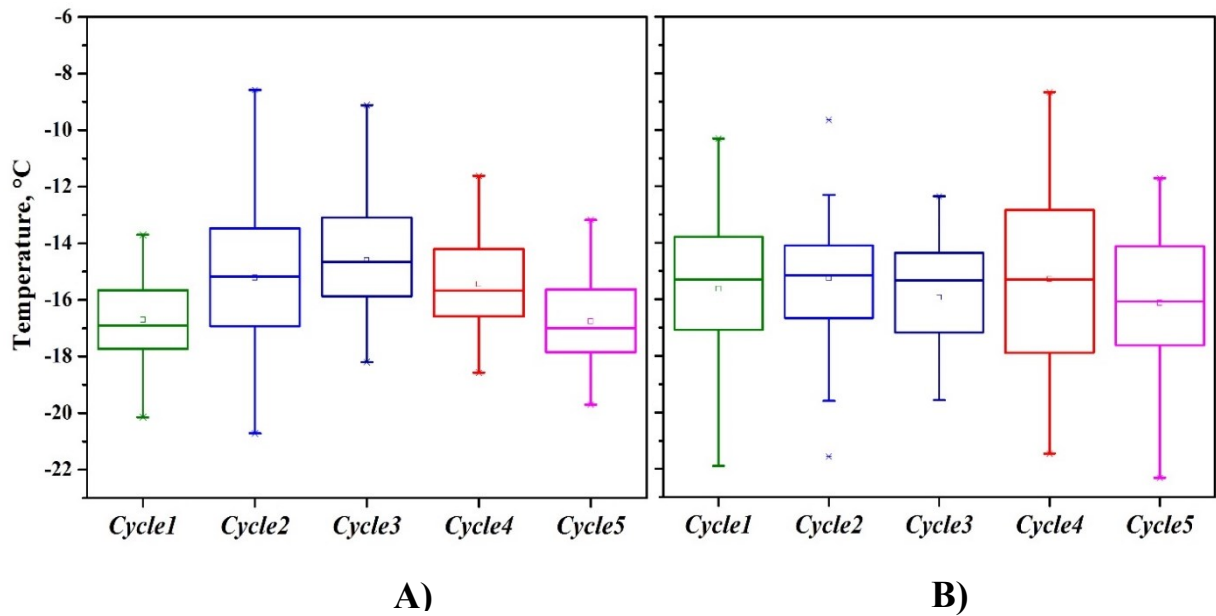


Figure 3.11: Box plots of the nucleation temperature distribution for different cycles A) Cooling rate: 0.1 °C/min. B) Cooling rate: 1 °C/min.

Table 3.4 and 3.5 present the descriptive statistics values of the nucleation temperature distribution of each cycle. For both cooling rates, the statistic values are similar for the 5 cycles.

Table 3.4: Descriptive statistics values of the nucleation temperature distribution for 5 different cycles, using a cooling rate of 0.1 °C/min.

COOLING RATE 0.1 °C/min					
	<i>Mean</i>	<i>Standard Deviation</i>	<i>Variance</i>	<i>Min value</i>	<i>Max Value</i>
<i>Cycle1</i>	-16.7	1.59	2.5	-20.1	-13.7
<i>Cycle2</i>	-15.2	2.36	5.6	-20.7	-8.6
<i>Cycle3</i>	-14.6	1.96	3.8	-18.2	-9.1
<i>Cycle4</i>	-15.4	1.72	3.0	-18.6	-11.6
<i>Cycle5</i>	-16.8	1.57	2.5	-19.7	-13.2

Table 3.5: Descriptive statistics values of the nucleation temperature distribution for 5 different cycles, using a cooling rate of 1 °C/min.

COOLING RATE 1 °C/min					
	<i>Mean</i>	<i>Standard Deviation</i>	<i>Variance</i>	<i>Min value</i>	<i>Max value</i>
<i>Cycle1</i>	-15.6	2.75	7.5	-23.1	-10.3
<i>Cycle2</i>	-15.3	2.13	4.5	-21.6	-9.6
<i>Cycle3</i>	-15.9	2.64	7.0	-24.5	-12.4
<i>Cycle4</i>	-15.3	3.35	11.2	-21.5	-8.7
<i>Cycle5</i>	-16.1	2.39	5.7	-22.3	-11.7

The final nucleation distribution for two different freezing protocols are shown in Figure 3.12 A and B. Their descriptive statistic values are presented in Table 3.6

The mean nucleation temperature for both freezing protocols is almost the same, and in both cases, a normal distribution was obtained. It is relevant to remark that there is an important difference in the value of the variance between the two protocols. In particular, the nucleation temperature distribution in the case of the higher cooling rate presented a higher variance. Contrary, the variance of the nucleation temperature distribution of a cooling rate of 0.1 °C/min was smaller.

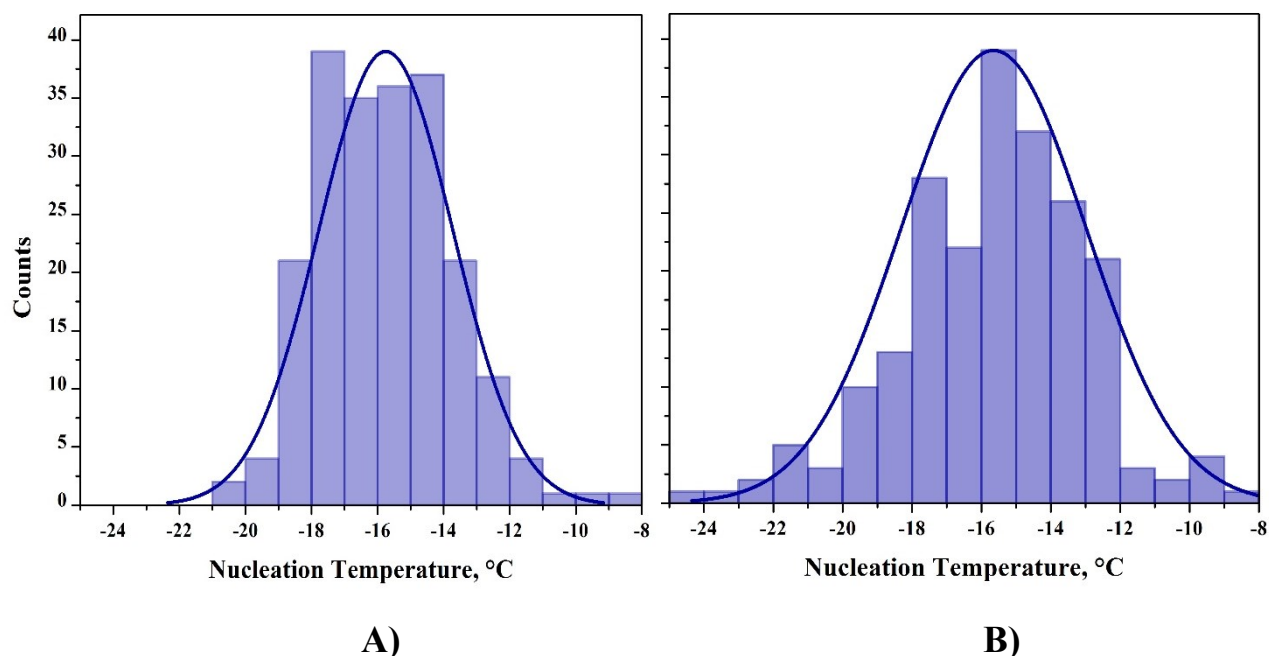


Figure 3.12: Nucleation temperature distribution for two different protocols (including 213 measurements). A) Cooling rate: 0.1 °C/min. B) Cooling rate: 1 °C/min.

This fact could be explained taking into account that in the case of the slower cooling rate, the vials remain at each temperature for more time and therefore the probability that more vials nucleates at the same range of temperature was higher than in the case of the higher cooling rate.

This difference in the variance of the nucleation temperature distribution leads to a difference on the inter-vial heterogeneity on the batch, and therefore, a higher inter-vial heterogeneity was expected in the case of the higher cooling rate (1°C/min).

Due to the heterogeneous morphology within a production, the behavior during primary drying varied from vial to vial, and therefore, the primary drying endpoint was not the same for all the vials. An analysis of the inter-vial heterogeneity was done in terms of the difference between the onset and offset time of the primary drying. Figure 3.13 shows the onset and offset time of the pressure ratio curve for both cooling rates. The onset and offset primary drying time were obtained with the same procedure described in chapter 2.

Theoretically, a higher heterogeneity within the batch leads to a higher difference between the onset and offset primary drying time (Oddone *et al.*, 2016). As figure 3.13 shows, the difference between the onset and offset point was slightly higher in the case of the cycle developed with a cooling rate of 1°C/min compared with that developed with a cooling rate of 0.1 °C/min. This result is consistent with the results obtained from the analysis of the nucleation temperature distribution.

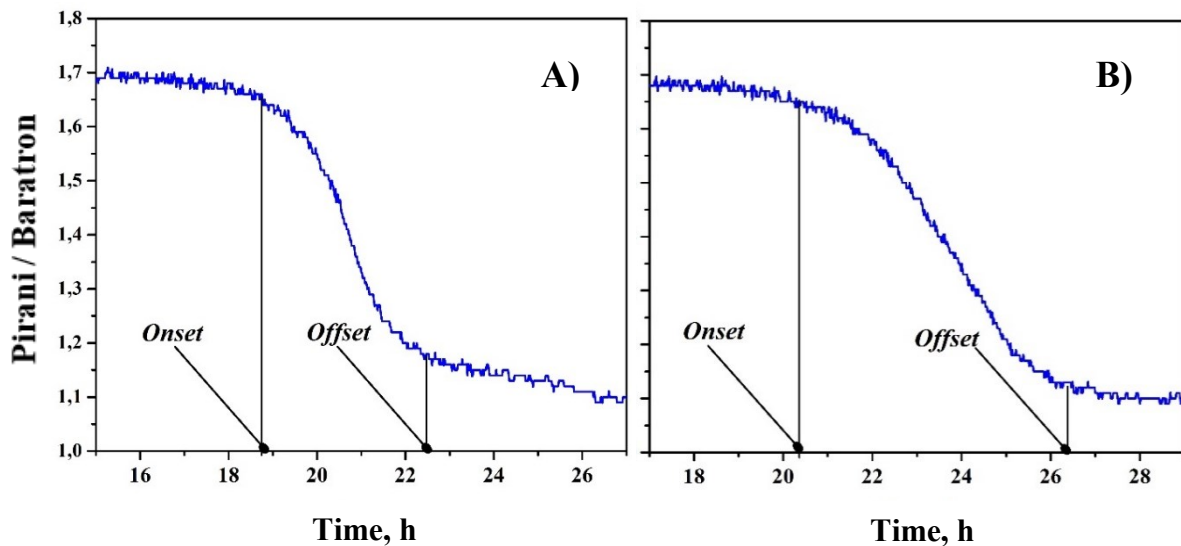


Figure 3.13: Onset-offset time of the pressure ratio curve (Pirani/Baratron) in the case of two different freezing protocols. A) Cooling rate: 0.1 °C/min. B) Cooling rate: 1 °C/min.

Table 3.6: Descriptive statistics values of the nucleation temperature distribution for two different freezing protocols.

Cooling rate	Sample Size	Mean	Standard Deviation	Variance	Min Value	Max Value
<i>1 °C/min</i>	213	-15.6	2.67	7.1	-24.5	-8.7
<i>0.1 °C/min</i>	213	-15.8	2.03	4.1	-20.7	-8.6

3.2.2 Impact of freezing conditions and T_n on within-batch and within-vial heterogeneity

Residual moisture content

Freezing conditions have an important effect on the characteristics of final products. For example, the use of different freezing protocols can lead to different physical-chemical properties, one of these properties is the specific surface area (Oddone *et al.*, 2017). Moreover, a freezing protocol could also determine differences on residual moisture content, because it determines the structure of the products. .

Even though the nucleation temperature usually affects the residual moisture content, in this work, no correlation between the nucleation temperature and the residual moisture was found and the values of residual moisture (%) were randomly spread for both cooling rates. This could be explained taking into account that the long secondary drying performed (15h) led to a so low residual moisture in the product, that data were all flattened to the same value , see Figure 3.14.

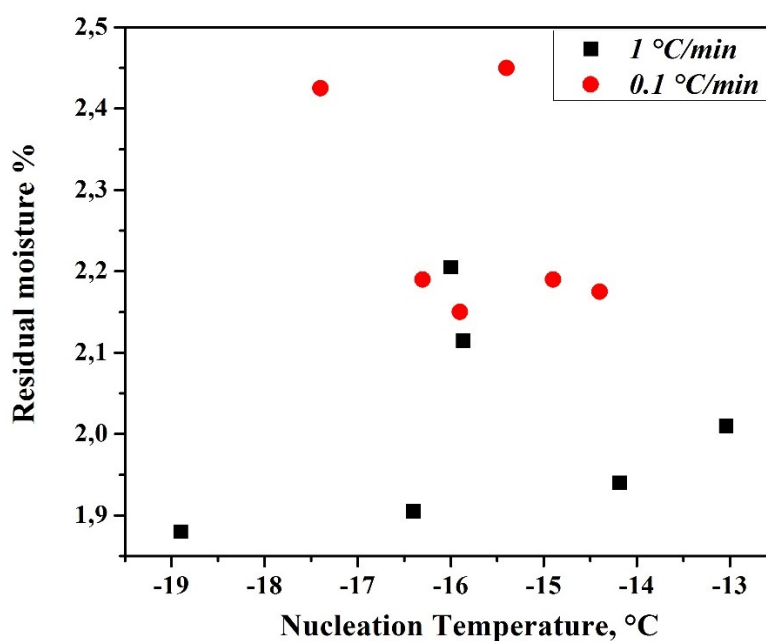


Figure 3.14: Residual moisture content after secondary drying in function of the nucleation temperature for two different freezing protocols.

Polymorphic state- Raman analysis

Impact of the freezing conditions on inter-vial heterogeneity

Center and Bottom

Figure 3.15 presents the reference spectra obtained using pure mannitol polymorphs. While in Figure 3.16 and 3.17, it is shown the loading line and the score plot of the spectra recorded

at the bottom and the center of the samples. The spectra collected at the top was not taken into account in the present analysis, because it was observed that the distribution of mannitol polymorphs within the sample was uniform, apart from near to the top of the cake.

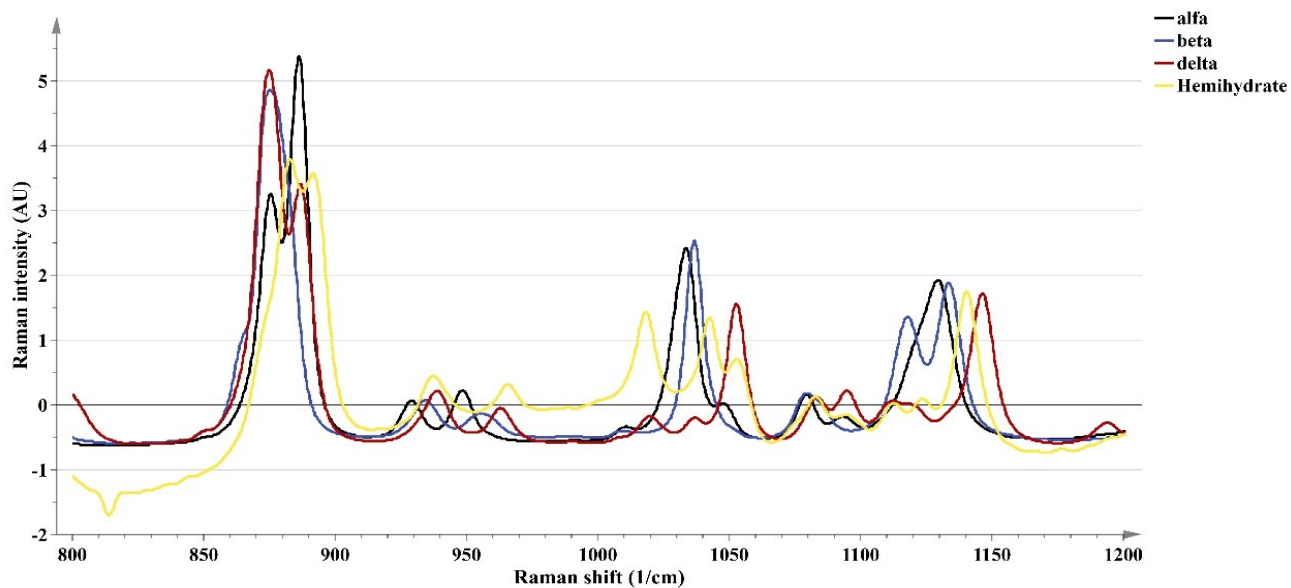


Figure 3.15: Raw spectra obtained using pure mannitol polymorphs (α , β , γ , and hemihydrate mannitol).

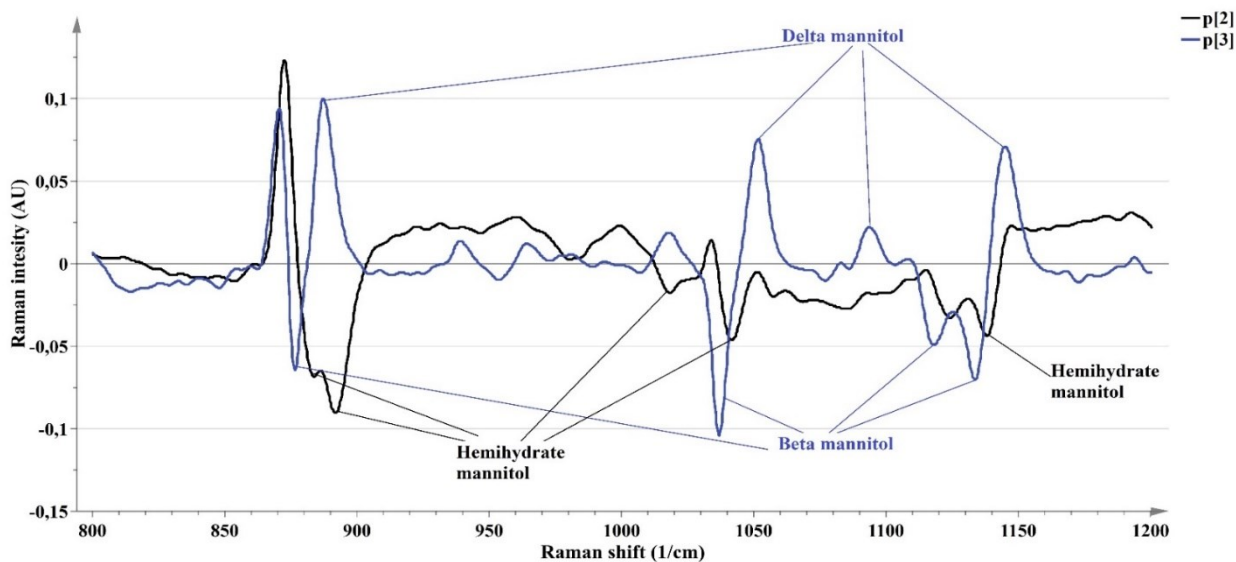


Figure 3.16: Loading line of the spectra recorded at the bottom and at the center of the samples.

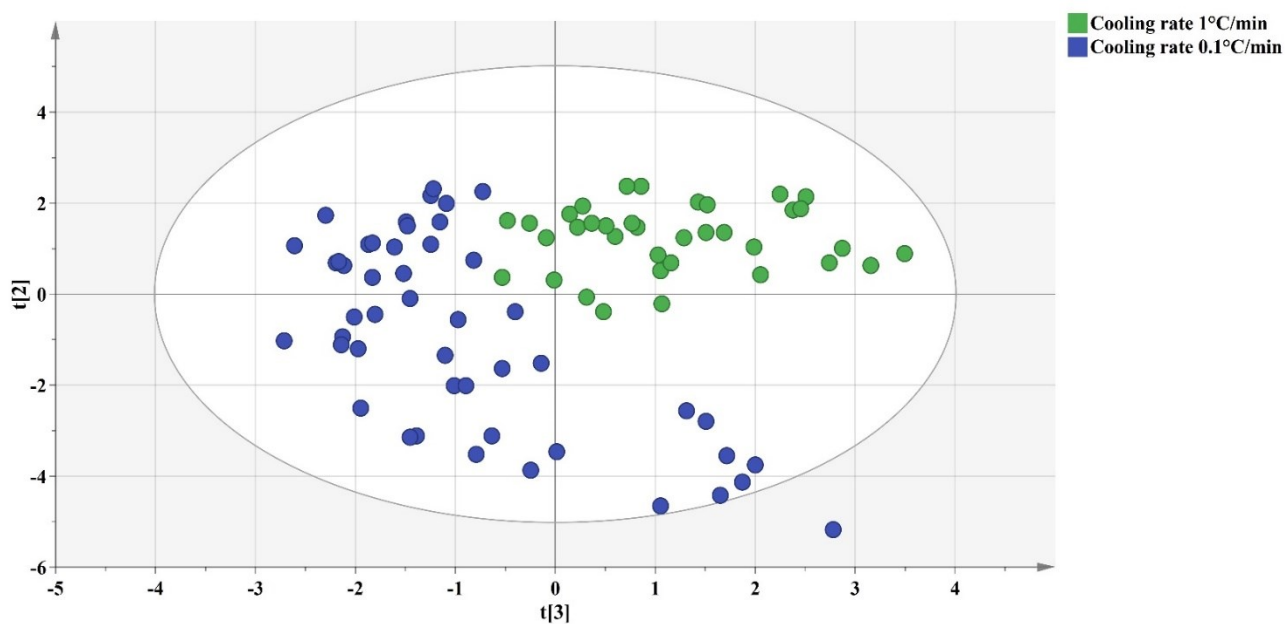


Figure 3.17: Score plot of the spectra recorded at the bottom and at the center of the samples.

The loading plot was compared with the reference spectra of pure mannitol polymorphs and, in this way, it was possible to identify specific peaks. As shown in Figure 3.16, in the case of the principal component 3 (PC3), the peaks pointing upwards matched with the characteristic peaks of delta mannitol (887 cm^{-1} , 1052 cm^{-1} , 1094 cm^{-1} , 1145 cm^{-1}), while the peaks pointing downwards matched with beta mannitol (876 cm^{-1} , 1037 cm^{-1} , 1118 cm^{-1} , 1134 cm^{-1}). The PC3 scores are plotted on the x-axis of the score plot. Consequently, the spectra near to the right side of the score plot present a higher amount of delta mannitol (and less beta mannitol) compared with those situated on the left side, in which the content of beta mannitol was higher. Based on this fact, the score plot shows a clear difference on the polymorph contained between the samples obtained with a cooling rate of $1\text{ }^{\circ}\text{C}/\text{min}$ and those with a cooling rate of $0.1\text{ }^{\circ}\text{C}/\text{min}$.

Summarizing, the samples obtained with a cooling rate of $1\text{ }^{\circ}\text{C}/\text{min}$ contained more delta mannitol (and less beta) than those with a cooling rate of $0.1\text{ }^{\circ}\text{C}/\text{min}$, which contained more beta mannitol.

To confirm these results, an individual spectral analysis was done. In Figure 3.18 is showed the raw spectra situated on three different sections of the score plot, on the left side, on the middle and the right-side (red dots). The Figure shows an increase of the intensity at 145 and 152 cm^{-1} (characteristic peak of delta mannitol) for the spectra near to the right side of the score plot (cooling rate $1\text{ }^{\circ}\text{C}/\text{min}$) and therefore, the analysis confirmed the differences in the amount of delta and beta mannitol for the two different cooling rates. Nevertheless, these differences were not dramatic, as the raw spectra of the samples presented only slight differences between the two cooling rates.

The scores of the PC2, are displayed on the y-axis. In this case, as the graph 3.16 shows, the peaks of the loading line PC2 pointing downwards matched with characteristic peaks of

hemihydrate mannitol (882 cm^{-1} , 889 cm^{-1} , 1018 cm^{-1} , 1143 cm^{-1} , 1140 cm^{-1}). Therefore, the spectra at the bottom of the score plot contained more hemihydrate mannitol than those in the top of the score plot. Analysis of the raw spectra confirmed this fact and as it is shown in Figure 3.19 the raw spectra near to the bottom of the score plot show characteristic peaks of hemihydrate mannitol.

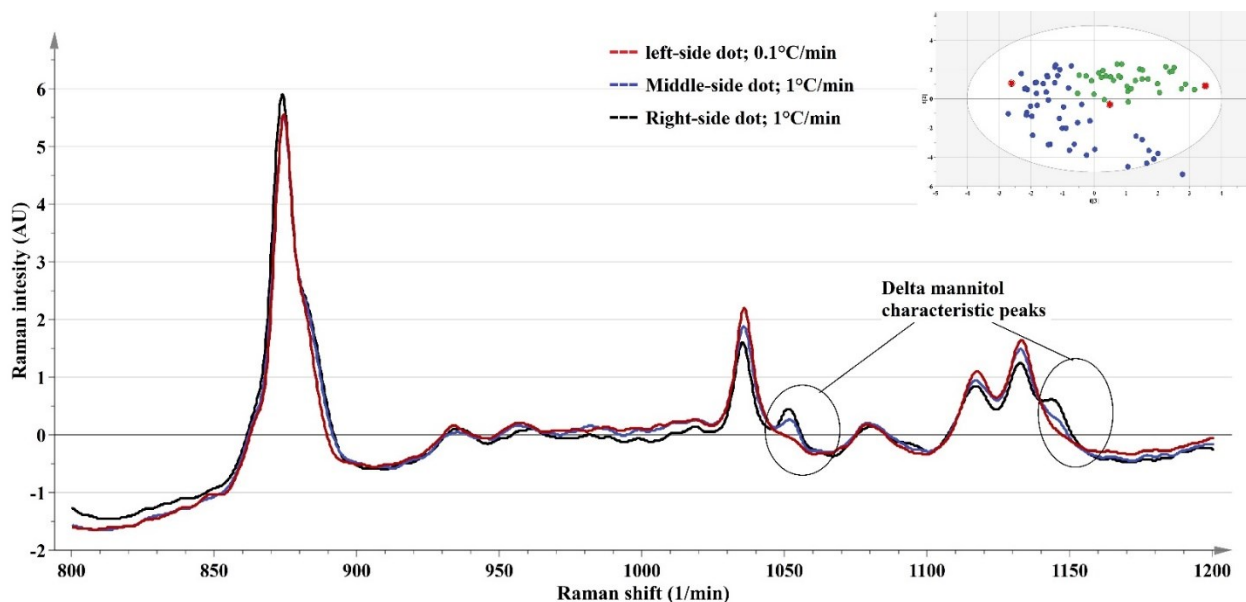


Figure 3.18: Comparison of the raw spectra situated in the left side, middle and right side of the score plot.

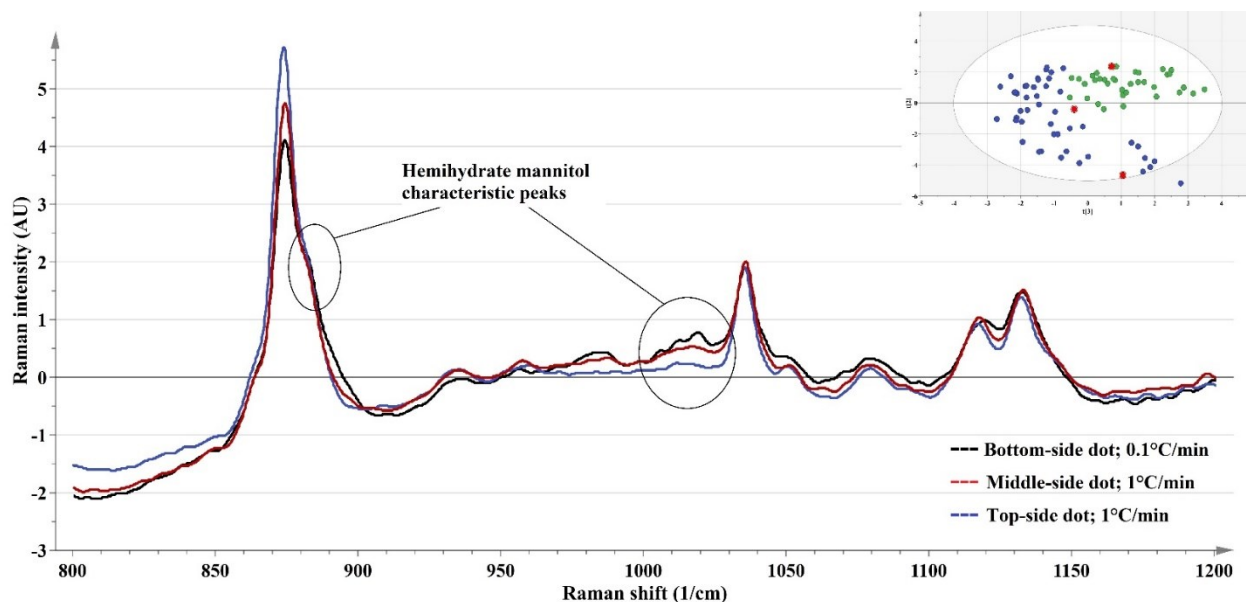


Figure 3.19: Comparison of the raw spectra situated in the top, middle and bottom of the score plot.

Top

The data assessment previously described was done also for the spectra collected at the top of the sample, and the score plot is shown on Figure 3.20; Figure 3.21 shows the loading line.

In the loading line of PC1, the peaks pointing downward coincided with characteristic peaks of delta mannitol and those pointing to the opposite direction matched with alfa mannitol. The scores of PC1 are plotted in the x-axis. Therefore, the spectra near to the right side (low cooling rate, 0.1 °C/min) contains more delta mannitol, while the spectra situated on the left side (1 °C/min) presents more alfa mannitol (and less delta). The loading line of PC2 shows characteristic peaks of beta mannitol (upwards directed peaks) and hemihydrate mannitol (downward directed peaks), see Figure 3.21. The score of PC2 is displayed on the y-axis and the same analogy used before is used to determinate the difference between the spectra located at the top or the bottom of the score plot.

The analysis of the raw spectra confirmed the information obtained from the PC analysis.

To summarize, the samples obtained with the higher cooling rate presented higher amounts of alfa mannitol (less delta) compared with those obtained using the lower cooling rate (see PC1)

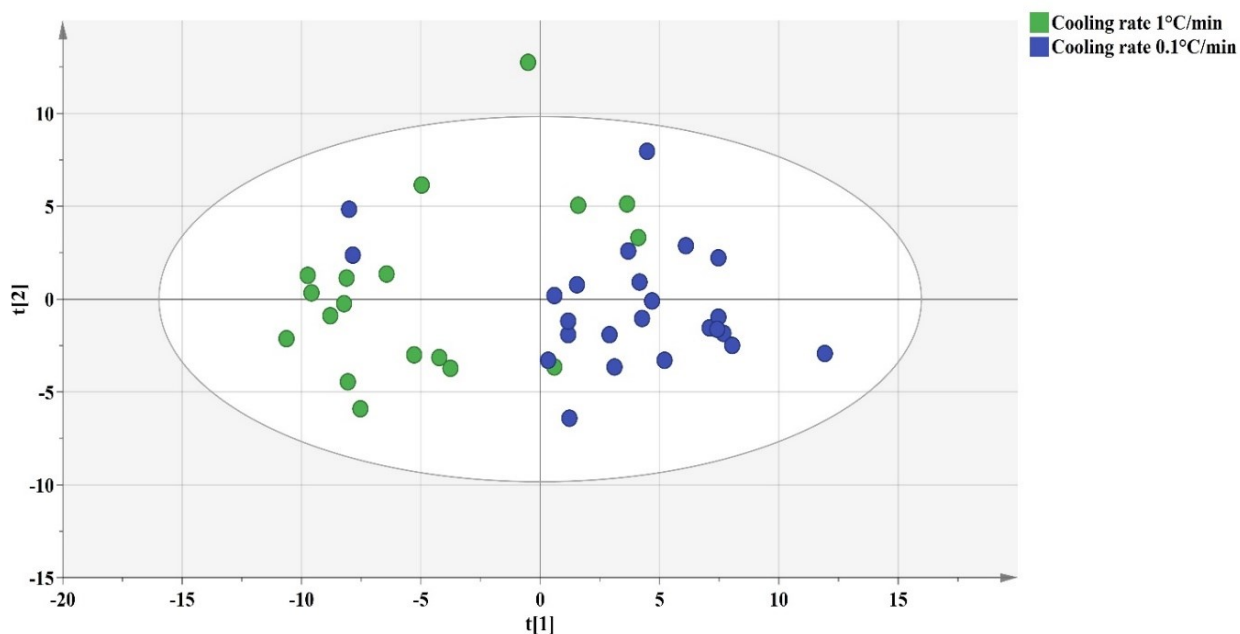


Figure 3.20: Score plot of the spectra recorded at the top of the samples.

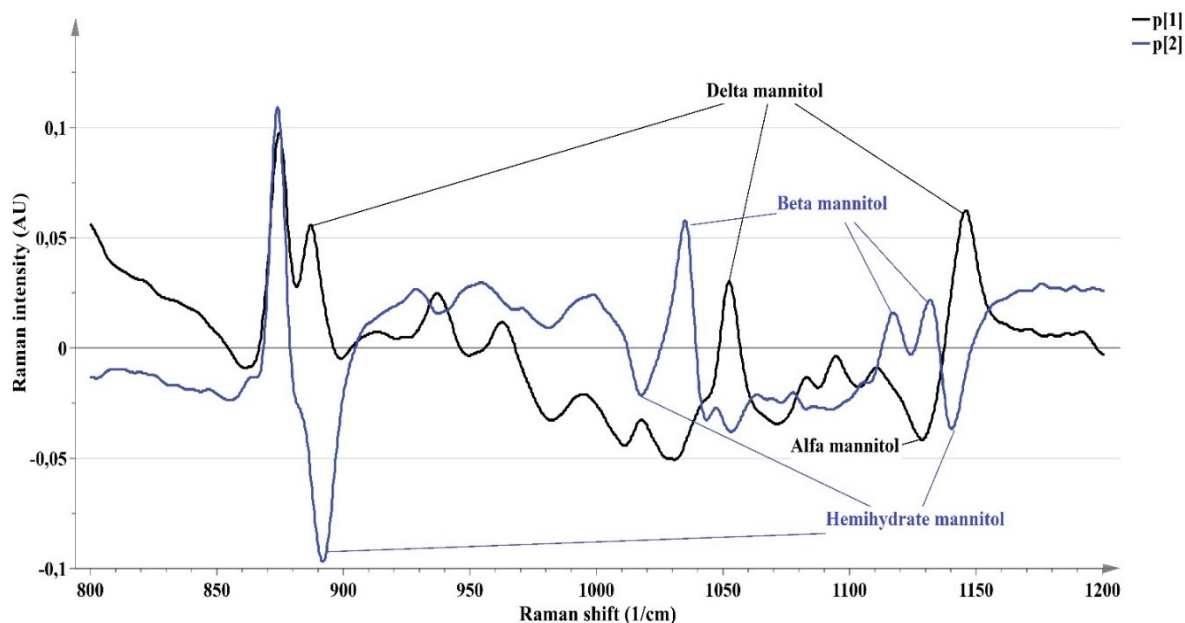


Figure 3.21: Loading line of the spectra recorded at the top of the samples.

Impact of the nucleation temperature on the polymorph contained

For both freezing protocols (high and low cooling rate), there was no correlation between the mannitol polymorph distribution and the nucleation temperature.

Intra-vial heterogeneity

As previously mentioned, the intra-vial distribution of mannitol polymorphs was uniform on the cake, with the exception of the polymorph contained near the top.

The score plot and the loading line for the spectra collected at the top, the center and the bottom of the samples are shown in Figure 3.22 and Figure 3.23, respectively. In the loading line of PC1 the peaks pointing upwards matched with the characteristic peaks of beta mannitol (876 cm^{-1} , 1037 cm^{-1} , 1118 cm^{-1} , 1134 cm^{-1}). While alpha, delta, and hemihydrate characteristic peaks are found in the opposite direction. The PC1 scores are plotted on the horizontal axis of the score plot. The spectra on the left-side of the score plot present a higher amount of delta, alfa, and hemihydrate mannitol compared with thus situated on the right side, which contains mainly beta mannitol.

The score plot (Figure 3.22) shows a clear difference between the top and the center/bottom, and the spectra collected on the top contained more alfa, delta, and hemihydrate mannitol while the spectra collected at the center and bottom presented higher amounts of beta, those for both cooling rates. No significant difference between the spectra collected in the center and the bottom (for the same cooling rate) was found. These facts were consistent with the results reported by Oddone *et al.* (2016).

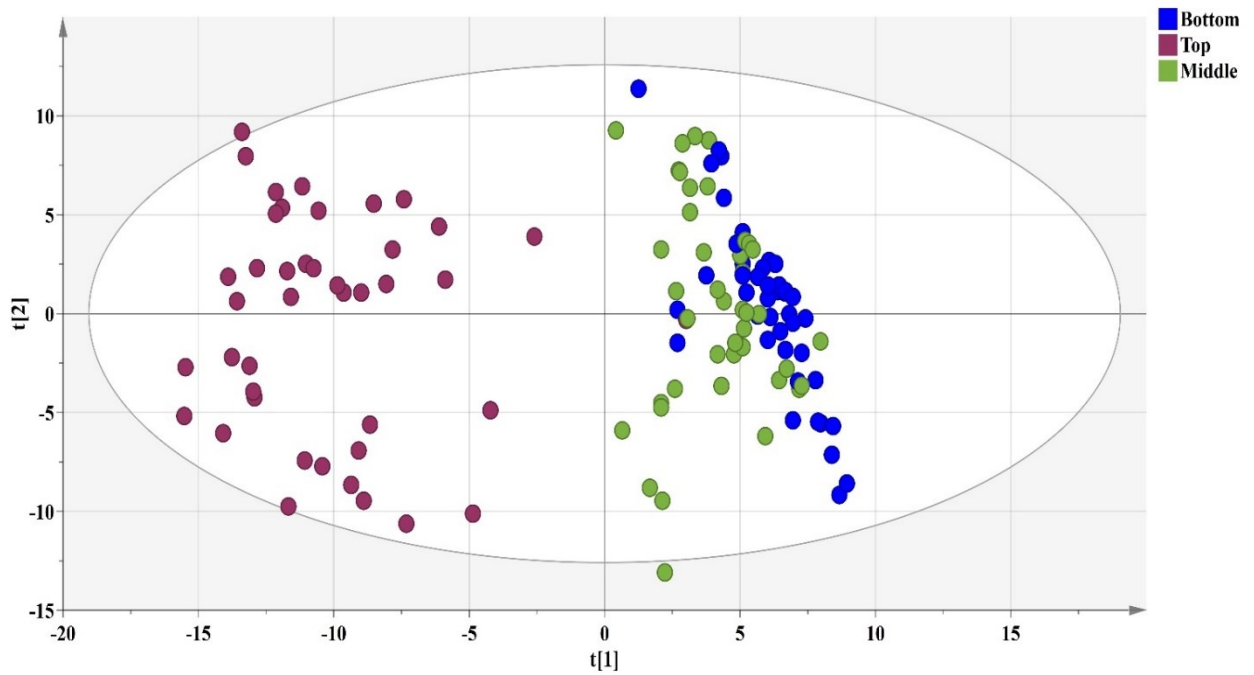


Figure 3.22: Score plot of the spectra recorded at the top, center and the bottom of the samples (for both cooling rates).

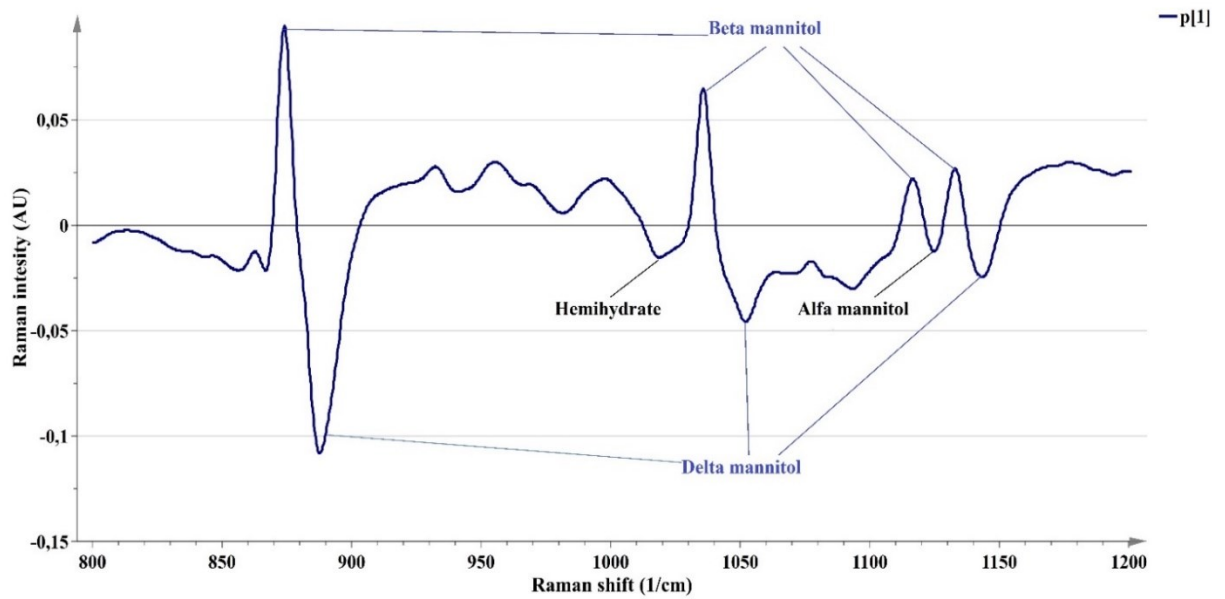


Figure 3.23: Loading line of the spectra recorded at the top, center and bottom of the samples.

The analysis of raw spectra confirmed the behavior previously described and predicted by the principal component analysis. The raw spectra taken at the top, center, and bottom of the

same sample (Figure 3.24) showed that the difference between the spectra on the top and those obtained on the center/bottom was evident.

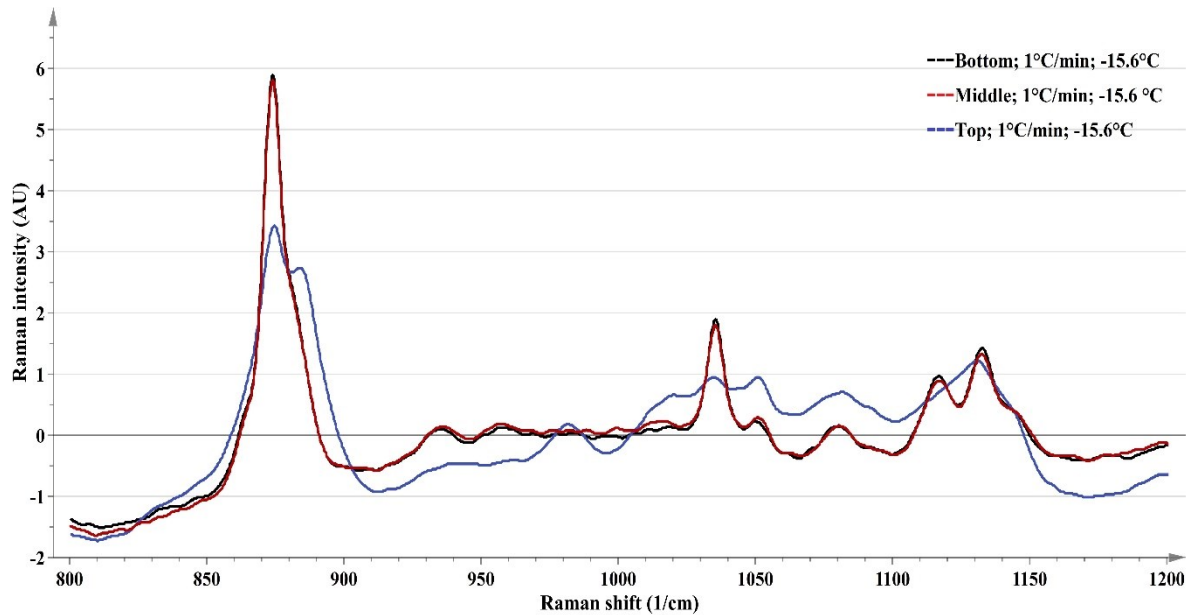
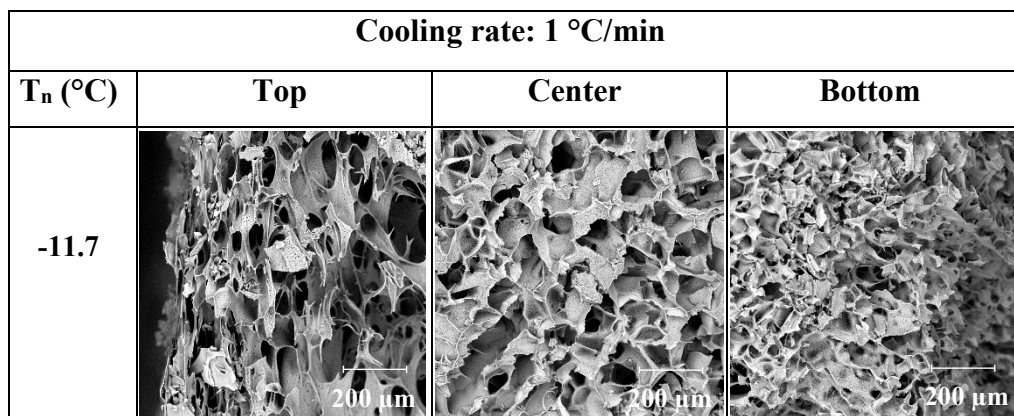


Figure 3.24: Comparison of the raw spectra collected at the top, center and bottom of one sample.

SEM-Analysis

Figure 3.25 shows the internal structure of samples (with different T_n) obtained using a cooling rate of 1°C/min. Figure 3.26 shows the internal structure of the samples obtained using a slower cooling (0.1°C/min) rate.



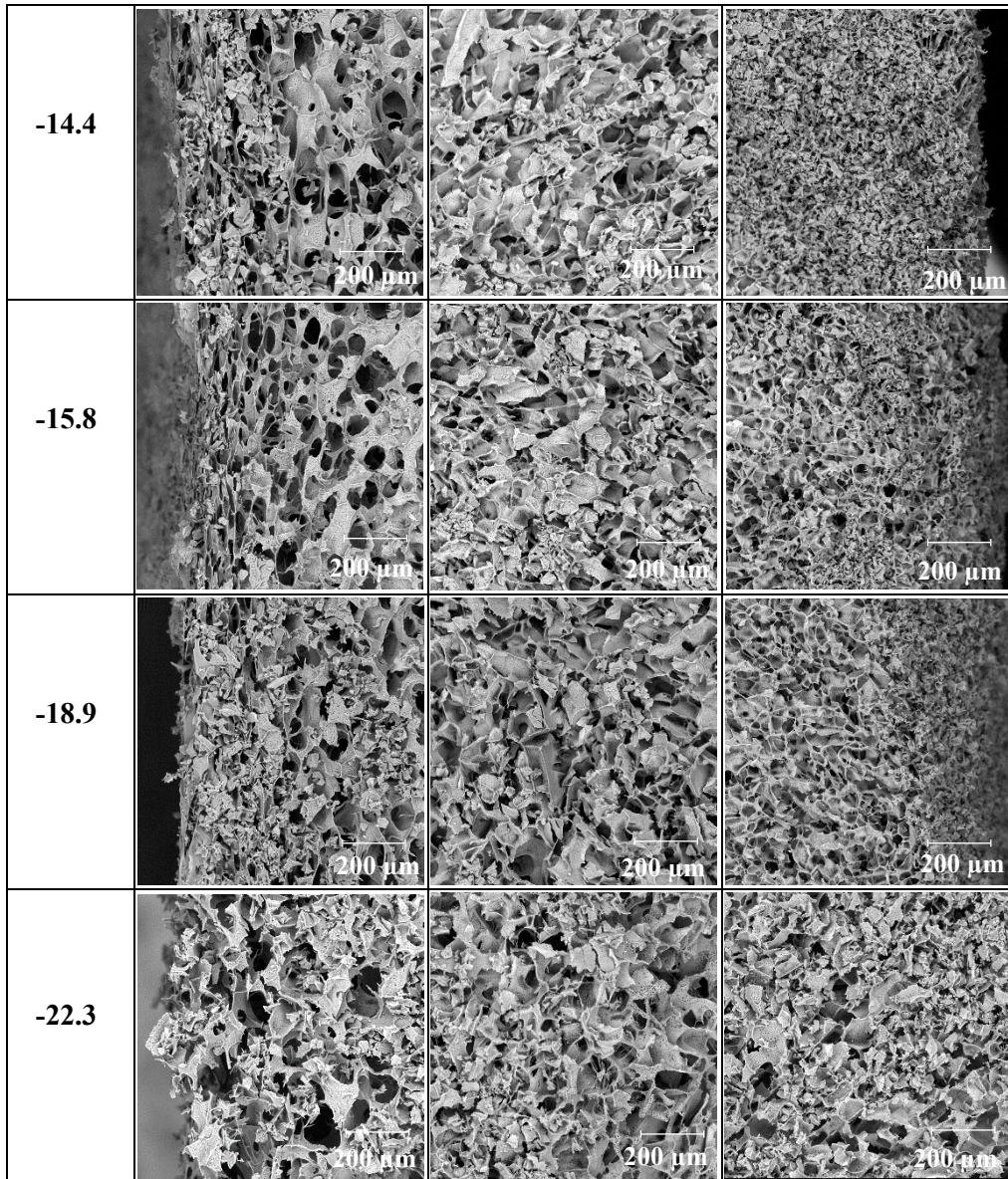
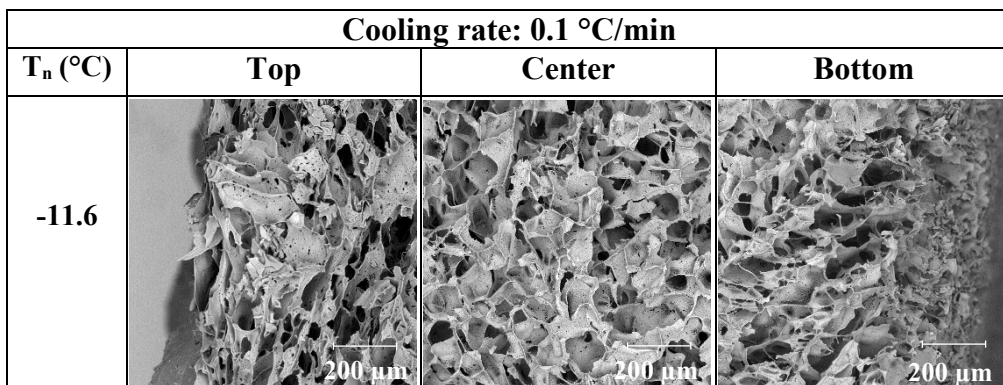


Figure 3.25: SEM images collected at the top, center and at the bottom of the sample. 5 samples with different T_n were analyzed.



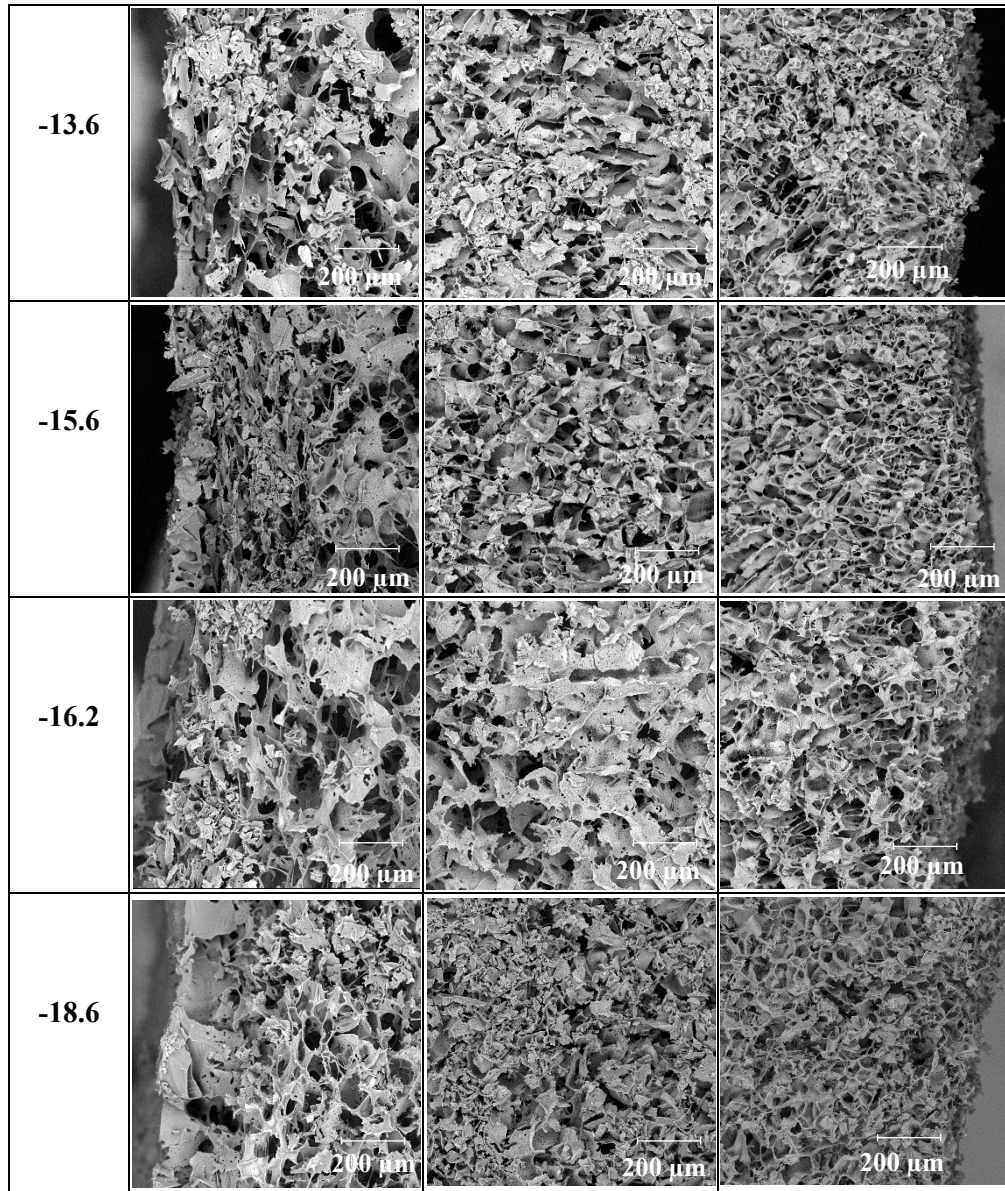


Figure 3.26: SEM images collected at the top, center and at the bottom of the sample. 5 samples with different T_n were analyzed.

The average pore size on the bottom, center, and top, for each sample are plotted in Figure 3.27; Figure 3.27 A shows the data obtained using the slower cooling rate (0.1°C/min) and Figure 3.27 B the values associated with a higher cooling rate (1°C/min).

As shown in the SEM images (Figure 3.25 and 3.26) and in Figure 3.27, in almost all the cases, at the center of the sample the average pore size is larger than at the top or at the bottom. These results are consistent with previous results reported by several researchers (Oddone *et al.*, 2016; Pisano and Capozzi, 2017).

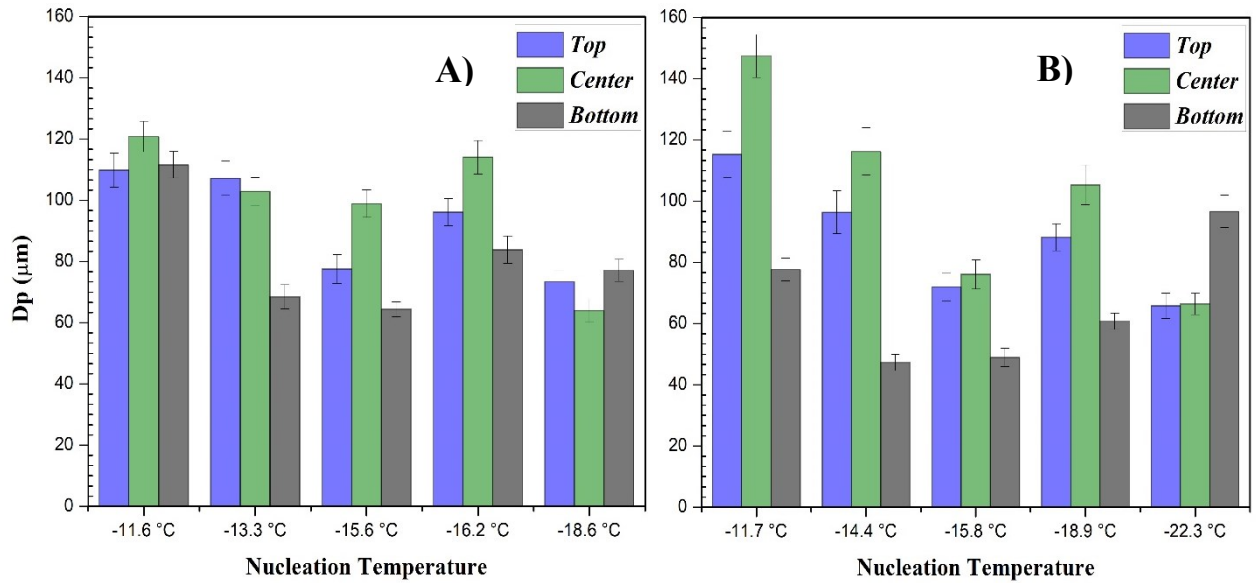


Figure 3.27: Average pore diameter at the top, center and Bottom of the sample. A) For the lower cooling rate (0.1°C/min). B) For the higher cooling rate (1°C/min).

The SEM images show that the intra-vial variability is higher in the case of the higher cooling rate. This could be explained considering the higher temperature gradient within the vial associated with higher cooling rates (Kasper and Friess, 2011).

Moreover, for both cooling rates, higher nucleation temperatures were usually related with larger pore sizes. While the opposite occurred in the case of lower nucleation temperature. Nevertheless, this behavior presented some deviations. Even though the pore size was strongly affected by the nucleation temperature, this was not the only factor that defines the product morphology.

3.2.3 Experimental determination of the heat transfer coefficient

K_v was determined for a chamber pressure equal to 10 Pa using the same vial arrangement (linear array) shown in Figure 3.7. The result obtained ($36.9 \text{ W m}^{-2}\text{k}^{-1}$) is higher than the value reported in the literature for the same vials and freeze-drier (Van Bockstal *et al.*, 2017). However, this difference can be explained taking into account the different distribution of the vials inside the chamber. This value was then used in section 3.2.4 for the prediction of product morphology.

3.2.4 Prediction of the product morphology.

Figure 3.28 and 3.29 present a comparison between the average pore diameter obtained via SEM observations and model predictions for samples obtained using a cooling rate of 0.1°C/min and 1°C/min, respectively (in the figures, each sample is related to a nucleation

temperature). These results show that there is a good agreement between the morphology predicted by the model and those obtained via SEM observations especially in the case of the lower cooling rate.

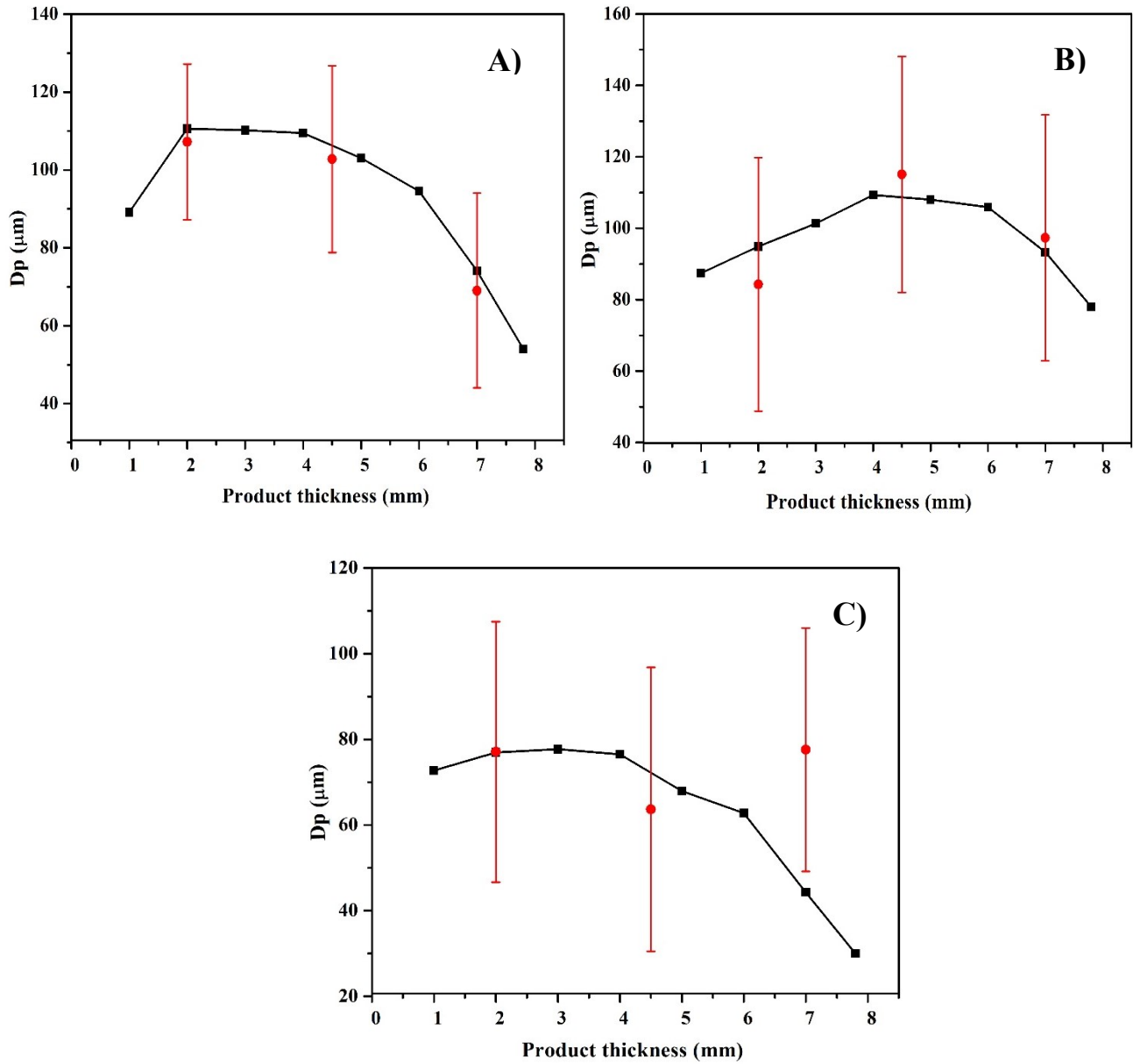


Figure 3.28: Comparison between the average pore diameter obtained via SEM observations and model predictions for samples obtained using a cooling rate of 0.1 °C/min. Sample with a nucleation temperature of: A) -13.3 °C. B) -16.6 °C. C) -18.6 °C.

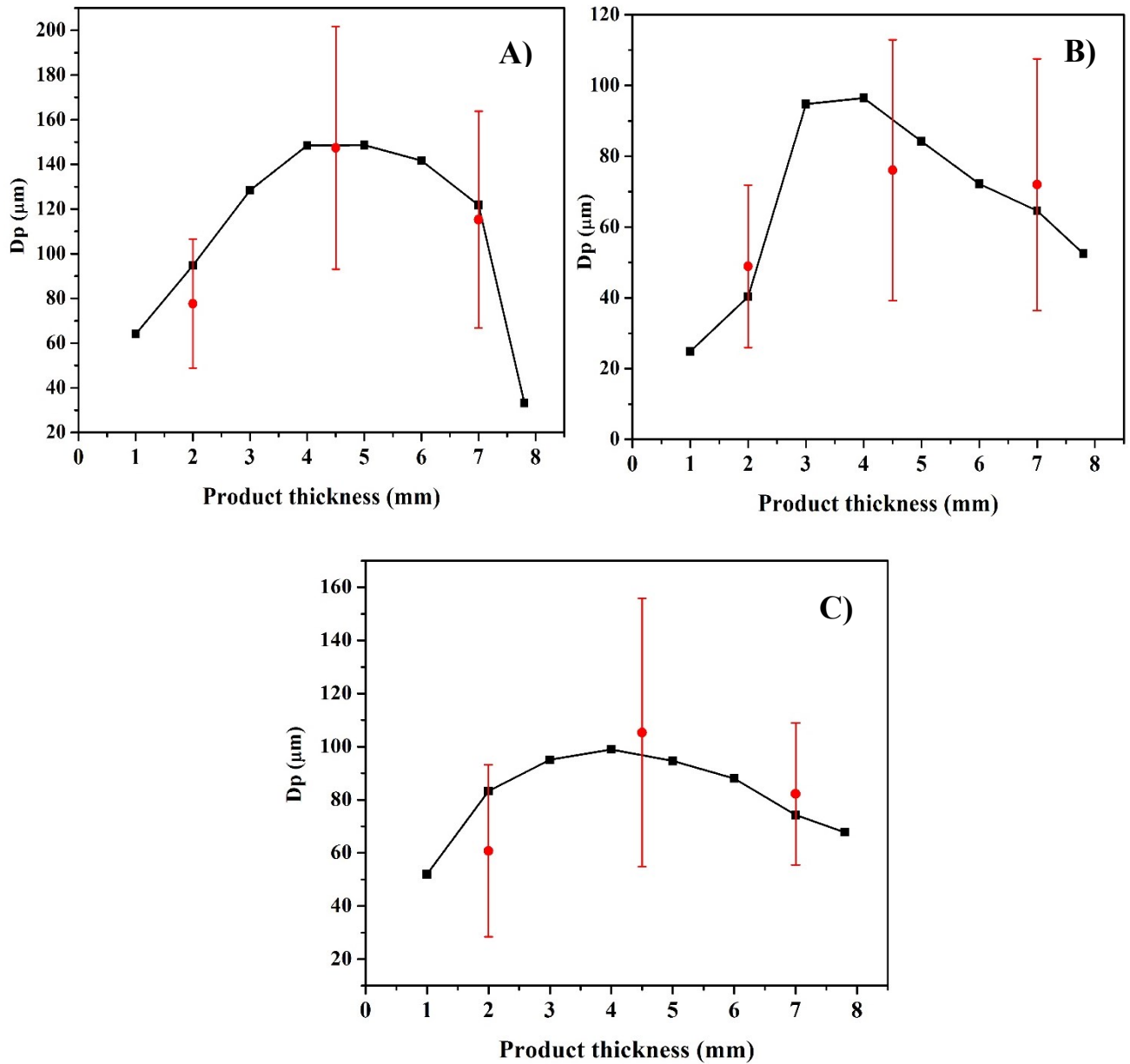


Figure 3.29: Comparison between the average pore diameter obtained via SEM observations and model predictions for samples obtained using a cooling rate of 1 °C/min. Sample with a nucleation temperature of: A) -11.4 °C. B) -15.8 °C. C) -18.9 °C.

Once the agreement between the model and the experimental results were verified, the sample population of each freezing protocol was divided into 9 classes. Each class is related to a nucleation temperature (T_n) and contains all the samples that nucleates between $T_n \pm \Delta y$, where Δy is 1 °C in the case of the slower cooling rate and 1.5 °C when a cooling rate of 1 °C/min was used.

For each class, the product morphology and the intra-vial variability were predicted. Figure 3.30 shows an example of the pore size distribution of 4 different classes (each related with

a T_n). Each class has a frequency associated (due to the frequency associated to each T_n), and a pore size distribution can be determined for each product thickness.

All the simulations predicted a larger average pore size in the center of the sample. This result is consistent with the observations (SEM images) in section 3.2.2.

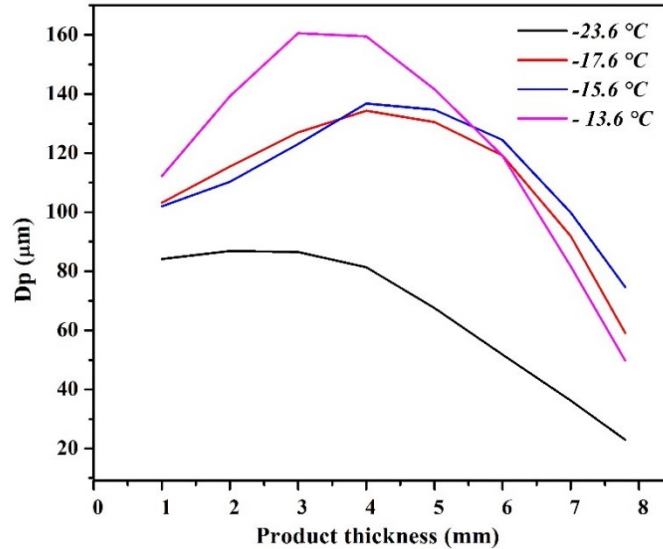


Figure 3.30: Pore size distribution of 4 different classes (each related with a T_n) (for a cooling rate of: 0.1 °C/min).

3.2.5 Determination of the mass transfer resistance.

Using the information of the predicted product morphology (section 3.2.4), R_p and its uncertainty level were calculated as a function of L_{dried} . The uncertainty level was defined as the relative standard deviations associated to each R_p distribution.

R_p as a function of L_{dried} is displayed in Figure 3.31 for each cooling rate. The dashed lines represent the upper and lower limit of R_p .

As previously was discussed, the R_p is a function of the pore size and as the SEM analysis and the simulation showed, the pore size changes with the product thickness. Therefore, the value of R_p will be affected for the intra-vial heterogeneity. In the calculation of the R_p value, this change of pore size as the L_{dried} increased was taken into account.

Overall, the uncertainty level is higher in the case of the higher cooling rate than in the case of the slower cooling rate (16% in front of 12 %). This result is consistent with the nucleation temperature distributions of the different freezing protocols (section 3.2.1), where a higher cooling rate leads to a higher variability in terms of nucleation temperature, and therefore a higher inter-vial variability is observed.

For both freezing protocols, non-linear regression was applied to fit Eq.3.10 to the data obtained and the R_p -coefficients were determined. Table 3.7 shows the final results. It is

important to remark that the uncertainty level used later in the dynamic design space, was defined respect the total R_p value and not respect to the R_p -coefficients.

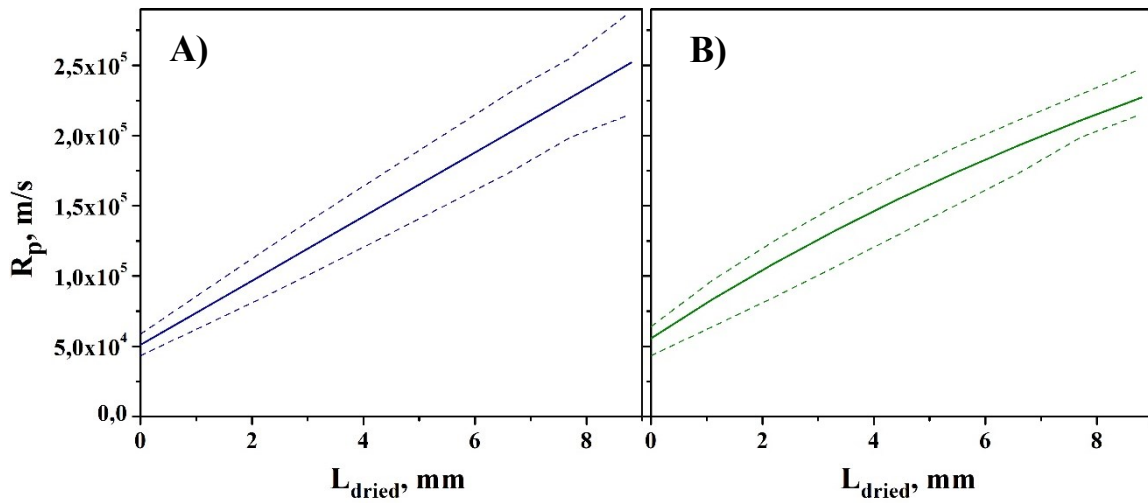


Figure 3.31: R_p in function of L_{dried} , the dashed lines represent the upper and lower limit of R_p . A) Cooling rate : $1^\circ\text{C}/\text{min}$. B) Cooling rate: $0.1^\circ\text{C}/\text{min}$.

Table 3.7: R_p -coefficients for two different freezing protocols.

	$1^\circ\text{C}/\text{min}$	$0.1^\circ\text{C}/\text{min}$
R_{po}	51051.27	55705.63
$A R_p$	22817.21	26239.42
$B R_p$	0.00	0.04

3.2.6 Dynamic Design space of primary drying for different risk of failure

Figure 3.32 represents the optimal values of P_c and T_{shelf} , for a RoF of 1% (in the case of a cooling rate of $1^\circ\text{C}/\text{min}$).

There are two stages simulated by the mechanistic model. Initially, T_{shelf} is equal to -55°C (the final temperature of the freezing step) and the chamber pressure is reduced from 100,000 Pa to 10 Pa in 10 min. During this step is assumed that the T_{shelf} remains constant. When the sublimation starts, the optimal value of T_{shelf} starts to increase at the maximum rate allowed by the equipment ($1^\circ\text{C}/\text{min}$), then after 1.50 h, the T_{shelf} reaches the highest value (-14°C) allowed.

After this, T_{shelf} remains almost constant and evolved with a slow rate towards a lower temperature (-15.5°C).

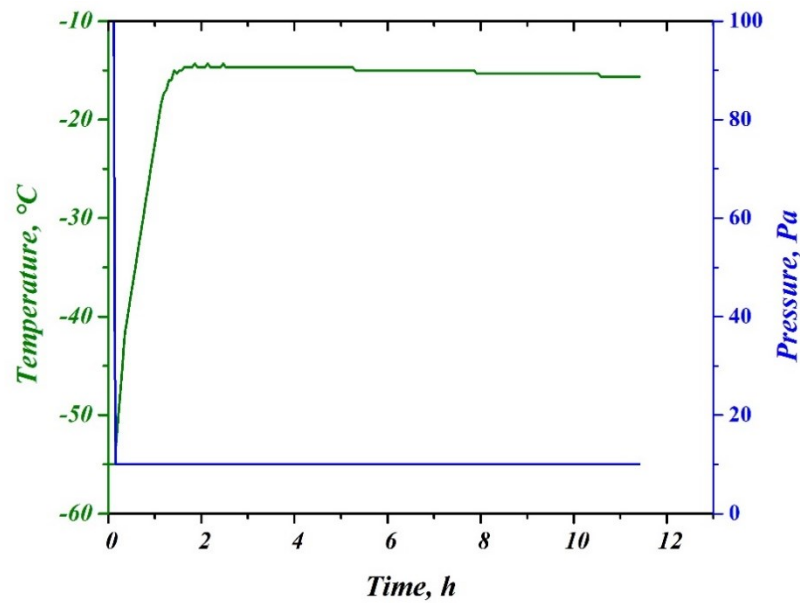


Figure 3.32: Optimal T_{shelf} and P_c in function of time for a RoF of 1% and a cooling rate of $1^{\circ}\text{C}/\text{min}$.

In Figure 3.33 the uncertainty of T_{shelf} is plotted. The T_{shelf} uncertainty varies from 2.5 to 10°C , and it is asymmetric (higher at the lower boundary) due to the thermal inertia (Van Bockstal *et al.*, 2017)

In the case of the chamber pressure, once its value reaches 10 Pa, it remains constant during the whole primary drying.

In Figure 3.34, the optimal values of T_{shelf} for different RoFs in function of time are represented, A) represents the case of a freezing protocol with a cooling rate of $1^{\circ}\text{C}/\text{min}$ and B) the case of the slower cooling rate ($0.1^{\circ}\text{C}/\text{min}$). The chamber pressure did not present differences between the different RoF and once its value reached 10 Pa, it remained constant.

As the Figures shown, a higher RoF is associated with a higher T_{shelf} and therefore, with a shorter primary drying. In the case of the higher cooling rate, the difference of the maximum value of T_{shelf} between a RoF of 1% and 99% was 16°C . While in the case of the lower cooling rate that difference was 11°C .

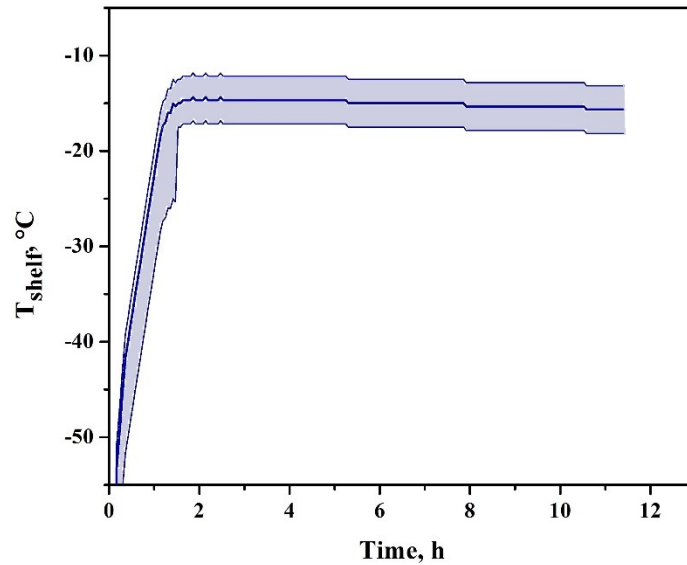


Figure 3.33: T_{shelf} uncertainty level for a RoF of 1% and a cooling rate of 1 °C/min.

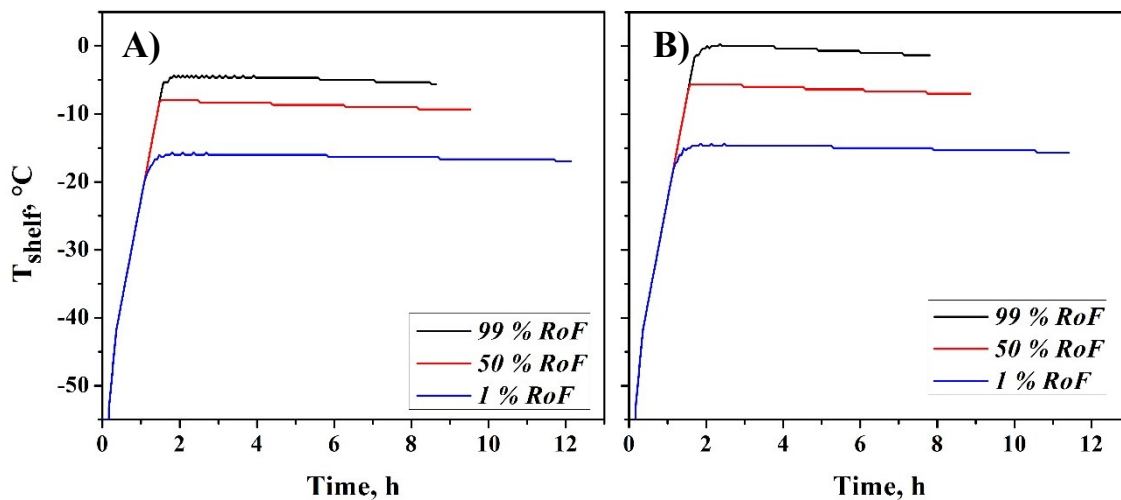


Figure 3.34: Optimal values for T_{shelf} in function of time for a RoF of 1%, 50% and 90 %. A) For a cooling rate of: 0.1°C/min. B) For a cooling rate of: 1 °C/min.

The evolution of L_{dried} during primary drying for different RoF is plotted on Figure 3.35 A) for a cooling rate of 1°C/min and in Figure 3.35 B) for a cooling rate of 0.1 °C/min. As the Figure shown, at the beginning of the process L_{dried} remained at 0 as long as the vapor pressure at the sublimation front (P_i) was lower than the chamber pressure (P_c) and the sublimation cannot occur.

Once P_i was higher than P_c the sublimation started and L_{dried} gradually increased. The slope of the evolution of L_{dried} in function of time increased when the RoF increased, and consequently, the sublimation rate was higher for the process conditions defined with a higher RoF.

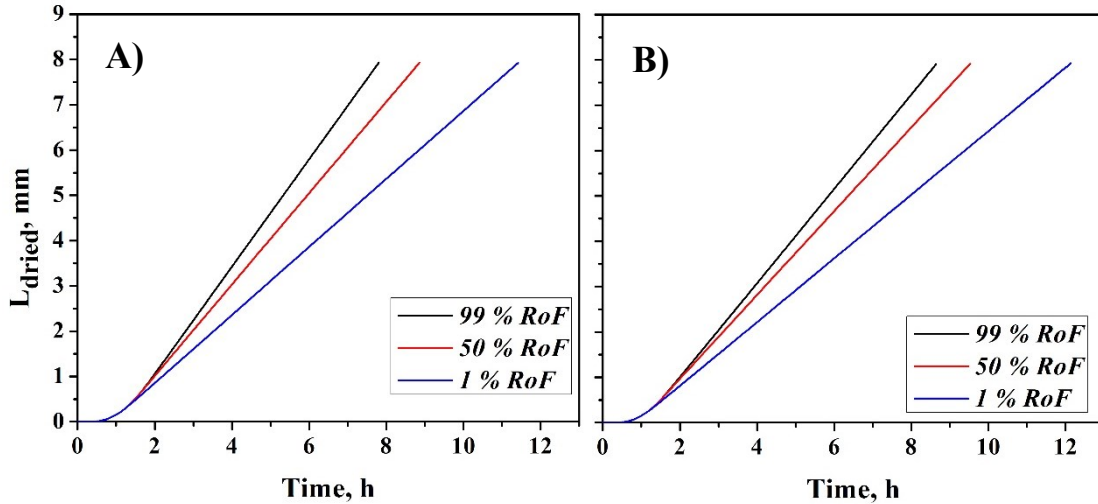


Figure 3.35: Evolution of L_{dried} during primary drying for a RoF of 1%, 50%, and 99%. A) Cooling rate: $1^{\circ}\text{C}/\text{min}$. B) Cooling rate: $0.1^{\circ}\text{C}/\text{min}$

In the case of a cooling rate of $1^{\circ}\text{C}/\text{min}$, Figure 3.36 shows the product temperature (T_i) monitored in function of time for different RoF (50% and 1%). The horizontal line in the Figure represents $T_{i,crit}$, that in this case was supposed to be equal to T_{c-50} (-34.8°C).

The temperature was monitored at the bottom of the vial; therefore, the temperature measured was slightly higher than the real temperature at the sublimation front. The sublimation front moved downwards during primary drying, and when the ice in contact with the thermocouple was sublimated the temperature increased sharply, due to more energy supplied to the vial than those removed by ice sublimation (Van Bockstal *et al.*, 2017).

As the Figure 3.36 A shown, T_i for the center-vials remained below $T_{i,crit}$ in the case of the 1% RoF. While T_i reached a value slightly higher than $T_{i,crit}$ when a 50% of RoF was used. In the case of the edge-vials (Figure 3.36 B), T_i slightly overcome $T_{i,crit}$ for both RoF.

Nevertheless $T_{i,crit}$ was overcome, no macroscopic collapse was observed in the final freeze-dried product. Several researchers reported that in some cases even though the collapse temperature was overcome, the macroscopic collapse of the structure did not occur (Rey and May, 2011).

This can be explain taking into account practical issues such as the fact that the temperature was monitored at the bottom and therefore at the point of maximum temperature, which could differ from the real temperature at the sublimation front (Rey and May, 2011). Moreover, the uncertainty on the temperature measurements (± 1) should be also considered.

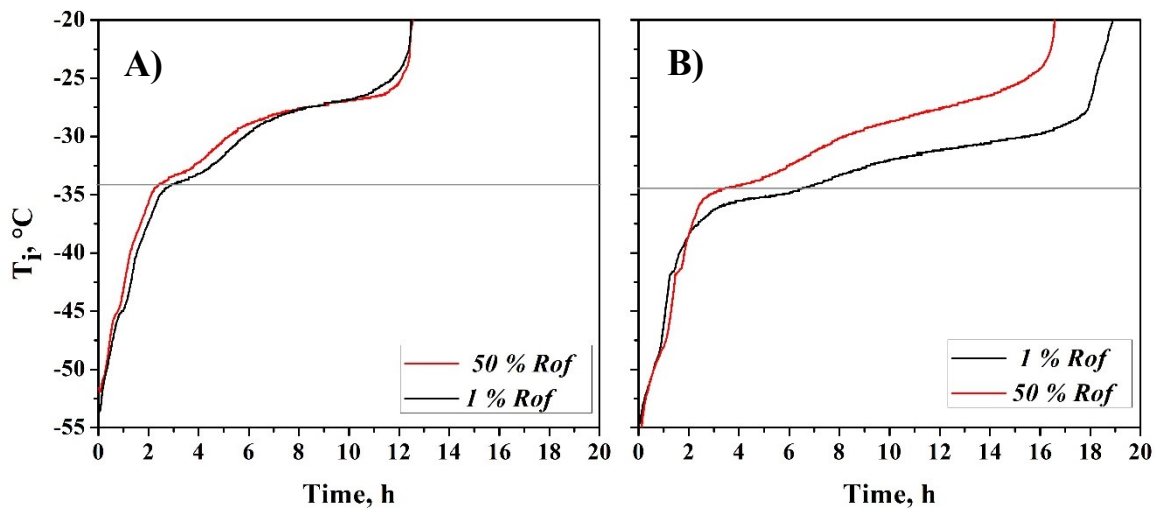


Figure 3.36: Product temperature (T_i) determined experimentally for a Risk of failure of 1% and 50% and a cooling rate of 1 °C/min. The grey line represents $T_{i,crit}$ (in this case -34.8 °C). A) T_i for an edge-vial. B) T_i for a center-vial.

In this case, the temperature taken as $T_{i,crit}$, was based on the T_{c-50} and not on the T_{fc} . Therefore, it is possible that only microcollapse occurred, and a complete loss of the structure was not present. Consequently, SEM analysis could be performed in order to evaluate whether a collapse at microscope level occurs or not.

Figure 3.37 presents the product temperature (T_i) monitored for different RoF (50% and 1%) in the case of the freezing protocol with the slower cooling rate (0.1 °C/min).

In both cases (both cooling rates), the edge-vials reach higher temperatures than those vials placed in the center of the shelf.

Table 3.8 reports the drying time computed by the model and the drying time obtained from the experimental validation. The first column shows the results obtained using the K_v -coefficients of the edge vials as input to the model. Since the ice sublimation takes longer for the center vials, the entire batch requires more time to finish primary drying.

The primary drying endpoint for the entire batch was calculated using the K_v -coefficients of the center-vials and the optimal process conditions (T_{shelf} and P_c , calculated previously) as input to the model. The uncertainty level of the parameters was taken into account, and as illustrated in Figure 3.38, the primary drying endpoint was determined with a certainty of 50% and 99%.

As it is shown, the computed drying time for the entire batch is lower than the drying time determined experimentally and higher than the drying time computed using the K_v of the edge vials.

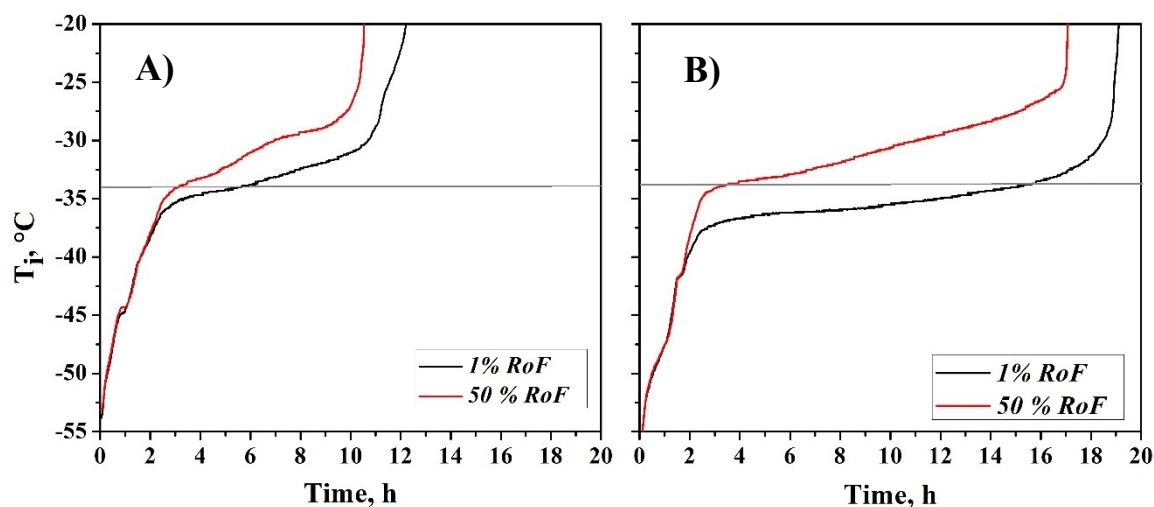


Figure 3.37: Product temperature (T_i) determined experimentally for a Risk of failure of 1% and 50% and a cooling rate of 0.1 °C/min. The grey line represents $T_{i,crit}$ (in this case -34.8 °C). A) T_i for an edge-vial. B) T_i for a center-vial.

Table 3.8: Computed primary drying endpoint by the model and the experimental determination of primary drying time for a RoF of 1% and 50 %.

<i>Cooling rate: 0.1 °C/min</i>				
Risk of failure	Computed primary drying endpoint-edge vials (h)	Computed primary drying endpoint-center vials (h)		Experimental Value (h)
		Mean	Certainty of 99%	
1%	12.14	14.4	16.2	22.67
50%	9.53	11.3	12.4	18.17

<i>Cooling rate: 1°C/min</i>				
Risk of failure	Computed primary drying endpoint-edge vials (h)	Computed primary drying endpoint-center vials (h)		Experimental Value (h)
		Mean	Certainty of 99%	
1%	11.42	13.6	15.2	0.00
50%	8.86	9.25	10.0	0.00

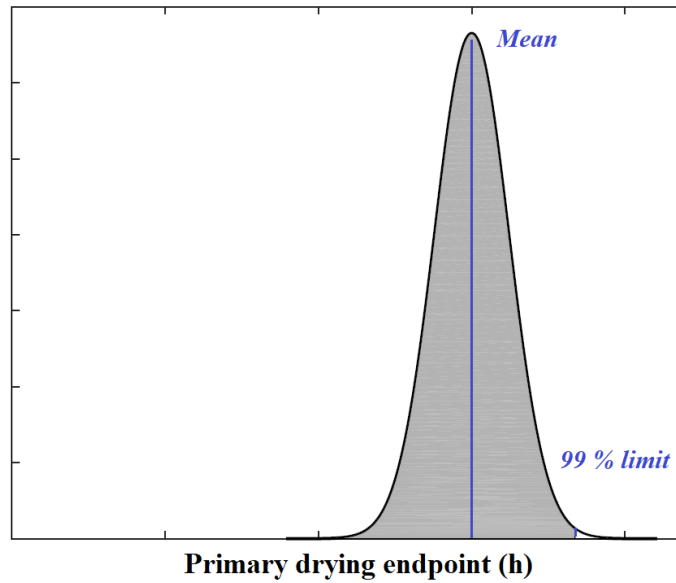


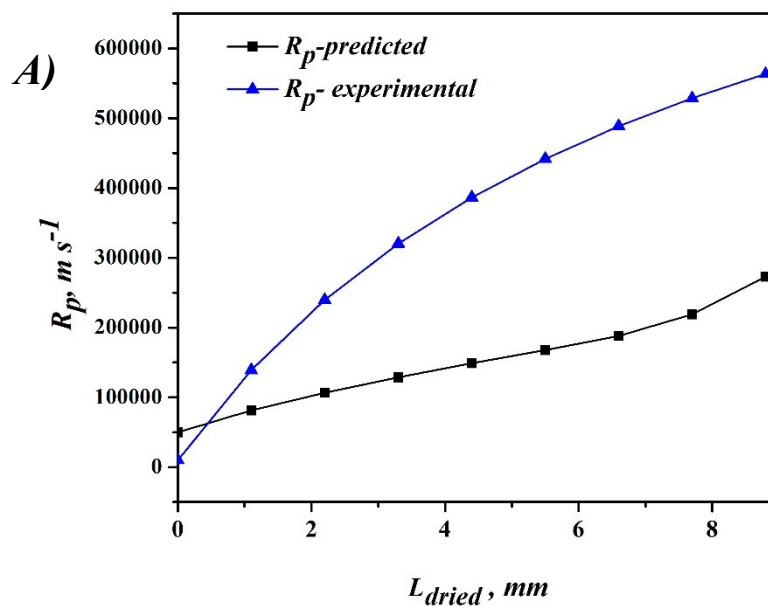
Figure 3.38: Primary drying endpoint with a certainty of 50% and 99% (from Van Bockstal *et al.*, 2017, with modifications)

3.2.7 R_p predicted and R_p experimentally determined

Once the R_p was predicted by using the mathematical model of the freezing step (section 3.2.6), the value was compared with the R_p value found experimentally (section 3.1.4).

Figure 3.39 shows the comparison of the R_p values (experimentally and predicted) in function of L_{dried} .

As it is shown, in the case of the higher cooling rate the R_p experimentally determined is significantly higher than that predicted.



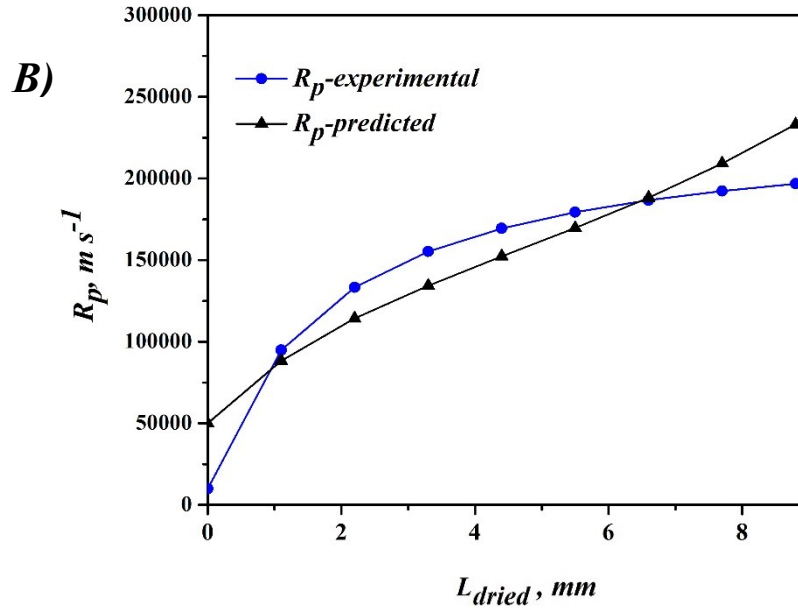


Figure 3.39: Comparison between the R_p value predicted and R_p experimentally determined. A) Cooling rate: $1^\circ C/min$. B) Cooling rate: $0.1^\circ C/min$.

Further analysis should be performed to find the reason for these differences, and it is advisable to do a second analysis of the SEM images due to the values of the average pore size obtained are higher than those obtained in previous researches and the methodology used to analyze the SEM images has a high level of subjectivity associated.

Notation

A_p	Inner vial area, m
A_{Rp}	R_p coefficient of Eq. 3.10, s^{-1}
A_v	Outer vial area, m
B_{Rp}	R_p coefficient of Eq. 3.10, m^{-1}
C_p^*	Apparent specific heat capacity, $J Kg^{-1}K^{-1}$
D	Data matrix
D_p	Size of ice crystal/pore, m
J_w	Sublimation flux, $Kg s^{-1}m^{-2}$
κ	Ratio of the specific heat for water
K_v	Heat transfer coefficient, $Jm^{-2}s^{-1}k^{-1}$

L_{dried}	Thickness of the dried layer, m
$\dot{m}_{sub,chock,vial}$	Maximum sublimation rate avoiding choked flow at vial level, kg s^{-1}
$\dot{m}_{sub,chock,drier}$	Maximum sublimation rate avoiding choked flow at drier level, kg s^{-1}
\dot{m}_{sub}	Sublimation rate, kg s^{-1}
n_{vials}	Maximum number of vials that can fit in the equipment
P	Loading matrix
p	Loading vector
P_c	Chamber pressure, Pa
P_i	Vapor pressure at the sublimation front, Pa
$P_{w,c}$	Water vapor partial pressure in the chamber, Pa
Q_c	Heat flux of crystallization, $\text{J s}^{-1}\text{m}^{-2}$
Q_n	Heat flux of nucleation, $\text{J s}^{-1}\text{m}^{-2}$
r_d	Radius of the duct of the dryer, m
R_p	Product resistance to vapor flow, ms^{-1}
R_{po}	Rp coefficient of Eq. 3.10, m s^{-1}
$r_{v,i}$	Inner radius of vial, m
$r_{v,n}$	Radius of vial neck, m
$r_{v,o}$	Outer radius of vial, m
T	Score matrix
t	Score vector
T_{c-50}	Mid-point collapse, $^{\circ}\text{C}$
T_{fc}	Full collapse temperature, $^{\circ}\text{C}$
T_i	Temperature at the sublimation front, $^{\circ}\text{C}$
$T_{i,crit}$	Critical product temperature, $^{\circ}\text{C}$
T_n	Nucleation temperature, $^{\circ}\text{C}$
T_{shelf}	Shelf temperature, $^{\circ}\text{C}$
V	Filling volume, ml
α	K_v coefficient of Eq. 3.9, $\text{J m}^{-2}\text{s}^{-1}\text{k}^{-1}$
α	Parameter of Eq. 3.6
β	K_v coefficient of Eq. 3.9, $\text{J m}^{-2}\text{s}^{-1}\text{k}^{-1}\text{Pa}^{-1}$

γ	K_v coefficient of Eq. 3.9, Pa ⁻¹
γ	Temperature gradient within the frozen zone, K
ΔH_{sub}	Latent sublimation heat, J mol ⁻¹
Δm	Mass of sublimated ice, kg
ΔT	Temperature across the ice layer, K
λ_1	Parameter of Eq. 3.6
λ_2	Parameter of Eq. 3.6
v	Freezing front rate, m s ⁻¹
ξ	Volume fraction of ice
ρ_I	Ice density, kg m ⁻³
τ	Tortuosity

Abbreviations

PC	Principal Component
SNV	Standard normal variate
SEM	Scanning Electron Microscope
RoF	Risk of Failure

References

- Bomben J. L., & King, C. J. (1982). Heat and mass transport in the freezing of apple tissue. *International Journal of Food Science & Technology*, **17**(5), 615–632.
- De Beer, T. R. M., Alleso, M., Goethals, F., Coppens, A., Vander Heyden, Y., Lopez De Diego, H., Baeyens, W. R. G. (2007). Implementation of a process analytical technology system in a freeze-drying process using Raman spectroscopy for in-line process monitoring. *Analytical Chemistry*, **79**(21).
- Fissore, D., Pisano, R., & Barresi, A. A. (2011). Advanced approach to build the design space for the primary drying of a pharmaceutical freeze-drying process. *Journal of Pharmaceutical Sciences*, **100**(11), 4922–4933.
- Geidobler, R., & Winter, G. (2013). Controlled ice nucleation in the field of freeze-drying: Fundamentals and technology review. *European Journal of Pharmaceutics and Biopharmaceutics*, **85**(2), 214–222.
- Giordano, A., Barresi, A. A., & Fissore, D. (2011). On the use of mathematical models to build the design space for the primary drying phase of a pharmaceutical lyophilization

- process. *Journal of Pharmaceutical Sciences*, **100**(1), 311–324.
- Jolliffe, I. T. (2002). Principal Component Analysis, *Second Edition. Encyclopedia of Statistics in Behavioral Science* (Vol. 30).
- Kasper, J. C., & Friess, W. (2011). The freezing step in lyophilization: Physico-chemical fundamentals, freezing methods and consequences on process performance and quality attributes of biopharmaceuticals. *European Journal of Pharmaceutics and Biopharmaceutics*, **78**(2), 248-263
- Kuu, W. Y., Hardwick, L. M., & Akers, M. J. (2006). Rapid determination of dry layer mass transfer resistance for various pharmaceutical formulations during primary drying using product temperature profiles. *International Journal of Pharmaceutics*, **313**(1–2), 99–113.
- Mortier, S. T. F. C., Van Bockstal, P. J., Corver, J., Nopens, I., Gernaey, K. V., & De Beer, T. (2016). Uncertainty analysis as essential step in the establishment of the dynamic Design Space of primary drying during freeze-drying. *European Journal of Pharmaceutics and Biopharmaceutics*, **103**, 71–83.
- Murphy, D. M., & Koop, T. (2005). Review of the vapour pressures of ice and supercooled water for atmospheric applications. *Quarterly Journal of the Royal Meteorological Society*, **131**(608), 1539–1565.
- Oddone, I., Barresi, A. A., & Pisano, R. (2017). Influence of controlled ice nucleation on the freeze-drying of pharmaceutical products: the secondary drying step. *International Journal of Pharmaceutics*, **524**(1–2), 134–140.
- Oddone, I., Van Bockstal, P. J., De Beer, T., & Pisano, R. (2016). Impact of vacuum-induced surface freezing on inter- and intra-vial heterogeneity. *European Journal of Pharmaceutics and Biopharmaceutics*, **103**, 167–178.
- Pisano, R., & Capozzi, L. C. (2017). Prediction of product morphology of lyophilized drugs in the case of Vacuum Induced Surface Freezing. *Chemical Engineering Research and Design*, **125**, 119–129.
- Pisano, R., Fissore, D., Barresi, A. A., Brayard, P., Chouvenc, P., & Woinet, B. (2013). Quality by design: optimization of a freeze-drying cycle via design space in case of heterogeneous drying behavior and influence of the freezing protocol. *Pharmaceutical Development and Technology*, **18**(1), 280–295.
- Rey, L., & May, J. C. (2011). Freeze-drying/ lyophilization of pharmaceutical and biological products, *Second Edition, Revised and Expanded. Drugs and the Pharmaceutical Sciences*. Taylor & Francis.
- Van Bockstal, P. J., Mortier, S. T. F. C., Corver, J., Nopens, I., Gernaey, K. V., & De Beer, T. (2017). Quantitative risk assessment via uncertainty analysis in combination with error propagation for the determination of the dynamic Design Space of the primary drying step during freeze-drying. *European Journal of Pharmaceutics and Biopharmaceutics*, **121**, 32–41.
- Zhang, L., Henson, M. J., & Sekulic, S. S. (2005). Multivariate data analysis for Raman imaging of a model pharmaceutical tablet. *Analytica Chimica Acta*, **545**(2), 262–278.

Chapter 4

Conclusions

The principal objective of this work was to develop, and optimize freeze-drying cycles using the approach of Quality by Design. This approach was widely applied in the development of pharmaceutical formulation and optimization of primary drying process conditions, and considered from regulatory agencies as an emerging paradigm in pharmaceutical industry.

Primary drying is the most expensive and longest step on lyophilization; therefore, the main concern on the development of freeze-drying cycles was the optimization of the process conditions of this step.

During primary drying is necessary to work with conservative drying conditions to keep the product temperature below the critical formulation temperature (i.e., collapse temperature), but on the other hand, it was necessary to develop this step at the maximum possible temperature and with a chamber pressure that allows the reduction of primary drying time. In this context, an optimization of the pharmaceutical formulation in terms of thermal properties and a definition of the optimal process conditions was required.

The work was divided into two parts; in the first part, a focus on the thermal characterization of different formulations was done. The second part involved the definition of the optimal process conditions during primary drying, while it was taken into account the uncertainty on process parameter as the heat and mass transfer coefficients.

The thermal characterization was done using two powerful tools; the Freeze-drying Microscope (FDM) and the Differential Scanning Calorimetry (DSC). In this way, the glass transition temperature and the collapse temperature were determined for combinations of Mannitol, used as a bulking agent, and sucrose, a lyoprotectant, in different buffers solutions (phosphate buffer, citrate buffer and HEPES). The characterization was performed for several formulations varying the weight ratio of mannitol to sucrose in order to analyze the effect of the excipient concentration on the physical state of the components and on the thermal characteristics of the formulations. In addition, different conditions into the cooling step during the DSC analysis were used to evaluate its effect on the thermal characteristics.

It was found that a higher amount of mannitol in the solutions reduced the glass transition temperature. For the three buffer solutions, it was observed a downward trend of the collapse temperature as the amount of mannitol increased, this until the amount of mannitol became higher than the amount of sucrose; from this point, the collapse temperature increased with the increase of mannitol concentration. This behavior could be explained taking into account the effect of sucrose on the inhibition of mannitol crystallization.

The effect of the different buffer solutions was evaluated and the collapse temperature of formulations with two different weight ratios of mannitol to sucrose (4:1 and 2:3; mannitol to sucrose) in three different buffers was confronted with the collapse temperature of formulations with the same weight ratios of mannitol to sucrose without buffer. In the case of the formulation with a weight ratio 4:1 mannitol to sucrose, the collapse temperature of the formulation without buffer was significantly higher than those with buffer. This could be associated with the inhibitory effect on mannitol crystallization caused by the presence of buffering salts. For the formulation with a weight ratio 2:3 mannitol to sucrose the collapse temperature of the formulation with and without buffer did not show the same significant difference than in the case of the formulation 4:1 mannitol to sucrose.

In addition, combinations of PVP/mannitol and dextran/mannitol were analyzed. The collapse temperatures obtained using these formulations were significantly higher than those obtained using combinations of mannitol and sucrose.

On the second part of this work, a mechanistic model developed at the University of Ghent was used to define a dynamic design space and therefore, the optimal process conditions during primary drying.

Traditionally, during the primary drying, the adaptable process conditions (T_{shelf} and P_c) were set as fixed values, leading to sub-optimal process conditions. It is important to consider that the model input variables change as the process evolves, for example, the increase of L_{dried} value as primary drying evolves correspond to an increase in R_p value; therefore the optimal process conditions change with the time and the use of a dynamic design space showed advantages.

In addition, the mechanistic model uses several input parameters that are usually an estimation of the real values. For example, the values of R_p and K_v are often defined for the entire production while their values change from vial to vial. To take into account of the uncertainty of the parameters an uncertainty analysis was performed to quantitatively estimate the batch rejection caused by the cake collapse, i.e., Risk of Failure (RoF). In previous works the assessment of the uncertainty of R_p was not done, but only supposed.

With this pursue, an analysis of the morphology variability within a production was done. The pore size is strongly dependent on the degree of supercooling of the sample and freezing rate. Therefore, the first step in the analysis was to determine the nucleation temperature distribution, using two different cooling ramps (0.1 °C/min and 1 °C/min).

The value of variance obtained in the case of the nucleation temperature distribution for the higher cooling rate was higher than that obtained using the slower cooling rate. This could be explained taking into account the fact that more samples nucleated within the same range of temperature if they remained in this condition for more time. This result is also consistent with the analysis done in terms of the difference between the onset and offset time of primary drying (using the pressure ratio curves). The difference between the onset and offset point was slightly higher in the case of the cycle developed with a cooling rate of 1 °C/min compared with that developed with a cooling rate of 0.1 °C/min. These results indicate that a higher cooling rate leads to a higher inter-vial variability.

Once the nucleation temperature distribution was defined for both freezing protocols, a mathematical model developed in the Politecnico di Torino was used to correlate each nucleation temperature to a product morphology, and therefore, use the nucleation temperature distribution to obtain a pore size distribution and then, to calculate a R_p in terms of mean value and standard deviation.

SEM analysis was done to find a pre-exponential factor used in this model and then to compare the results from the prediction of the product morphology and those obtained by SEM observations.

The uncertainty level of R_p were 16% and 12% for the high cooling rate and the lower cooling rate, respectively. These results confirmed that a higher cooling rate leads to a higher inter-vial variability.

Once all the parameters needed were fixed, the mechanistic model was used to define the adaptable process conditions for three Risk of Failure (1%, 50%, 99%) for each freezing protocol. As it was expected, more conservative conditions are related to a lower risk of failure.

The experimental verification of the dynamic design space was performed for two RoF (1% and 50%), in both cases, no collapse was observed (for both freezing protocols). In all cases, the computed primary drying time for the whole production was lower than the endpoint of primary drying calculated experimentally.

Further analysis should be performed to find the specific reason for these differences. Particularly, the determination of the average pore size using the SEM images should be repeated because the values obtained were higher than those obtained in previous researches.

Acknowledges

First, I would like to thank my thesis supervisor, Dr. Roberto Pisano, who leads me into this interesting topic and gave to me the opportunity to become in a better professional.

Thanks to Dr. Thomas De Beer, who gave me the opportunity to develop part of my thesis in the laboratories of the Gent University. This experience allowed me to growth professionally and personally. I have enjoyed deeply the time I spent there.

In addition, I would like to acknowledge Luigi and PJ, who helped me during the development of this project. Their advice and recommendations were an invaluable contribution to this work. I have learned so much working with them.

I must express my very profound gratitude to my parents and my sister for providing me with unfailing support and continuous encouragement during my life; I am who I am thanks to you. This accomplishment would not have been possible without them. Thank you.

Thanks to Hernan, with whom I started this adventure years ago. Thanks for supporting me and encourage me during these years of study.

Thank you, Ale, for sharing these two years with me and always being there for me. I will not forget all the moments we have shared together-from those unforgettable trips to even those stressful moments in study rooms-. Thank you for been there always in the good moments and in those bad also.

During these two years in Italy, I had also the opportunity to meet good friends who accompanied me during this experience, thanks Gabo for all the good moments we shared together. Thanks Migue for been my friend, I have enjoyed every moment that we spent together.

Thank you all very much.

Estefany Carolina Flores Brun